

# **EVALUATION OF RECYCLED ASPHALT SHINGLES AS STRUCTURAL FILL**

By Ali Soleimanbeigi, Tuncer Edil and Craig Benson

Recycled Materials Resource Center

University of Wisconsin-Madison

Madison, WI 53706, USA

10 December 2011

[www.recycledmaterials.org](http://www.recycledmaterials.org)

<b>TABLE OF CONTENTS</b>	<b>PAGE</b>
Chapter 1 Introduction.....	2
Chapter 2 Recycled Asphalt Shingles Mixed with Granular Byproducts as Structural Fills.....	5
Chapter 3 Evaluation of Fly Ash Stabilization of Recycled Asphalt Shingles for Use in Structural Fills.....	47
Chapter 4 Effect of Temperature on Geotechnical Properties of Recycled Asphalt Shingles Mixtures .....	86
Chapter 5 Summary and Conclusion .....	143
Appendix I Evaluation of shredded reclaimed asphalt shingles mixed with foundry slag as highway embankment fill .....	148

# Chapter 1

## Introduction

The amount and type of generated solid waste grow as the world population increases. While landfills are the primary end place of the majority of solid waste, there have been increasing motivation and research towards feasibility, and performance of reusing certain types of solid waste in highway construction. A wide variety of solid waste including coal combustion byproducts, foundry slags, tire shreds, and reclaimed paving materials have been studied and successfully used in the construction of highway embankments (RMRC 2011). In addition to promising a solution to the disposal problem and an economic alternative to natural soils, certain solid waste materials may have lower dry unit weight, which makes them favorable alternative to traditional material for construction of embankments over weak grounds.

Discarded asphalt shingles is another type of solid waste that has recently been prioritized by Environmental Protection Agency (EPA) and Federal Highway Administration (FHWA) for reuse application. Asphalt shingle waste is produced by removing the asphalt shingles from the roofs of existing structures during renovation (called post-consumer asphalt shingle or tear-off shingle) or rejecting asphalt shingles/shingle tabs discarded in the manufacturing process of new asphalt shingles (called manufactured shingle scrap). Approximately 11 million Mg of asphalt roofing shingle waste are generated in the U.S. per year (Krivit, 2007, NERC 2011). Re-roofing jobs account for 10 million Mg, with another 1 million Mg manufacturing scrap. Different applications including as a component of hot mix asphalt (HMA), cement kiln fuel, cold patch in paved roads and dust control in gravel roads account for reuse only between 10 to 20% of the total asphalt shingle waste and therefore the remaining large amount is landfilled (Townsend,

2007; Turley, 2011). Use of the asphalt shingle waste as fill material in highway fills consuming large volume of materials will open up potentially a large reuse option for the asphalt shingle waste.

The objective of the proposed research is to evaluate the geotechnical properties of recycled asphalt shingles (RAS) as structural fill material in highway embankments or backfill material behind retaining structures and to provide relevant design guidelines. The research outlined in this proposal addresses the following hypotheses:

- 1- RAS as a granular material has sufficient shear strength and drainage capacity to qualify as a structural fill. Since RAS contains asphalt cement and cellulose felt, the material may exhibit higher compressibility compared to traditional fill material.
- 2- Addition of less compressible materials to RAS or stabilization of RAS can reduce the compressibility and increase shear strength and drainage capacity of RAS.
- 3- Since RAS contains asphalt cement, temperature variation affects its engineering properties.
- 4- Since RAS contains asphalt cement, time-dependent shear or volumetric strain under sustained deviatoric stress may be significant.

The main chapters (Chapter 2, 3, and 4) are written as individual self-contained technical articles. In Chapter 2 entitled “Recycled Asphalt Shingles Mixed with Granular Byproducts as Structural Fill”, physical and mechanical properties of RAS and RAS mixed with granular industrial byproducts including bottom ash (BA) and foundry slag (FS) are evaluated in a systematic manner. Results show that although pure RAS has suitable drainage capacity and shear strength as structural fill, compressibility of RAS is significant compared to natural soils. Systematic addition of BA and FS to RAS reduced the compressibility and increased shear

strength and drainage capacity of RAS:BA and RAS:FS mixtures. Design graphs were developed to estimate geotechnical properties of RAS:BA and RAS:FS mixtures for a given RAS content and stress level.

In Chapter 3 entitled “Evaluation of Fly Ash Stabilization of Recycled Asphalt Shingles for Use in Structural Fills”, self-cementing (Class C) fly ash was used to stabilize RAS. Results show that stabilization remarkably reduces compressibility and increases the shear strength of RAS. However, stabilization also reduces the drainage capacity of RAS to that of silty sand or silty clay soil.

Chapter 4 entitled “Effect of Temperature on Geotechnical Properties of Recycled Asphalt Shingles Mixtures” evaluates the effect of temperature change on geotechnical properties of compacted RAS:BA mixture and stabilized RAS. The development of a thermo-mechanical system and test procedures at elevated temperature are described. Systematic mechanical tests at elevated temperatures were conducted on RAS:BA and stabilized RAS specimens. The results show that when temperature increases, the shear strength decreases but compressibility and hydraulic conductivity increases. The shear strength and hydraulic conductivity of RAS containing embankments or stabilized RAS are sufficient to provide stability and drainage capacity of road embankments at different climates in North America. However; to minimize long-term settlement, compaction and construction of RAS embankments are recommended in warm season of the year.

Chapter 5 contains summary and conclusion of the research conducted on RAS. Appendix I includes a paper that investigates geotechnical properties of RAS mixed with foundry slag in greater detail as well as the practical implications for estimation of settlement of typical highway embankment constructed with RAS:FS mixture.

## Chapter 2

### **Recycled Asphalt Shingles Mixed with Granular Byproducts as Structural Fills**

**ABSTRACT:** In this research, possible reuse of discarded asphalt shingles as structural fill was investigated. Bottom ash (BA) and foundry slag (FS) were also investigated as additives to recycled asphalt shingles (RAS) to enhance its mechanical properties. The engineering properties of RAS:BA/FS mixtures including compaction characteristics, hydraulic conductivity, compressibility, shear strength, and coefficient of lateral earth pressure at rest were evaluated in a systematic manner. Results show that addition of bottom ash and foundry slag significantly reduces compressibility of RAS while increasing drainage capacity and shear strength. RAS:BA/FS mixtures are favorable light weight material for use as embankment fills or backfill behind retaining walls.

**KEYWORDS:** Recycled asphalt shingle, bottom ash, foundry slag, structural fill, engineering properties.

#### **Introduction**

Approximately 11 million Mg of waste asphalt roofing shingles are generated per year in the U.S. of which 10 million Mg are tear-off roofing shingles and 1 million Mg is factory scraps

(Townsend et al. 2007). Asphalt shingle waste is produced over 250,000 Mg per year in Wisconsin and is categorized as the third largest waste item by weight in the state (Recycling Connections Corporation, 2010). Reuse of recycled asphalt shingles (RAS) has been identified by the U.S. Environmental Protection Agency (EPA) as a top priority. Constituents of typical asphalt shingle include 20-35% asphalt cement, 2-15 % cellulose felt, 20-38 % mineral granule/aggregates, and 8-40% mineral filler/stabilizer.

The primary reuse application of RAS is in production of hot mix asphalt (HMA). Research results have shown however, that more than 5% by weight RAS in HMA will adversely affect the creep stiffness and tensile strength of HMA (Button et al. 1995, Grodinsky, 2002). Consequently, this application uses only between 10 to 20 % of the total asphalt shingle waste (Turley, 2010). Another potential application, which could use large volume of asphalt shingle waste is structural fill including highway embankment fills or backfill behind retaining walls.

Preliminary compression test results showed that pure RAS is too compressible for use as structural fill (Benson et al. 2010). To reduce compressibility of RAS, addition of granular materials with verified suitability as structural fill was considered. Bottom ash (BA) is a coarse granular coal combustion product, which is collected at the bottom of the furnaces in power plants. Previous investigation has verified suitability of engineering properties and field performance of bottom ash in construction of highway embankments or working platforms (Seals et al. 1972; Moulton et al. 1973; Huang 1990; Karim 1997; Edil et al. 2002; Kim 2003; Tanyu et al. 2005; Kim et al. 2005; Yoon et al. 2009). According to American Coal Ash Association (ACAA, 2008) about 16.5 million Mg bottom ash was produced in 2009 of which 44 % was reused in different applications like structural fills, embankments, road base and sub-base,

soil modifications and concrete products. Of the total reused bottom ash, 42 % was used as structural fills.

Foundry slag (FS) is a combination of limestone and metal impurities in metal casting industry, which is collected from top of the molten metal in the furnace. The molten slag is cooled, crushed and screened to create granular slag. According to the U.S. Geological Survey about 17 to 24 million Mg foundry slag was produced in 2008 of which about 90 % were reused in a variety of engineering applications as aggregate in portland cement concrete, asphalt concrete, aggregate base, fill material and railroad ballast. Of the total reused foundry slag 40 % was used as road basement and 10 % was used as fill material. The engineering properties of foundry slag are suitable for use as structural fill and working platforms (Emery 1982, Ahmed 1993; Edil et al. 2002; Tanyu et al. 2005). In this study, bottom ash and foundry slag were investigated as granular additives to improve the engineering properties of RAS.

The objective of this research is to investigate suitability of RAS:BA/FS mixtures as construction material for structural fills. For this purpose, relevant engineering properties of RAS:BA/FS mixtures including compaction characteristics, hydraulic conductivity, compressibility, shear strength and coefficient of earth pressure at rest were evaluated in a systematic manner and presented herein.

## **Background**

While mechanical properties of recycled asphalt pavement (RAP) have been evaluated for use as structural fill (Viyasant et al. 2007; Wen and Edil 2007; Li et al. 2008), few scientific investigations have been completed on engineering properties of RAS. Most of the findings are

based on field observations. Iowa Department of Transportation studied the use of ground shingles as a surface treatment on an unpaved road. Nearly 900 tons of tear-off shingles were ground to pieces less than 25 mm to 50 mm and mixed with crushed limestone to achieve a uniform shingle/limestone mixture of about 65 mm thick. After two years of observations, the study concluded that shingles are very effective for dust control in rural roads, result in better lateral control of vehicles, reduce the loss of granular materials into the ditches, and resulted in a quieter and smoother roadway (Marks 1997).

Vermont Agency of Natural Resources (Vermont ANR) incorporated 10 % by weight RAS with the maximum size ( $d_{\max}$ ) of 9.5 mm, 30 % recycled asphalt pavement (RAP) with  $d_{\max}$  of 37.5 mm and 60 % of gravel with  $d_{\max}$  of 37.5 mm. The material was placed and compacted on a series of municipal roadways and spread with calcium chloride solution. Over a two-year evaluation period, Vermont ANR reported that the mixture compacts very well, resists rutting and erosion, mitigates dust and in general requires less maintenance than the conventional gravel control section (Grodinsky et al. 2002).

Hooper and Marr (2004) obtained some baseline quantitative data on the physical and mechanical effects that shingles have on soils. California bearing ratio (CBR) tests on RAS samples with  $d_{\max}$  of 25 mm showed that the CBR strength is 6 % which categorizes RAS as a questionable to fair material for subgrade. The results showed that addition of 33% by volume of RAS to clay increased CBR of the RAS:clay mixture from 8 % to 20 %. However; addition of 33 % by volume of RAS reduced CBR of crushed stone gravel from 92% to 23%, silty sand from 33% to 19% and clean sand from 21% to 13%. Hooper and Marr (2004) concluded that RAS behaves like granular particles in clay but may cause deterioration of inter-particle friction between sand and gravel particles.

Warner (2007) evaluated beneficial use of RAS as base course and subbase layers. Compaction tests on RAS samples with the  $d_{\max}$  ranging from 5 mm to 50 mm showed that the maximum dry unit weight ( $\gamma_{d\max}$ ) of RAS varied between 8.8 kN/m<sup>3</sup> and 12.3 kN/m<sup>3</sup>. The types of soil used for the mixture were Boardman silt (ML) and Grade 2 granular backfill (GP-GM). Compaction test results showed that increase in RAS content decreased dry unit weight ( $\gamma_d$ ) of both types of soil. Resilient modulus ( $M_r$ ) of pure RAS was 30 MPa, which is lower than the minimum 75 MPa recommended by NCHRP project 1-37A for base course layer. Addition of 50% by weight of Grade 2 gravel increased the resilient modulus to 78 MPa, which made the mixture suitable for use as base course and subbase layer.

## **Test Materials**

RAS samples used in this study were taken from Stratford Building Supply Company in Stratford, WI. Visual inspection indicated that RAS samples were free of impurities like wood chips, plastics, and nails. The Stratford Building Supply grinds the waste shingles once over and screens them through 50 mm, 25 mm and 19 mm sieve sizes. Warner (2007) concluded that RAS particles with 10 mm maximum size result in higher  $\gamma_d$ , higher CBR and  $M_r$ . Therefore, in this study, the RAS supply was screened to limit the  $d_{\max}$  to 10 mm. Bottom ash and foundry slag samples were taken respectively from the Columbia Power Station and the Grede Foundries in Wisconsin. To compare the engineering properties of RAS:BA/FS mixtures to those of natural soil, a sample of Wisconsin glacial outwash sand was also used in this study.

## **Test Methods**

### *Physical Property Tests*

The physical property tests including grain size analysis, specific gravity, and microscopic examination were conducted on RAS, BA and FS samples. The physical properties of the Wisconsin glacial outwash sand sample were taken from Bareither et al. (2008).

### *Grain Size Analysis*

The grain size distribution of RAS, BA and FS samples were determined according to ASTM D 422. The samples were first wet sieved through sieve No. 200 to separate coarse and fine particles. The coarse portions of BA and FS samples were oven dried for 24 hours prior to mechanical sieving. The coarse portion of RAS sample was air dried to prevent binding of the particles at oven temperature.

### *Specific Gravity*

The specific gravities of RAS, BA and FS samples were measured according to ASTM D854 (Method B). To prevent clogging of RAS particles during the test and to remove any entrapped air in the slurry, the pycnometer was continuously agitated for about one hour under a constant vacuum. De-airing was accomplished by vacuuming distilled water.

### *Microscopic Examination*

Shape, angularity and surface texture of RAS, BA, FS and outwash sand particles were examined using a light microscope to understand interaction mechanisms between the particles during different mechanical testing.

### *Mechanical Property Tests*

The mechanical property tests including compaction, hydraulic conductivity, one-dimensional compression, and consolidated drained triaxial compression tests were performed on RAS:BA/FS mixtures with BA or FS contents of 0, 25, 50, 75 and 100%. To evaluate suitability of RAS:BA/FS mixtures as backfill behind retaining walls,  $K_o$ -Consolidation tests were performed on the mixtures with BA or FS contents of 0, 50 and 100%.

### *Compaction*

Standard Proctor compaction tests following ASTM D 698 (method B) were performed on RAS:BA/FS mixtures. One modified Proctor compaction test following ASTM D 1557-09 (method B) was performed on pure RAS to obtain compaction characteristics of RAS under higher compaction effort and to see if higher compaction energy will help reduce compressibility of RAS.

### *Hydraulic Conductivity*

Flexible wall hydraulic conductivity tests were conducted on RAS:BA/FS mixtures according to ASTM D 5084-03 to evaluate the effect of confining stress ( $\sigma'_c$ ) on hydraulic conductivity of the mixtures. Each RAS:BA/FS mixture was compacted to 95% of the  $\gamma_{dmax}$  at optimum water content ( $w_{opt}$ ) and consolidated to the desired effective stress ( $\sigma'_c=35$  kPa, 70 kPa and 140 kPa) for 24 hours. After consolidation phase, the hydraulic conductivity was measured according to the falling-head rising-tail method.

### *One-dimensional Compression*

Settlement of an embankment with large lateral extension can be considered one-dimensional and estimated from the results of one-dimensional consolidation tests. To evaluate compressibility of RAS:BA/FS mixtures, one-dimensional compression tests were performed following ASTM D 2435-96 using a standard consolidometer ring with 64-mm diameter and 25-mm height. Each specimen was compacted at the  $w_{opt}$  and relative compaction level of 95%. The compaction in the consolidometer ring was conducted in three lifts of equal thickness by a manual hammer. RAS:BA/FS specimens were then soaked in the consolidometers for 24 hours before applying vertical loads. Pore pressure piezometers were connected to consolidometer cells to measure any generated excess pore water pressures under each stress level. The specimens were loaded incrementally from 12.5 kPa with load increment ratio (LIR) of 1.0 and load increment duration (LID) of 24 hours until the maximum vertical stress level of 1600 kPa. The one-dimensional consolidation test was also performed on a glacial outwash sand sample for comparison. The LABVIEW software (National Instruments, Austin, TX) and a data acquisition card (UPC601-U) were used for automated incremental loading and recording of vertical deformation.

### *Triaxial Compression Tests*

To evaluate stress-strain and volumetric behavior of RAS:BA/FS mixtures under shearing and to determine the shear strength; consolidated drained (CD) triaxial compression tests were performed on compacted RAS:BA/FS mixtures. For each mixture composition three tests were performed under effective confining pressure,  $\sigma'_c$  of 35 kPa, 70 kPa and 140 kPa. The confining pressures were selected to represent the range of typical effective stresses in highway

embankments or retaining wall backfills. Each RAS:BA/FS mixture was compacted in five layers in a split mold with 74 mm diameter and 148 mm height to achieve the compaction level of 95%. The number of tamps per layer using a standard Proctor hammer was determined such that the same compaction energy as in the standard compaction effort (592 kN.m/m<sup>3</sup>) is applied to each sample mixture. After assembling the cell chamber, the specimens were backpressure-saturated according to ASTM D4767 so that a B value greater than 95 % was attained. The specimens were then isotropically consolidated under  $\sigma'_c$  of 35 kPa, 70 kPa and 140 kPa. The specimen volume change during consolidation phase was monitored in the backpressure tubing until no significant change in volume was observed. The shearing of each mixture specimen in drained condition was performed under constant strain rate. The axial deformation rate of 0.2 mm/min was selected based on the time for primary consolidation and the ultimate strain of the specimen at failure. The pore water pressure was monitored during shearing to ensure no excess pore water pressure is generated. The volume change of each specimen during shearing was recorded from the volume change of water in backpressure tubing.

### *K<sub>o</sub>-Consolidation Tests*

To evaluate the coefficient of lateral earth pressure at rest ( $K_0$ ) of RAS:BA/FS mixtures a specifically developed  $K_0$ -Consolidation cell by Edil and Wang (2000) was used. Fig. 1 shows the schematic of the apparatus. The cell has the dimensions of a conventional consolidation ring (64-mm diameter and 25-mm height) and consists of a hallowed ring with a thickness of 1 mm instrumented with strain gages. The air pressure is applied into the lateral pressure chamber around the inner ring to maintain the lateral displacement of the inner ring to a minimum during application of vertical stress. A program was written in LABVIEW to automate the test and

acquire the data.  $K_o$  is calculated by measuring the lateral air pressure upon application of vertical pressure on the specimen. The Poisson's ratio,  $\nu$  is assessed from  $\nu = K_o / (1 + K_o)$ .

## **Test Results**

### *Grain size distribution*

Fig. 2 shows the grain size distribution of RAS, BA, FS and outwash sand particles. More than 80 % of particles of each material are sand size with fine contents less than 5 %. RAS, BA and FS particles have almost similar grain size distributions; therefore, grain size distribution of different RAS:BA/FS mixtures will fall within a narrow range. According to the Unified Soil Classification System (USCS) RAS and FS are classified as well graded sand whereas BA and outwash sand are classified as poorly graded sand. Basic grain size indices and the USCS classification are included in Table 1.

### *Specific Gravity*

The specific gravities of RAS, BA, FS and outwash sand samples are included in Table 1. The specific gravity of RAS is 1.74, which is lower than the specific gravity of outwash sand (2.71). The low specific gravity of RAS is attributed to organic cellulose felt and asphalt cement contents which together constitute about 50% by mass of RAS. The specific gravity of asphalt binder is generally between 1.0 and 1.04 (Roberts et al. 1996). The specific gravity of BA is 2.67, which is comparable to specific gravity of the outwash sand. FS has the specific gravity of 2.36 which is lower than the specific gravity of the outwash sand. The measured specific gravity of BA and FS samples fall within the range reported in the literature (RMRC 2010).

### *Morphological Characteristics*

Fig. 3 shows typical particle shape of RAS and LM photomicrographs of BA, FS and outwash sand. RAS particles are plate-like, irregular in shape, highly angular and have rough surface texture. The angularity of RAS particles reduces to semi-round to round as the particle size decreases. During manufacturing, one side of the asphalt shingles is covered by sand to protect them against physical damages. The other side is covered by mineral filler to protect the shingles against adhesion during packing and shipment. Fig. 3 (a) shows the sand and mineral surface covers on the RAS particle surfaces.

BA and FS particles are angular to highly angular, internally porous and have rough surface texture. Some pores of the particles are filled with dust. On the other hand, particles of outwash sand are solid, semi-round to round and have smooth surface texture. Particle surfaces are clean, shiny and free of dust.

### *Compaction Characteristics*

Fig. 4 (a) shows the variation of dry unit weight ( $\gamma_d$ ) versus water content ( $w$ ) of different RAS:BA and RAS:FS mixtures. Pure RAS has a well-defined compaction curve with the maximum dry unit weight ( $\gamma_{dmax}$ ) of  $11.3 \text{ kN/m}^3$  and optimum water content ( $w_{opt}$ ) of 8 %. The  $\gamma_d$  of RAS:BA mixture increases with increasing BA content. Although BA and outwash sand have comparable specific gravities, the high porosity of BA particles reduces the  $\gamma_{dmax}$  to  $15 \text{ kN/m}^3$  which is lower than  $\gamma_{dmax}$  of typical compacted sand. As the BA content increases the  $\gamma_d$  of the mixture becomes less susceptible to water content. The  $\gamma_{dmax}$  of RAS compacted using modified Proctor test is the same as the  $\gamma_{dmax}$  of RAS:BA mixture with 50 % BA content compacted using

standard Proctor test. The  $\gamma_d$  of pure RAS becomes less susceptible to water content when compacted using modified Proctor test. Although pure RAS under higher compaction energy has the same  $\gamma_{dmax}$  as that of RAS:BA mix with 50% BA content, the RAS:BA mixture uses less energy to produce the same  $\gamma_{dmax}$  thus is preferred to RAS compacted using modified Proctor test.

Systematic addition of FS to RAS only slightly reduces  $\gamma_{dmax}$  of the RAS:FS mixture. The  $\gamma_{dmax}$  of RAS:FS mixture varies between 11.3 kN/m<sup>3</sup> to 10.8 kN/m<sup>3</sup>. Low specific gravity and high porosity of FS particles result in low  $\gamma_{dmax}$  of FS with respect to typical compacted sand. Figure 4 (b) shows that addition of FS to RAS does not essentially change  $\gamma_{dmax}$  of the RAS:FS mixture while addition of BA to RAS increases  $\gamma_{dmax}$  of the RAS:BA mixture from 11.3 kN/m<sup>3</sup> to 15.0 kN/m<sup>3</sup>.

### *Hydraulic conductivity*

Fig. 5 shows the hydraulic conductivity of RAS:BA/FS mixtures from the flexible wall hydraulic conductivity tests. Except for pure RAS under  $\sigma'_c$  of 140 kPa, the hydraulic conductivity of RAS:BA/FS mixture falls between  $1 \times 10^{-2}$  cm/s and  $1 \times 10^{-4}$  cm/s. The hydraulic conductivity of RAS:BA/FS generally decreases as the  $\sigma'_c$  increases. High compressibility of RAS particles and densification of RAS:BA/FS mixtures at higher  $\sigma'_c$  possibly explain the decrease in hydraulic conductivity of RAS:BA/FS mixtures with  $\sigma'_c$ . As the bottom ash/foundry slag content increases the hydraulic conductivity of RAS:BA/FS mixture becomes less sensitive to  $\sigma'_c$ . For the mixtures with bottom ash/foundry slag content more than 50 %, the hydraulic conductivity is almost constant at different  $\sigma'_c$ . At a particular  $\sigma'_c$ , the hydraulic conductivity of RAS:BA/FS

mixture increases with increasing BA/FS content. This is attributed to increase in void ratio. The void ratio of compacted RAS is 0.59 while the void ratios of BA and FS are 0.87 and 1.44; respectively. As the BA/FS content increases the void ratio of the compacted mixture increases which consequently increases the hydraulic conductivity. In general, according to USBR (1987) classification for drainage capacity based on hydraulic conductivity, the RAS:BA/FS mixtures under low to moderate confining pressures have *good drainage capacity* for use as structural fill.

### *Compressibility*

Fig. 6 (a) shows the compression curves of RAS:BA mixtures as vertical strain,  $\epsilon_v$ , versus logarithm of vertical effective stress,  $\sigma'_v$ . The compression curve of outwash sand sample is also included for comparison. Compared to outwash sand, pure RAS is highly compressible for structural fill applications. High compressibility of RAS is attributed to the asphalt cement and cellulose felt components which together constitute about 50% by weight of RAS particles. The compressibility of BA is only slightly higher than the compressibility of outwash sand which makes the BA an appropriate additive to reduce compressibility of RAS. The higher compressibility of BA than outwash sand may be attributed to angularity and rough surface texture of BA particles (Fig. 3b), which would tend to increase the stress concentration at particle contact surfaces. Increase in stress concentration at particle surface contacts is likely to result in particle damage due to abrasion or breakage of particle surface asperities or sharp particle corners which consequently increases the compressibility (Robert and de Souza 1958; Marshal 1967; Pestana and Whittle 1995; Chuhan et al. 2003). Fig. 6 (a) shows that systematic addition of BA to RAS reduces compressibility of RAS:BA mixtures. Under  $\sigma'_v$  up to 200 kPa, which is a

typical overburden pressure in highway embankments, addition of 50 % bottom ash to RAS significantly reduces  $\epsilon_v$  of the RAS:BA mixture from 17% to 5%.

The compressibility curves of RAS:FS mixtures are shown in Fig. 6 (b). Systematic addition of FS to RAS reduces compressibility of RAS:FS mixture. FS is more compressible than BA at  $\sigma'_v$  higher than 200 kPa. In addition to high angularity and rough surface texture that increase the possibility of particle breakage, the individual FS particles are more crushable than BA particles. Some popcorn-like slag particles were observed to break under finger pressure. Figure 7 shows degradation of BA and FS particles after compaction test and after compression test under  $\sigma'_v$  of 1600 kPa in terms of changing grain size distribution curves. Grain size distribution of BA sample shows increased amount of finer particles after compaction and compression tests. Degradation effect on FS particles after compaction and consolidation tests is more significant than bottom ash particles due to more crushable nature of the individual slag particles.

Compressibility of soils is classified based on modified recompression index,  $C_{r\epsilon} = C_r / (1 + e_o)$ , and modified compression index,  $C_{c\epsilon} = C_c / (1 + e_o)$ , as summarized in Table 2 (Coduto 1998). The preconsolidation pressure ( $\sigma'_p$ ) as well as  $C_{r\epsilon}$  and  $C_{c\epsilon}$  of RAS:BA/FS mixtures were determined from the graphs of void ratio versus  $\log \sigma'_v$  according to the graphical construction of Casagrande (Casagrande 1936b). Fig. 8 shows the variation of  $\sigma'_p$  of RAS:BA/FS mixtures with bottom ash/foundry slag content. The  $\sigma'_p$  of the mixtures increases with increase in bottom ash/foundry slag content indicating that yield pressure of RAS is improved with BA and FS addition. Fig. 9 illustrates the variation of  $C_{r\epsilon}$  and  $C_{c\epsilon}$  with respect to bottom ash/foundry slag content in RAS:BA/FS mixtures determined from the compression

curves. For RAS:BA mixtures, both  $C_{re}$  and  $C_{ce}$  decrease with increasing BA content. For RAS:FS mixtures,  $C_{re}$  decreases but  $C_{ce}$  increases with increasing FS content. The increase in  $C_{ce}$  with increasing FS content is attributed to significant particle crushing at  $\sigma'_v$  higher than 200 kPa during compression test as explained from Figs. 6(b) and 7(c). The settlement design of typical highway embankments with overburden pressure less than 200 kPa and constructed using RAS:BA/FS mixtures can be based on compressibility parameters in the recompression range. Therefore, addition of BA and FS to RAS reduces the compressibility of the mixture from moderately compressible to slightly and very slightly compressible for  $\sigma'_v$  in the recompression range according to classification criteria (Table 2).

Figs. 8 and 9 and Table 2 can be used as design tools to determine the required BA and FS content in the RAS:BA/FS mixtures given a  $\sigma'_v$  and a desired compressibility. For example if a *very slightly compressible* mixture of RAS:BA is desired for an embankment with  $\sigma'_v$  of 200 kPa, the designer selects a  $C_{re}$  between 0 and 0.05, say 0.03, from Table 2. Assuming that  $\sigma'_v$  is in the recompression range, from Fig. 9 the corresponding BA content is 50 %. From Fig. 8, the  $\sigma'_p$  corresponding to the BA content of 50 % is 300 kPa which is higher than the given  $\sigma'_v$  of 200 kPa.

Fig. 10 shows the variation of  $\epsilon_v$  with time for different RAS:BA/FS mixtures under  $\sigma'_v$  of 100 kPa. The time at which excess pore water pressure,  $\Delta u$  as measured, is dissipated marks the end of primary consolidation,  $t_p$ . The generated  $\Delta u$  in RAS:BA/FS mixtures dissipates in less than 2 min. The end of primary consolidation marked on the compression curves on Fig. 10 indicates that negligible settlement occurs due to primary consolidation in RAS:BA/FS mixtures and the majority of settlement is due to secondary compression. The secondary compression is

characterized by modified secondary compression index which is defined as the slope of  $\varepsilon_v$  versus  $\log t$  curve,  $C_{\alpha\varepsilon} = C_{\alpha} / (1 + e_p) = \Delta\varepsilon_v / \Delta \log \sigma'_v$  where  $e_p$  is the void ratio at the end of primary consolidation. The secondary compression part of the compression curves shows that  $\varepsilon_v$  nonlinearly increases with time. The  $C_{\alpha\varepsilon}$  increases with time for both RAS:BA and RAS:FS mixtures. A similar compression behavior was observed by Fox et al. (1992) and Mesri et al. (1997) for Middleton peat. Long term consolidation test on pure RAS under  $\sigma'_v=100$  kPa ( $\sigma'_v / \sigma'_p=1.80$ ) shows that  $C_{\alpha\varepsilon}$  becomes constant after the standard LID of 24 h whereas in RAS:BA/FS mixtures with 50 % bottom ash/foundry slag under  $\sigma'_v=100$  kPa ( $\sigma'_v / \sigma'_p=0.33$ ), the  $C_{\alpha\varepsilon}$  increases with time after 24 h. All mechanisms of compression (including particle rearrangement through interparticle slip, rotation and particle damage; and particle deformation including bending and compression) that operate during primary compression continue into secondary compression (Robert and de Souza 1958; Lee and Farhoomand 1967; Lade et al. 1997; Mesri and Vardhanabhuti 2009). Flexible, plate-like RAS particles seem to reach a stable position after a rapid rearrangement under  $\sigma'_v / \sigma'_p=1.80$  thus the long term compression of the specimen might be only due to particle deformation as a result of compressibility of asphalt cement and cellulose felt constituents in RAS. Addition of BA or FS to RAS may increase particle rearrangement during secondary compression. In particular, crushability of foundry slag particles may help particle damage during secondary compression resulting in higher secondary compression index over time.

To compare long term compression of different RAS:BA/FS mixtures quantitatively,  $C_{\alpha\varepsilon}$  was calculated over one log cycle of time before LID of 24 hr. Fig. 11 shows the variation of  $C_{\alpha\varepsilon}$  with bottom ash/foundry slag content under different  $\sigma'_v$ . For a given  $\sigma'_v$  the secondary

compression of RAS:BA/FS mixtures decreases significantly as the bottom ash/foundry slag content increases. As illustrated in Fig. 11, for typical highway embankments with  $\sigma'_v$  less than 200 kPa, addition of 50 % bottom ash/foundry slag to RAS reduces  $C_{\alpha\epsilon}$  from 0.023 to 0.006.

Figure 12 shows the effect of secondary compression on  $\sigma'_p$  of pure RAS and a RAS:BA mixture. The LID under  $\sigma'_v=100$  kPa was extended to 150 days for pure RAS and the RAS:BA mixture with 50 % bottom ash during one-dimensional consolidation test. After the 150-day time period the consolidation test with standard LID=24 h continued until  $\sigma'_v=1600$  kPa. The long-term secondary compression increased  $\sigma'_p$  of pure RAS from 65 kPa to 250 kPa and of the RAS:BA mixture from 300 kPa to 400 kPa. The effect of secondary compression on  $\sigma'_p$  is more significant on pure RAS than the RAS:BA mixture. The  $C_{r\epsilon}$  of RAS decreases from 0.07 to 0.03 as a result of preconsolidation effect. Consequently, preloading is an alternative way to reduce compressibility of RAS.

### *Shear Strength*

Figs. 13 and 14 show respectively the stress-strain and volumetric behavior of RAS:BA and RAS:FS mixtures sheared in triaxial compression cells under CD condition at  $\sigma'_c$  of 140 kPa. The stress-strain and volumetric behavior of pure RAS resembles those of sandy soils in loose state. For BA or FS content up to 50%, the volumetric behavior of RAS:BA/FS mixture is contractive and the maximum deviator stress,  $\sigma'_{d\max}$ , remains almost unchanged. Increase in BA or FS content beyond 50 % increases  $\sigma'_{d\max}$  and the volumetric behavior changes to dilative. Deviator stress at failure,  $\sigma'_{df}$ , was selected as the  $\sigma'_{d\max}$  or the  $\sigma'_d$  corresponding to 10% axial strain whichever is reached earlier. Pure RAS exhibited an apparent cohesion of 7 kPa in Mohr-

Coulomb failure envelop due to a slight binding of RAS particles during compaction. This apparent cohesion is neglected for practical purposes. Fig. 15 (a) shows the variation of effective friction angle,  $\phi'$ , of RAS:BA mixtures with BA content and Fig. 15 (b) shows the variation of  $\phi'$  of RAS:FS mixtures with FS content for different  $\sigma'_c$ . Similar to  $\sigma'_{d\max}$ , the  $\phi'$  remains almost unchanged with bottom ash/foundry slag content up to 50 % after which the  $\phi'$  increases. The range of  $\phi'$  for RAS:BA mixtures is between  $37^\circ$  and  $53^\circ$  and for RAS:FS mixtures is between  $37^\circ$  and  $56^\circ$  which are higher than the  $\phi'$  range ( $31^\circ$  to  $45^\circ$ ) for typical compacted sandy soils (US Navy 1986). Therefore, the shear strength of RAS:BA/FS mixtures are sufficient for use as structural fill material for construction of highway embankments.

### *Coefficient of Lateral Earth Pressure and Poisson's Ratio*

Fig. 16 shows the results of  $K_0$ -Consolidation tests. The  $K_0$  of pure RAS nonlinearly decreases with  $\sigma'_v$  from about 1.0 for  $\sigma'_v$  less than 100 kPa to 0.36 for  $\sigma'_v$  higher than 500 kPa. Correspondingly, Poisson's ratio decreases from 0.5 to 0.26. On the other hand, BA has almost a constant  $K_0$  of 0.25 and Poisson's ratio of 0.2 and FS has  $K_0$  of 0.30 and Poisson's ratio of 0.25 at different  $\sigma'_v$ . Mesri and Hayat (1993) concluded that stronger interlock and friction between particles reduce  $K_0$  while disengagement of particle interlocks due to particle damage increases  $K_0$ . Once the particle framework restructures at higher stress level,  $K_0$  starts to decrease. Under small to moderate  $\sigma'_v$ , the compressibility of RAS particles seems to help disengage the interlocks and reorient the particles. Therefore, pure RAS seems to pose lateral earth pressure almost equivalent to its overburden pressure behind retaining walls. Similarly, a typical embankment constructed using pure RAS would face relatively large lateral deformation. At higher  $\sigma'_v$ , densification as well as apparent cohesion between RAS particles due to asphalt

cement content seem to help particle interlock and engagement which consequently reduces  $K_o$ . As illustrated in Fig. 16, addition of 50 % BA or FS to RAS significantly reduces  $K_o$  and Poisson's ratio of the RAS:BA/FS mixture close to those of bottom ash and foundry slag.

## Conclusions

In this study, recycled asphalt shingles (RAS) were evaluated for potential use as structural fill in highway embankments or backfills behind retaining walls. Because of high compressibility of RAS, two byproducts, i.e., bottom ash (BA) and foundry slag (FS), were selected as granular additives to improve the mechanical properties of RAS and render it as an acceptable fill material. The following specific observations are made based on the test results:

1. RAS:BA/FS mixtures have lower  $\gamma_{dmax}$  than typical compacted soils. Low dry unit weight of RAS:BA/FS mixtures make them favorable alternatives to natural compacted soils for construction of structural fill over soft soils.
2. RAS:BA/FS mixtures have good drainage capacity as structural fills. The hydraulic conductivity of the mixture slightly decreases with increasing confining pressure due to high compressibility of RAS particles. The hydraulic conductivity of the mixture increases with increase in bottom ash/foundry slag content and becomes almost insensitive to confining pressure when the bottom ash/foundry slag content of the mixture increases to more than 50 %.
3. The short-term and long-term compressibility of pure RAS are significantly higher than those of compacted sandy soils. The high compressibility is due to asphalt cement and cellulose felt contents in RAS. Systematic addition of bottom ash/foundry slag to RAS

reduces compressibility of the mixture. At small to moderate stress levels typical in highway embankments, addition of more than 50 % by weight bottom ash/foundry slag to RAS greatly reduces the short-term and the long-term compression and categorizes the RAS:BA/FS mixtures as slightly to very slightly compressible material.

4. Stress-strain and volumetric behavior of pure RAS is similar to those of loose sandy soils. Addition of bottom ash/foundry slag up to 50 % to RAS does not have any noticeable effect on volumetric behavior and shear strength; however, the volumetric behavior tends to be dilative and shear strength starts to increase when the bottom ash/foundry slag content of the RAS:BA/FS mixture increases to more than 50 %. Shear strength of different RAS:BA/FS mixtures are similar to those of compacted sandy soils and is sufficient for construction of structural fills.
5. Coefficient of lateral earth pressure of RAS:BA/FS mixtures is comparable to those of compacted sand. Good drainage capacity and lower dry unit weight of RAS:BA/FS mixtures make them favorable alternatives to sand and gravel in terms of lower lateral earth pressures behind retaining structures.

Based on the results of this research, RAS:BA/FS mixture is a viable material for use as structural fill. Such an application will provide a large-volume beneficial use for RAS, which is largely disposed in landfills. Asphalt cement content in RAS may make the RAS:BA/FS mixture sensitive to temperature change and warrant further research.

## **Acknowledgement**

Support for this study was provided by the Recycled Materials Resource Center, which is supported by the Federal Highway Administration. The opinions, findings, conclusions, or recommendations expressed herein are those of the author(s) and do not necessarily represent the views of the sponsors.

## References

- Ahmed, I. (1993). *Use of Waste Material in Highway Construction*. Noyes Data Corporation, Park Ridge, NJ.
- American Coal Ash Association (2009). Coal Combustion Product (CCP) Production & Use Survey Results. ACAA, Aurora, CO. September 15, 2009 [online].
- American Society for Testing and Materials (ASTM). (1963). "Standard test method for particle-size analysis of soils." *Designation D422-63*, PA.
- American Society for Testing and Materials (ASTM). (2000). "Standard test methods for specific gravity of soil solids by water pycnometer." *Designation D854-00*, PA.
- American Society for Testing and Materials (ASTM). (2000). "Standard test methods for laboratory compaction characteristics of soil using standard effort [[f12,400 ft lbf/ ft<sup>3</sup> (600 kN m/m<sup>3</sup>)]." *Designation D698-00a*, PA.
- American Society for Testing and Materials (ASTM). (1995). "Standard test methods for measurement of hydraulic conductivity of saturated porous materials using a flexible wall permeameter." *Designation D5084-03*, PA.
- American Society for Testing and Materials (ASTM). (1996). "Standard test method for one-dimensional consolidation properties of soils." *Designation D2435-96*, PA.
- Bareither, C., Edil, T., Benson, C., and Mickelson, D. (2008). "Geological and Physical Factors Affecting the Friction Angle of Compacted Sands." *Journal of Geotechnical and Geoenvironmental Engineering*, Vol. 134, No. 10, pp. 1476-1489.
- Benson, C., Edil, T., and Soleimanbeigi, A. (2010). "Use of recycled asphalt shingles in highway embankments" *Proceeding of 2010 Mid-Continent Transportation Research Forum*, August 19-21, Madison, WI.

- Button, J. W., Williams D., and Scherocman, J.A. (1995). “Roofing Shingles and Toner in Asphalt Pavements”, Research Report 1344-2F, Texas Transportation Institute, College Station, Texas.
- Casagrande, A. (1936a). “The determination of the pre-consolidation load and its practical significance.” Discussion D-34, *Proc. First Int. Conf. Soil Mech. Found. Engr.*, Cambridge, Vol. 3, pp. 60-64.
- Chuhan, F. A., Kjeldstad, A., Bjorlykke, K., and Hoeg, K. (2003). “Experimental compression of loose sands: relevance to porosity reduction during burial in sedimentary basins.” *Canadian Geotechnical Journal*, Vol. 40, No. 5, pp. 995–1011.
- Coduto, D. P. (1998). *Geotechnical Engineering Principles and Practices*. Prentice Hall.
- Edil, T., Benson, C., Bin-Shafique, M., Tanyu, B., Kim, W., and Senol, A. (2002). “Field evaluation of construction alternatives for roadway over soft subgrade,” *Transportation Research Record*, 1786, Transportation Research Board, National Research Council, Washington, DC, pp. 36-48.
- Edil, T. B., and Wang, X. (2000). “Shear strength and  $K_o$  of peats and organic soils”, *Geotechnics of High Water Content Materials, ASTM Special Technical Publication*, pp. 209-225.
- Emery, J. J. (1985). “Slag utilization in pavement construction.” *Extending Aggregate Resources*, ASTM STP No. 774, ASTM, pp. 95-118.
- Fox, P. J., Edil, T. B. and Lan, L. T. (1992). “ $C_u/C_c$  concept applied to compression of peat,” *Journal of Geotechnical Engineering*, ASCE, Vol. 118, No. 8, pp. 1256-1263.
- Grodinsky, C., Plunkett, N., and Surwilo, J. (2002). “Performance of Recycled Asphalt Shingles for Road Applications.”, *Final Report*, State of Vermont’s Agency of Natural Resources.
- Huang, H. W. (1990). “The use of bottom ash in highway embankments, subgrade, and subbases.” Joint Highway Research Project, Final Report, FHWA/IN/JHRP-90/4, Purdue University, West Lafayette, Indiana.
- Karim, A., Lovell, C., Salgado, R. (1997). *Building Embankments of Fly/Bottom Ash Mixtures*, FHWA/IN/JTRP-97/01, SPR-2115, Joint Transportation Research Program, Purdue University.
- Kim, B. (2003). *Properties of Coal Ash Mixtures and their Use in Highway Embankments*. PhD Thesis, Purdue University, Indiana, USA.

- Kim, B., Prezzi, M. and Salgado, R. (2005). "Geotechnical Properties of Fly and Bottom Ash Mixtures for Use in Highway Embankments." *Journal of Geotechnical and Geoenvironmental Engineering*, ASCE, Vol. 131, No. 7, pp. 914-924.
- Krivit, D. (2007). Recycling of Tear-Off Shingles: Best Practices Guide. Final report prepared for the Construction Materials Recycling Association (CMRA).
- Hooper, F., and Marr, W. (2004). "Effects of Reclaimed Asphalt Shingles on Engineering Properties of Soils," *Recycled Materials in Geotechnics, Geotechnical Special Publication*, No. 127, ASCE, pp. 137-149.
- Lade, P. V., Yamamuro, J. A., and Bopp, P. A. (1997). "Influence of time effects on instability of granular materials." *Computers and Geotechnics*, Vol. 20, pp. 179–193.
- Lee, K. L., and Farhoomand, I. (1967). "Compressibility and crushing of granular soil in anisotropic triaxial compression." *Canadian Geotechnical Journal*, Vol. 4, No. 1, pp. 68–99.
- Li, L., Benson, C. H., Edil, T. B., and Hatipoglu, B. (2008). "Sustainable Construction Case History: Fly Ash Stabilization of Recycled Asphalt Pavement Material." *Geotechnical and Geological Engineering*, Vol. 26, No. 2, pp. 177-188.
- Marks, V. J., and Petermeier, G. (1997). "Let Me Shingle Your Roadway", *Research Project HR-2079, Iowa Department of Transportation*, Ames, Iowa
- Marsal, R. J. (1967). "Large scale testing of rockfill materials." *Journal of the Soil Mechanics and Foundations Division, ASCE*, 93, pp. 27–43.
- Mesri, G., and Hayat, T. M. (1993). "The coefficient of earth pressure at rest." *Canadian Geotechnical Journal*, Vol. 30, No. 4, pp. 647–666.
- Mesri, G., Stark, T. D., Ajlouni, M. A., and Chen, C. S. (1997). "Secondary compression of peat with or without surcharging." *Journal of Geotechnical and Geoenvironmental Engineering, ASCE*, Vol. 123, No. 5, pp. 411–421.
- Mesri, G., and Vardhanabhuti, B. (2009). "Compression of granular materials", *Canadian Geotechnical Journal*, Vol. 46, pp. 369-392.
- Moulton, L. K., Seals, R. K., and Anderson, D. A. (1973). "Utilization of ash from coal burning power plants in highway construction." *Transportation Research Record*, Vol. 430, pp. 26-39.
- Pestana, J. M., and Whittle, A. J. (1995). "Compression model for cohesionless soils." *Géotechnique*, 45, pp. 611–631.

- Recycled Materials Resource Center (2010). *User Guidelines for By-products and Secondary Use Materials in Pavement Construction*, <http://www.rmrc.unh.edu/tools/uguidelines/index.asp>, Accessed December 2010.
- Recycling Connections Corporation (2010). *Wisconsin Statewide Waste Characterization Study*. Prepared for Wisconsin Department of Natural Resources.
- Roberts, J. E., and de Souza, J. M. (1958). "The compressibility of sands." *Proc., American Society for Testing and Materials*, 58, pp. 1269-1277.
- Roberts, F. L., Kandhal, P. S., Brown, E. R., Lee, D. Y. and Kennedy, T. W. (1996). *Hot Mix Asphalt Materials, Mixture Design, and Construction*. National Asphalt Paving Association Education Foundation. Lanham, MD.
- Seals, R. K., Moulton, L. K., and Ruth, B. E. (1972). "Bottom ash: An engineering material." *Journal of Soil Mechanics and Foundation Division*, Vol. 98, No. 4, pp. 311–325.
- Tanyu, B.F., Benson, C.H., Edil, T.B., and Kim, W.H. (2005), "Equivalency of crushed rock and three industrial by-products used as a working platform during pavement construction," *Transportation Research Record*, 1874, Transportation Research Board, National Research Council, Washington, DC, pp. 59-69.
- Townsend, T., Powell, J., and Xu, C. (2007). Environmental issues associated with asphalt shingle recycling. *Construction Materials Recycling Association, US EPA Innovations Workgroup*.
- Turley, W. (2010). Personal Communication. *Construction Materials Recycling Association*, Eola, IL.
- U.S. Bureau of Reclamation. (1987). *Design of Small Dams*. U.S. Department of the Interior, Bureau of Reclamation.
- U.S. Geological Survey. (2008). *Minerals Yearbook*. USGS, [http://minerals.usgs.gov/minerals/pubs/commodity/iron\\_&\\_steel\\_slag/myb1-2008-fesla.pdf](http://minerals.usgs.gov/minerals/pubs/commodity/iron_&_steel_slag/myb1-2008-fesla.pdf), Accessed December 2010.
- U.S. Navy. (1986). "Design manual—Soil mechanics, foundations, and earth structures." *NAVFAC DM-7*, Department of the Navy, Washington, D.C.
- Viyanant, C., Rathje, E. M., and Rauch, A. F. (2007). "Creep response of recycled asphalt pavement." *Canadian Geotechnical Journal*, Vol. 44, pp. 687-697.
- Warner, J. D. (2007). "The beneficial reuse of asphalt shingles in roadway construction", *MSc thesis, Department of Civil and Environmental Engineering, University of Wisconsin-Madison*.

- Wen, H., and Edil, T. B. (2007). "Laboratory Study of Recycled Asphalt Pavement Materials as BaseCourse." *Proc. of 5<sup>th</sup> International Conference on Maintenance and Rehabilitation of Pavements and Technological Control*, Park City, UT, pp. 457-462.
- Yoon, S., Balunaini, U., Yildirim, I. Z., Prezzi, M. and Siddiki, N. Z. (2009). "Construction of an embankment with a fly and bottom ash mixture: Field performance study." *Journal of Material in Civil Engineering, ASCE*, Vol. 21, No. 6, pp. 271-278.

Table 1-Grain size indices and USCS classifications of RAS, bottom ash and outwash sand

Material	d <sub>10</sub> (mm)	d <sub>50</sub> (mm)	C <sub>u</sub>	C <sub>c</sub>	% fines	G <sub>s</sub>	USCS symbol	USCS name
RAS	0.17	1.1	7.6	1.6	3.8	1.74	SW	Well graded sand
Bottom ash	0.19	0.9	6.3	0.8	1.9	2.67	SP	Poorly graded sand
Foundry slag	0.18	1.6	11.4	2.7	4.8	2.36	SW	Well graded sand
Glacial outwash sand <sup>a</sup>	0.21	0.5	3.1	0.8	0.0	2.71	SP	Poorly graded sand

<sup>a</sup> Data were taken from Bareither et al. (2008)

Table 2-Classification for material compressibility (after Coduto 1998)

<b>(C<sub>c</sub> or C<sub>r</sub>)/(1+e<sub>0</sub>)</b>	<b>Classification for compressibility</b>
0-0.05	Very Slightly compressible
0.05-0.10	Slightly compressible
0.10-0.20	Moderately compressible
0.20-0.35	Highly compressible
> 0.35	Very Highly compressible

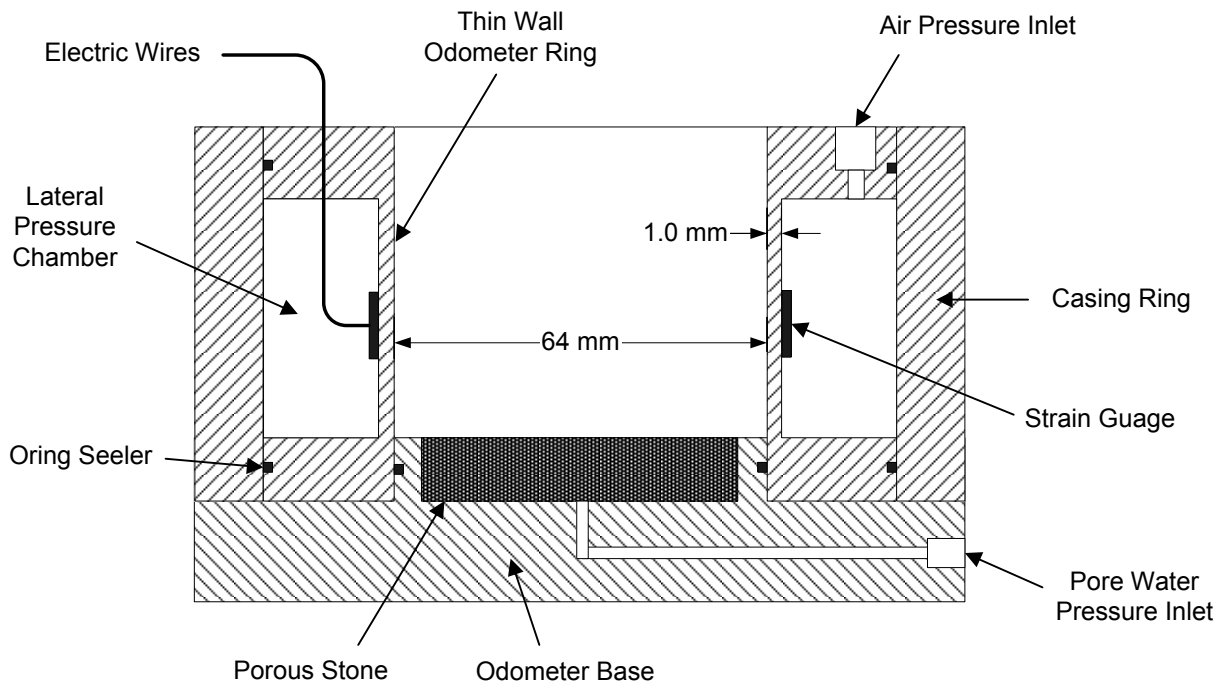


FIG. 1- $K_0$ -Consolidation cell (after Edil and Wang 2000)

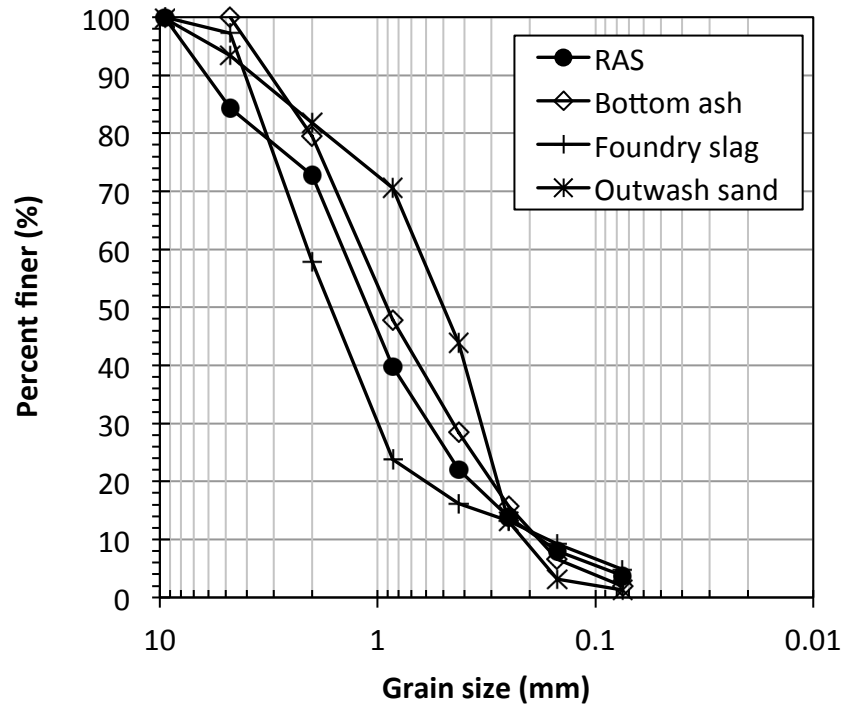
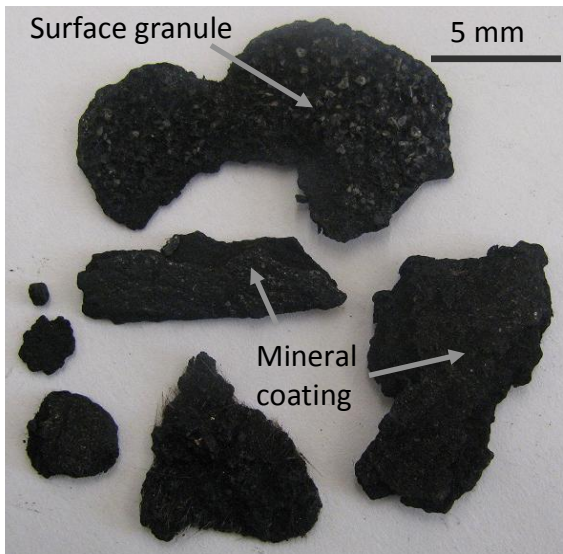


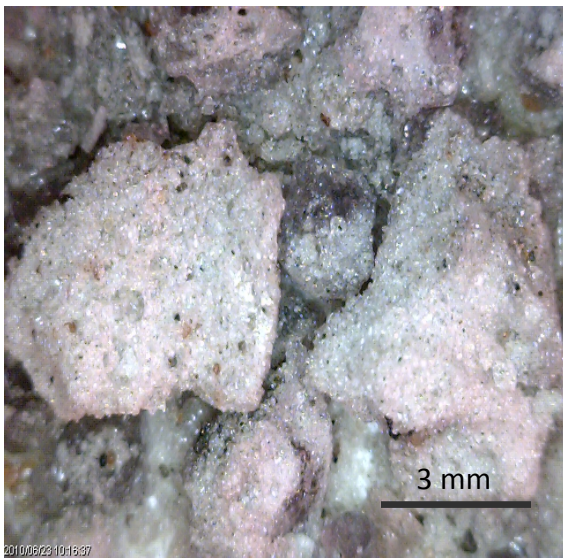
FIG. 2-Grain size distribution of RAS, bottom ash, foundry slag and glacial outwash sand



(a)



(b)



(c)



(d)

FIG. 3-(a) Photographs of RAS, (b) LM photomicrographs of bottom ash, (c) foundry slag, and (d) glacial outwash sand particles

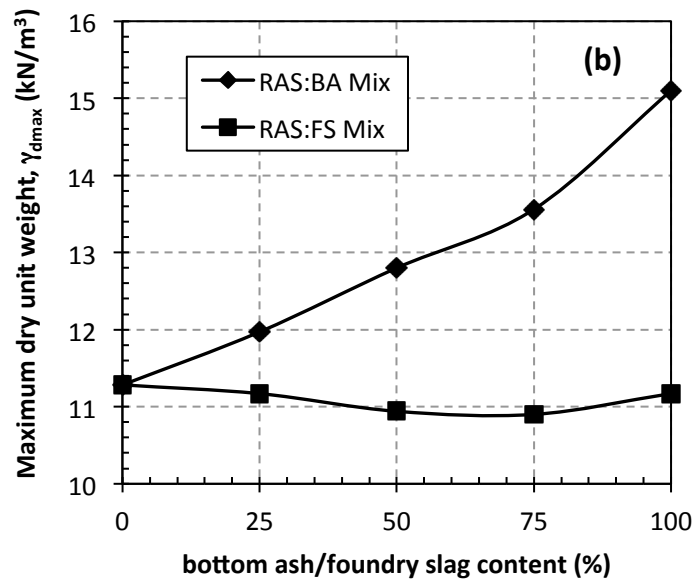
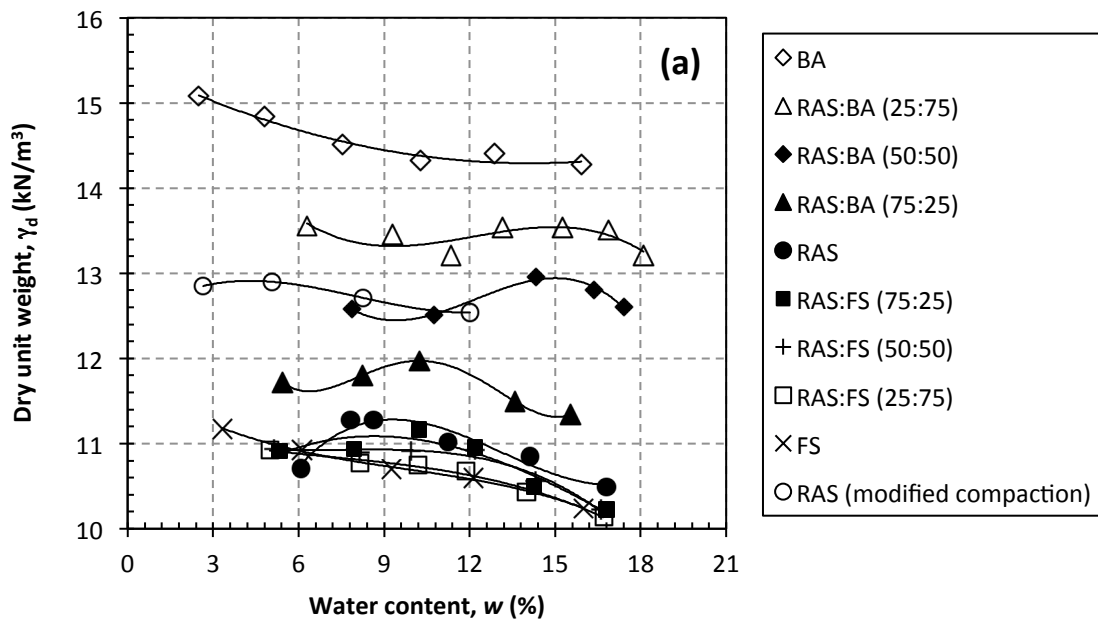


FIG. 4- (a) Standard Proctor dry unit weight versus water content of RAS:BA/FS mixtures (b) maximum dry unit weight of RAS:BA/FS mixture versus bottom ash/foundry slag content

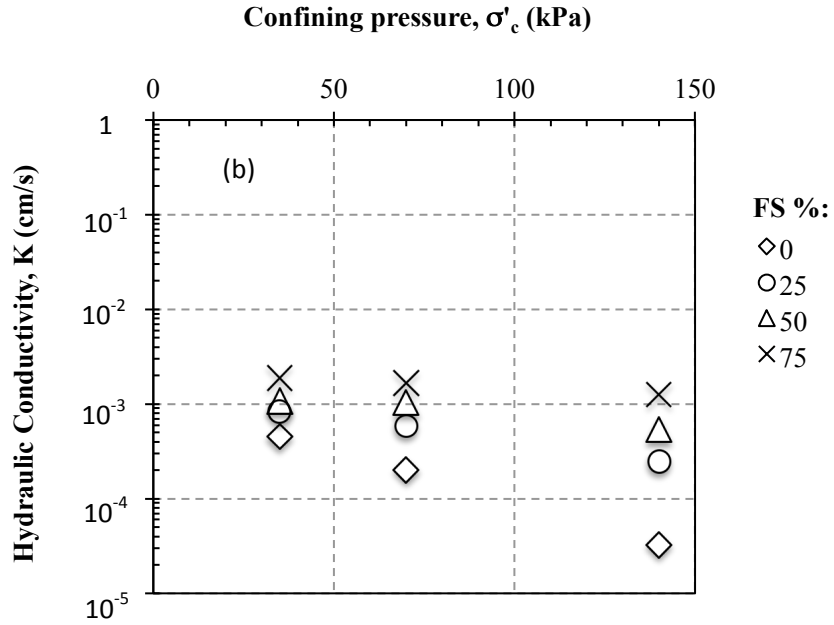
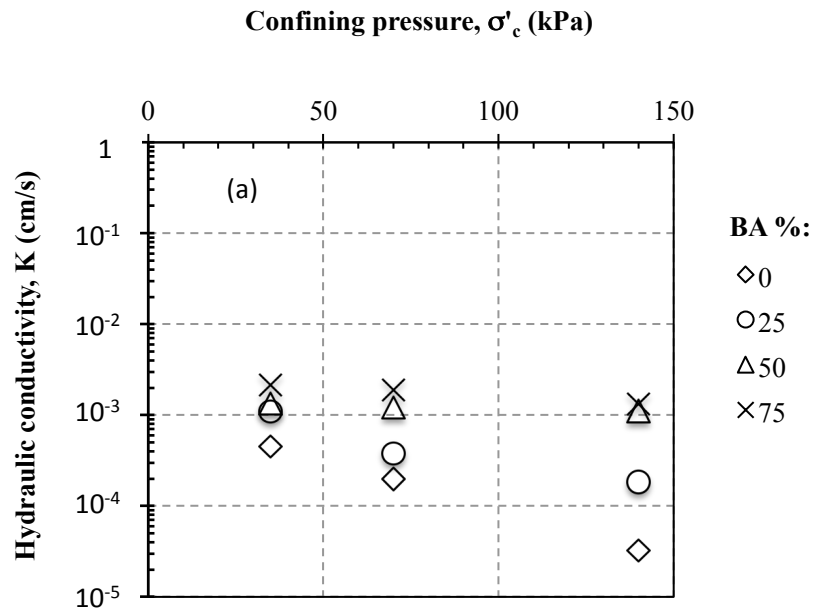


FIG. 5-Hydraulic conductivity of (a) RAS:BA mixtures and (b) RAS:FS mixtures versus effective confining pressure

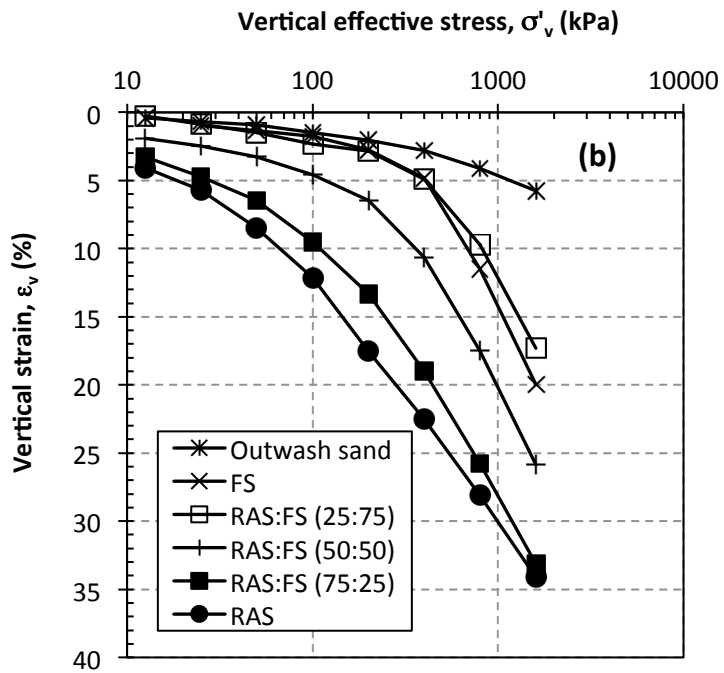
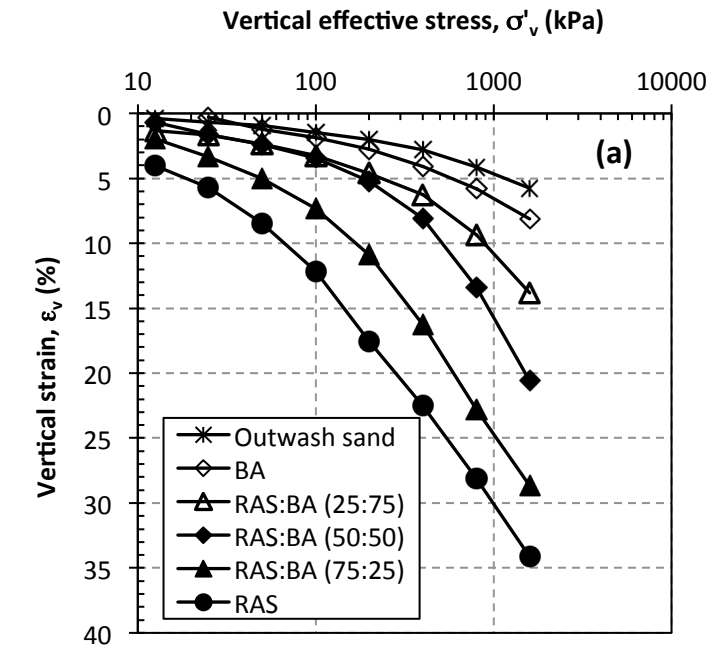


FIG. 6- One-dimensional compression curves of (a) RAS:BA mixtures and (b) RAS:FS mixtures

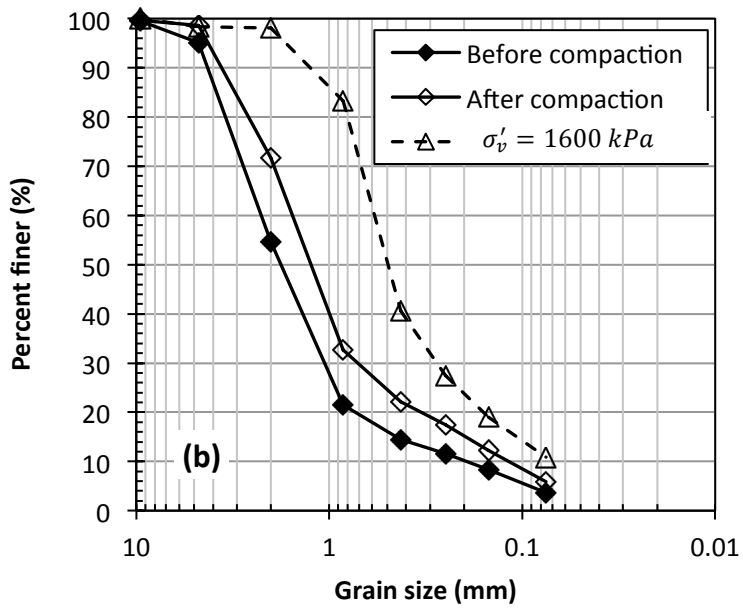
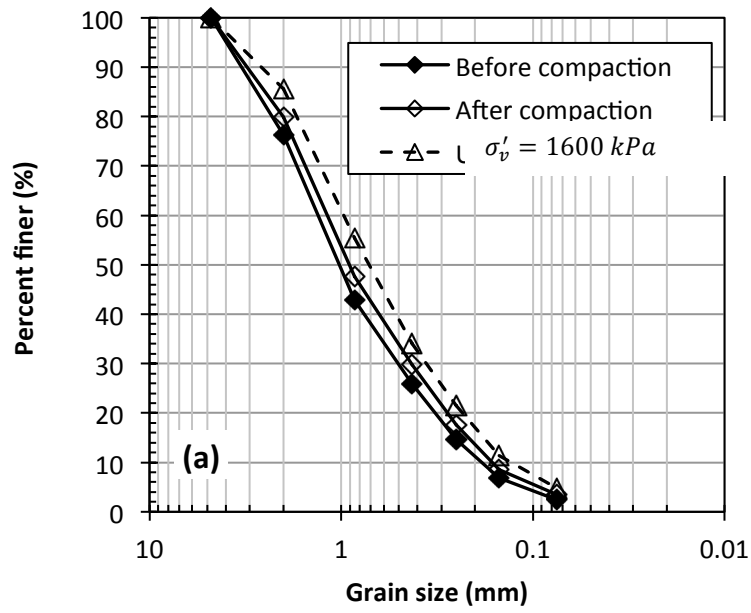


FIG. 7- Material degradation after compaction and compression tests (a) bottom ash and (b) foundry slag

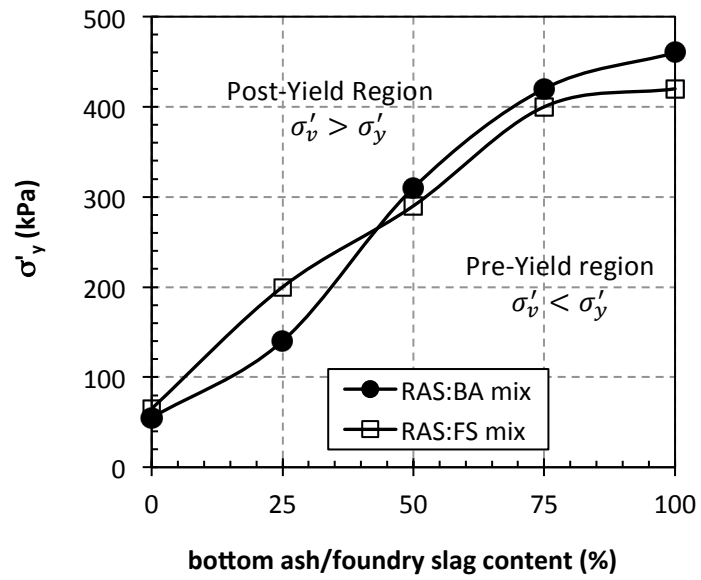


FIG. 8- Variation of yield pressure of RAS:BA/FS mixture with bottom ash/foundry slag contents

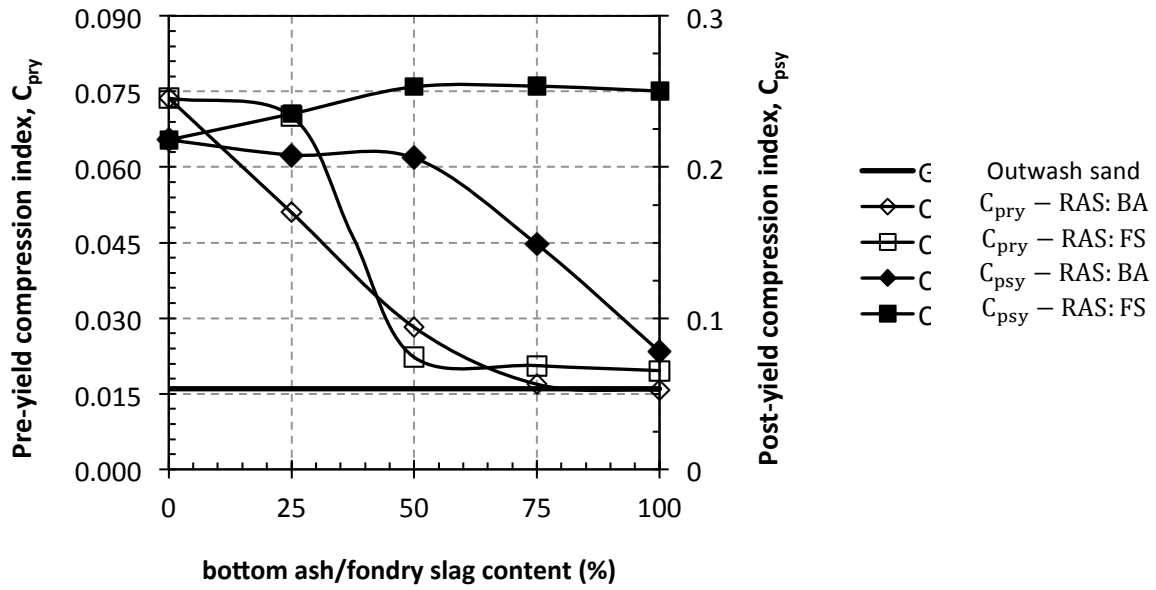


FIG. 9-Variation of post-yield and pre-yield compression indices of RAS:BA/FS mixtures with bottom ash/fondry slag content

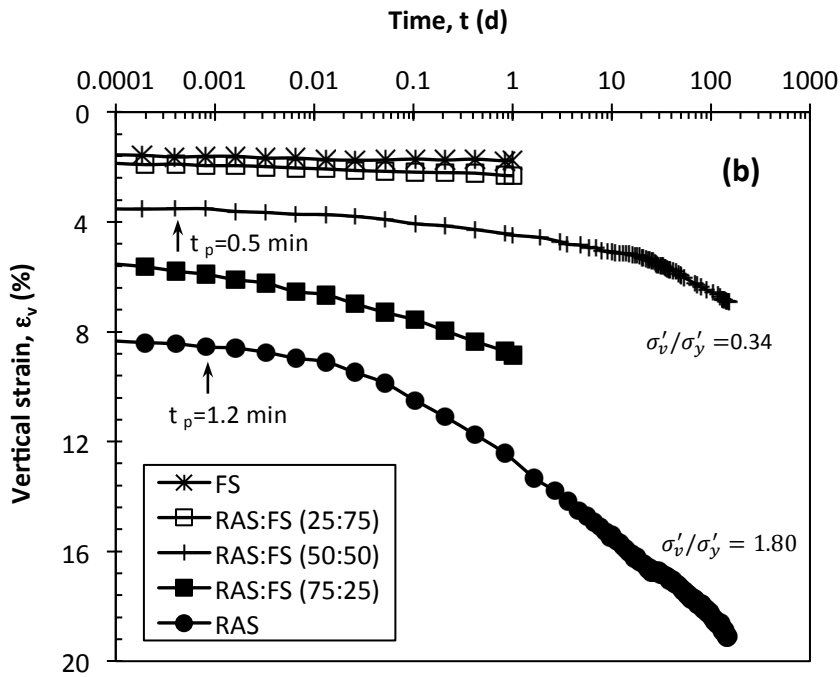
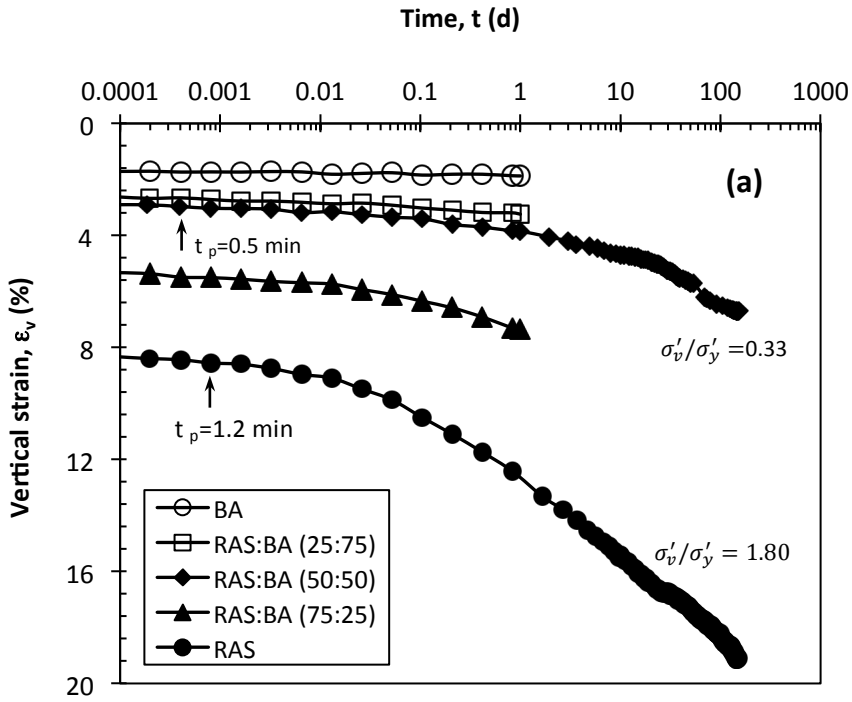


FIG. 10-Variation of  $\epsilon_v$  with time for (a) RAS:BA mixtures and (b) RAS:FS mixtures

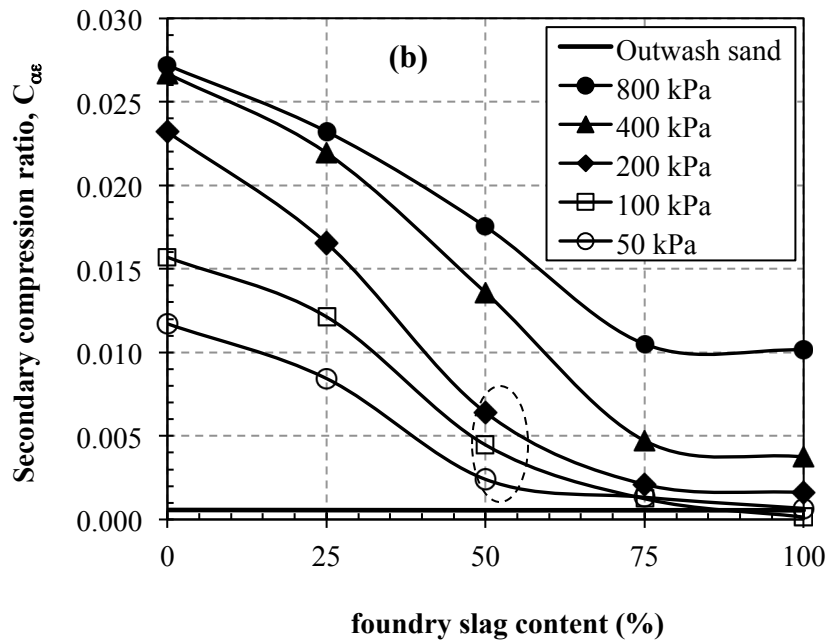
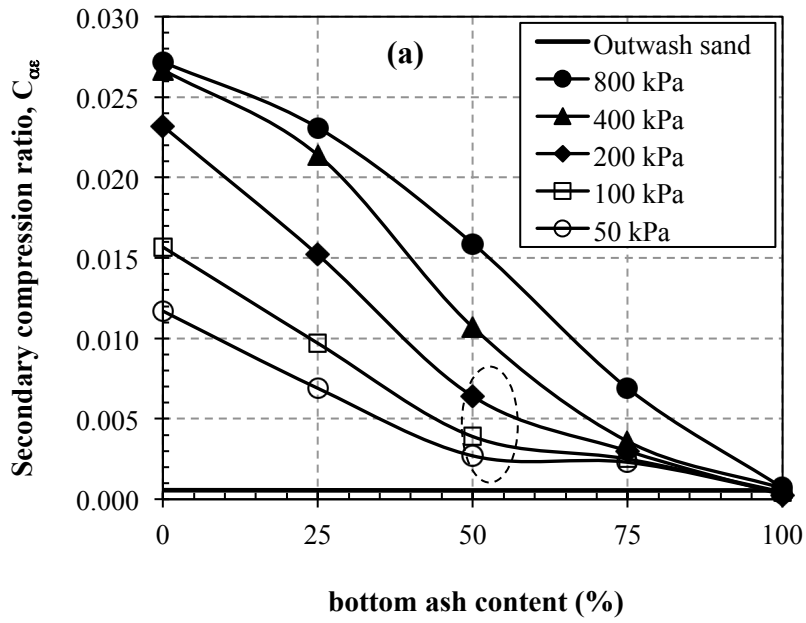


FIG. 11-Variation of secondary compression of (a) RAS:BA mixtures with BA content and (b) RAS:FS mixtures with FS content.

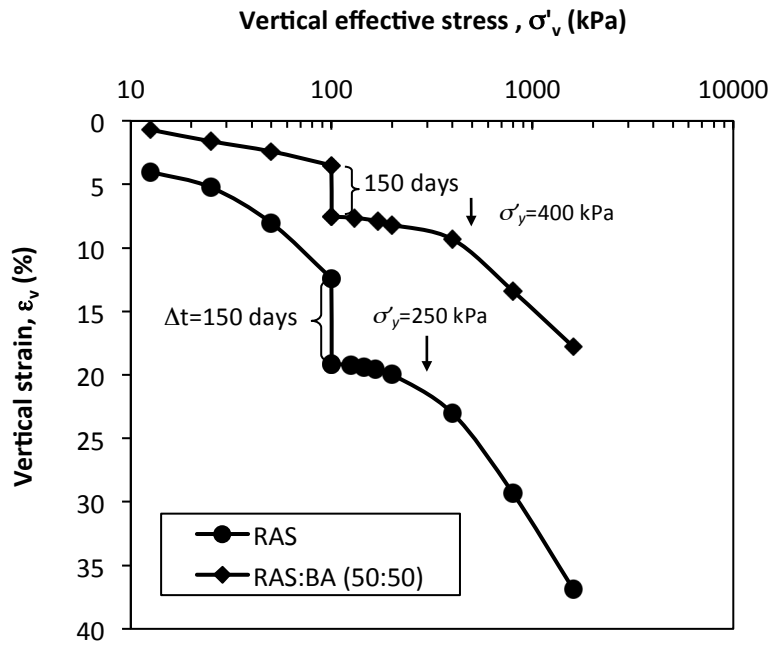


FIG. 12-Preconsolidation pressure of RAS:BA mixture resulting from secondary compression

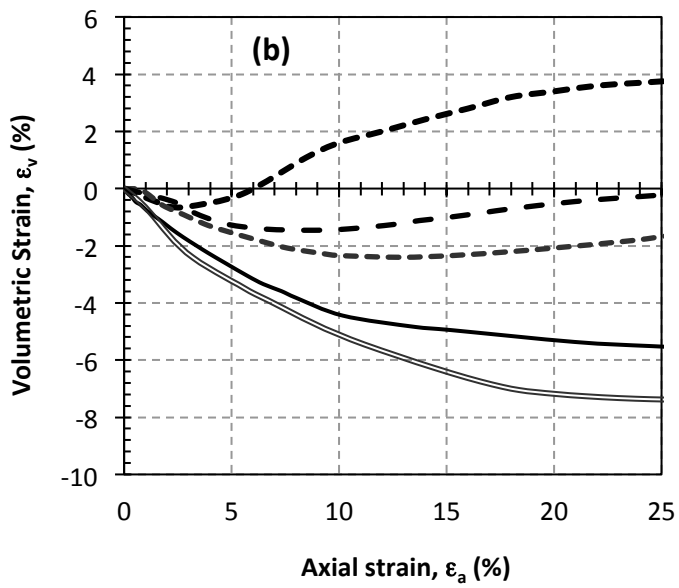
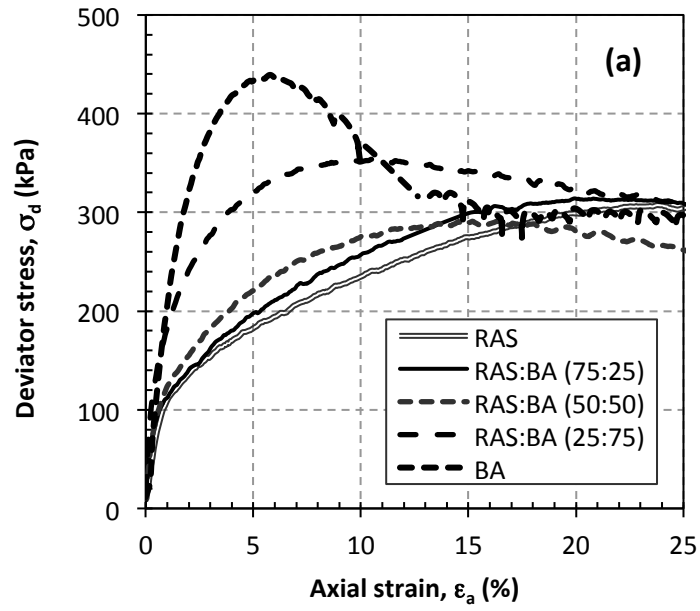


FIG. 13-Results of CD triaxial tests: (a) stress-strain behavior of RAS:BA mixtures; (b) volumetric change behavior of RAS:BA mixtures

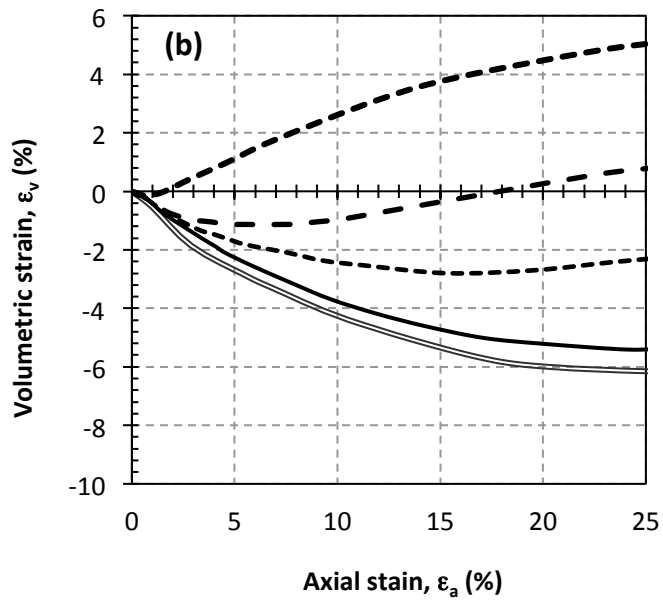
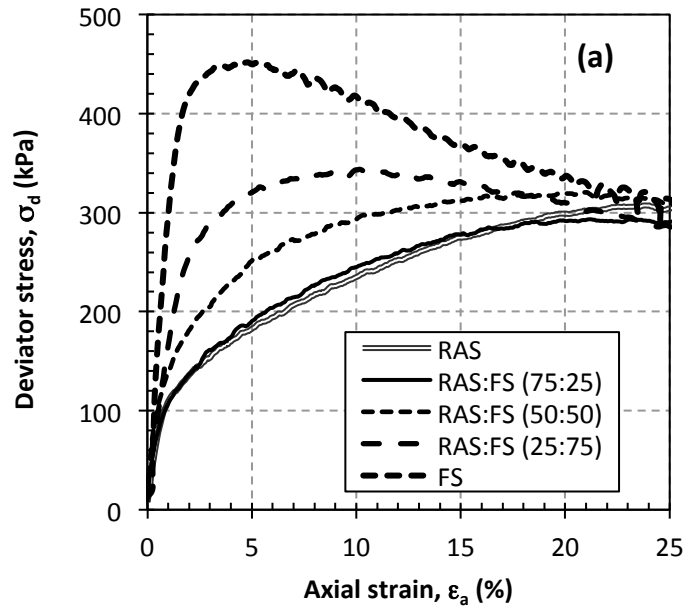


FIG. 14-Results of CD triaxial tests: (a) stress-strain behavior of RAS:FS mixtures; and (b) volumetric change behavior of RAS:FS mixtures

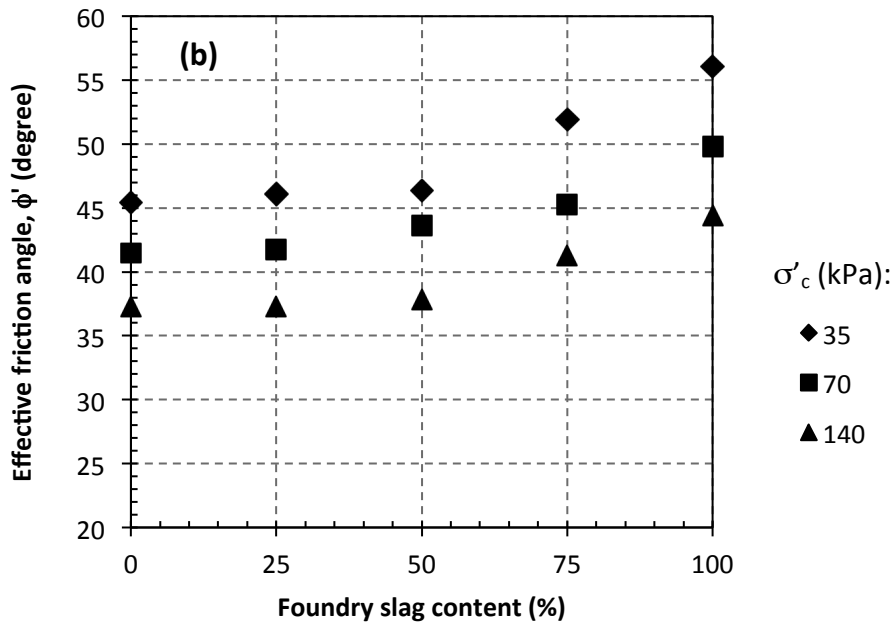
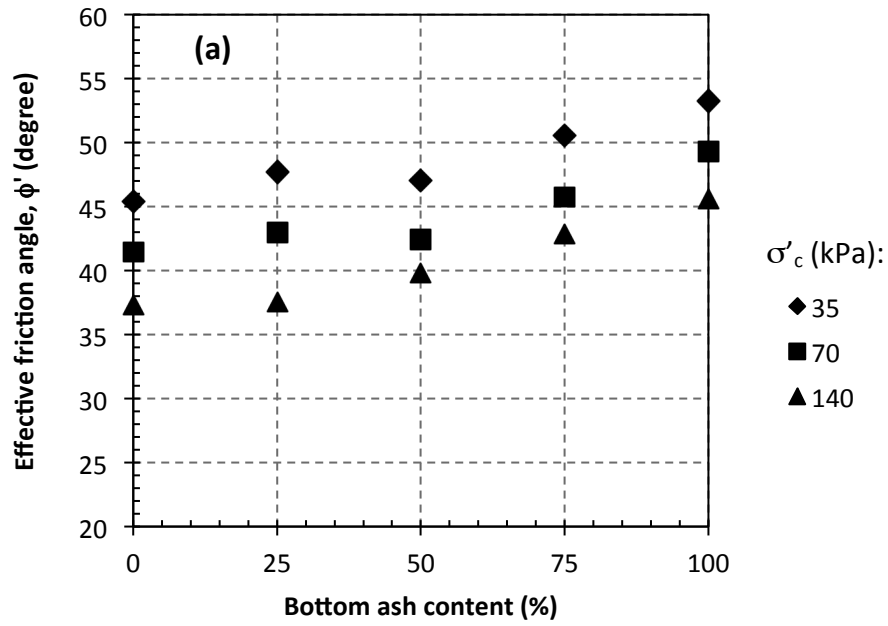


FIG. 15-Variation of friction angle of (a) RAS:BA mixtures with BA content and (b) RAS:FS mixtures with FS content at different confining stresses

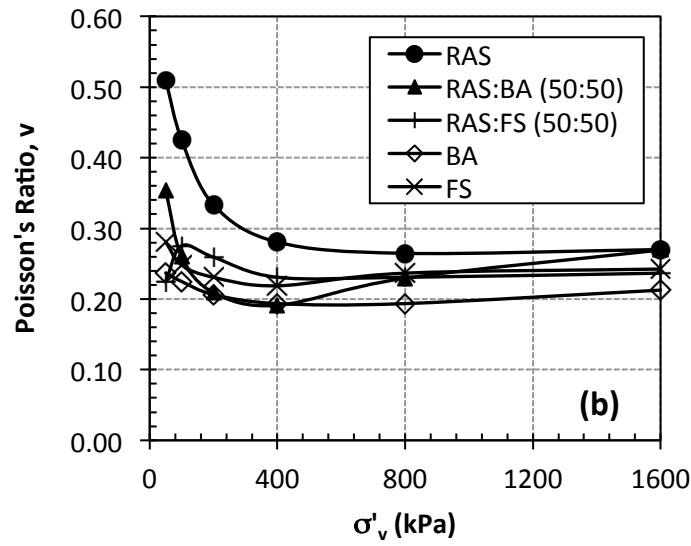
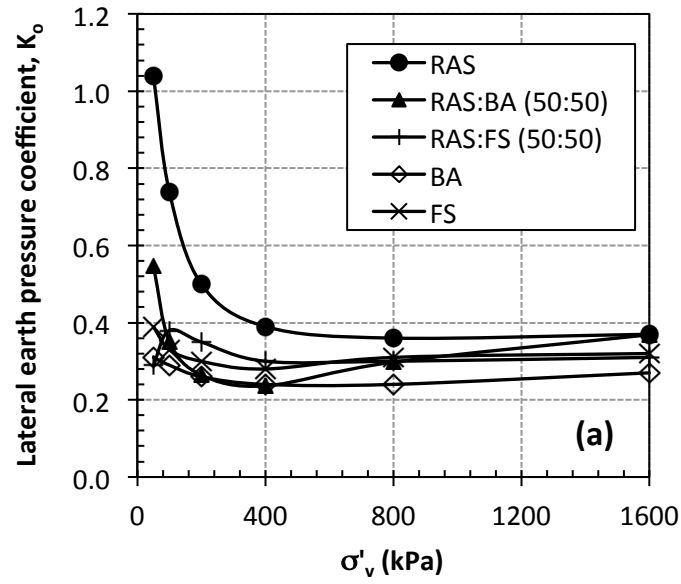


FIG. 16-Variation of  $K_0$  (a) and Poisson's ratio (b) of RAS:BA/FS mixtures with overburden pressure

## Chapter 3

# Evaluation of Fly Ash Stabilization of Recycled Asphalt Shingles for Use in Structural Fills

**Abstract:** The majority of tear-off roofing shingles and manufacturing shingle scraps are currently disposed as solid waste in landfills. Landfills are also the end place for the majority of coal combustion byproducts like fly ash. In this study, geotechnical properties of recycled asphalt shingles (RAS) stabilized with a self-cementing fly ash for use as structural fill material were systematically evaluated. Compaction, hydraulic conductivity, compressibility, shear strength and coefficient of lateral earth pressure at rest of stabilized RAS were evaluated. Results show that stabilized RAS has potential as a lightweight material for use as highway embankment fill or retaining wall backfill.

**KEYWORDS:** Recycled asphalt shingle, fly ash, structural fill, engineering properties.

### Introduction

Using industrial solid waste in construction contributes to savings in energy consumed in production of virgin aggregates and reduction in greenhouse gas emissions, consequently resulting in more sustainable construction (Edil 2006, Lee et al. 2010). Nearly 80% of structures in the U.S. are covered by asphalt shingles. Asphalt shingle waste is produced by removing the asphalt shingles from the roofs of existing houses during renovation (called post-consumer

asphalt shingle or tear-off shingle) or rejecting asphalt shingles/shingle tabs discarded in the manufacturing process of new asphalt shingles (called manufactured shingle scrap). Approximately 11 million Mg of asphalt roofing shingle waste are generated in the U.S. per year (Krivit 2007). Re-roofing jobs account for 10 million Mg, with another 1 million Mg manufacturing scrap. Currently the majority of produced asphalt shingle waste in the U.S. is disposed in landfills (Zickell 2003, Townsend 2007). The majority of current reuse application of recycled asphalt shingles (RAS) consists of incorporation in hot mix asphalt (HMA) to benefit from the asphalt cement and sand contents of RAS. However, many DOT specifications limit the incorporation of RAS in HMA to 5% due to adverse effect of higher percentages of RAS on mechanical properties of HMA (Button et al. 1995, Grodinsky 2002, Krivit 2007). Other applications of RAS include as fuel and mineral supplement in cement kilns, as dust control in gravel roads, as compacted road base and subbase, and as cold patch on paved roads. Reuse of RAS in these applications is also limited due to unavailability of basic knowledge of properties and standard specifications. Consequently, current applications of RAS reuse consists of only 10 to 20% of the total produced asphalt shingle waste in the U.S. (Turley, 2011).

Another possible application that will potentially generate large-volume use of the asphalt shingle waste is its use as structural fill material in highway embankments and backfill behind retaining walls. For these applications, certain geotechnical properties are required and there is a dearth of such information. RAS is a highly compressible material (Soleimanbeigi et al. 2011), which limits its ability for use as a structural fill material. To control its excessive compressibility, stabilization of RAS with self-cementing fly ash, which is a widely available industrial byproduct, is considered. In this study, the geotechnical properties of RAS stabilized with self-cementing fly ash are evaluated for structural fill applications. The beneficial use of

self-cementing fly ash has been investigated by several researchers and several demonstration projects have been successfully constructed using self-cementing fly ash in conjunction with a variety of materials from natural soils to recycled asphalt pavements (Patelunas 1986; DiGioia 1986; McLaren and DiGioia 1987; Misra 2000; Srivastava and Collins 1989; Ferguson, 1989; Ferguson and Levorson, 1999; Edil et al. 2002; Bin-Shafique et al. 2004; Lin et al. 2008; ACAA 2008; Lin et al. 2009; Wen and Edil 2009; Wen et al. 2011). According to the American Coal Ash Association (ACAA 2009) survey about 63 million Mg fly ash (FA) was produced in 2009 of which only about 39% was reused in different applications like concrete production, structural fills, waste stabilization, road base/subbase and soil modification. The remaining fly ash is typically disposed in utility disposal sites. Reuse of RAS stabilized with self-cementing fly ash will potentially have beneficial contribution in saving landfill space and reducing energy consumption and green house gas emissions due to production of natural aggregates through the beneficial use of two under recycled industrial byproducts.

The objective of this research is to evaluate mechanical properties of RAS stabilized with self-cementing fly ash for use as structural fill in highway embankment fill and retaining wall backfill thus opening up an application for both waste materials. The compaction, hydraulic conductivity, compressibility, shear strength, and coefficient of earth pressure at rest of stabilized RAS have been evaluated in a systematic manner and improvements and suitability as a structural fill are assessed. The environmental implications are considered beyond the scope of this investigation; however, there are procedures available to implement such an assessment (Li et al. 2006; Kosson et al. 1996; Kosson et al. 2002; Komonweeraket et al. 2011).

## **Background**

A typical asphalt shingle is produced by impregnating a layer of organic or fiberglass mat with air-blown liquid asphalt. Once coated with appropriate thickness of asphalt, one side of the shingle is covered by granules to protect the shingle against physical damage and damage from ultraviolet rays of sun, and the other side is coated by fine sand or fly ash to prevent adhering of individual shingles to each other during packing and transport. The compositions of a typical, new residential asphalt shingle produced today include 32 to 42% coating filler, 28 to 42% granules, 16 to 25% asphalt content, 2 to 15% mat, and 0.2 to 2% adhesive (Grodinsky et al. 2002; Krivit 2007).

Only a few scientific investigations have been conducted on engineering properties and field performance of RAS in geotechnical applications. A qualitative study conducted by Iowa Department of Transportation showed that ground shingles mixed with crushed limestone as a surface treatment were effective for dust control in unpaved rural roads, resulted in better lateral control of vehicles, reduced the loss of granular onto the ditches, and resulted in a quieter and smoother roadway (Marks 1997). Vermont Agency of Natural Resources (Vermont ANR) reported that a mixture of RAS:RAP:Gravel with 10:30:60 ratio placed and compacted on a series of municipal roadways, resists rutting and erosion, mitigates dust and in general requires less maintenance than the conventional gravel control section (Grodinsky et al. 2002).

Laboratory investigations on geotechnical properties of RAS were first conducted to evaluate performance of RAS as base-course (Hooper and Marr 2004; Warner 2007). The maximum dry unit weight ( $\gamma_{dmax}$ ) of RAS from the standard Proctor compaction tests varied between 8.8 kN/m<sup>3</sup> and 12.3 kN/m<sup>3</sup>. The California bearing ratio (CBR) of RAS was 6%, which categorized RAS as only a suitable material for subgrade (Hooper and Marr 2004). The resilient modulus of RAS was only appropriate for base/subbase layers when mixing 50% by weight of

Grade 2 granular backfill (GP-GM) to RAS (Warner 2007). RAS mixed with granular material is however appropriate for use as structural fill in highway embankment or backfill behind retaining walls (Soleimanbeigi et al. 2012). The RAS content in the RAS:“Granular Material” mixture is selected based on the desired shear strength, compressibility and overburden pressure.

## **Materials**

Samples of RAS were taken from Stratford Building Supply Co. in Stratford, Wisconsin. The non-friable RAS samples were processed from tear-off roofing shingle waste to remove common impurities including nails, paper, plastic and wood chips. The percent impurities measured from the RAS sample was less than 0.3% by weight. Fig. 1 (a) shows the typical shape of RAS particles as well as sand cover and mineral coating on RAS particle surfaces. The particles are plate-like, irregular in shape, highly angular, and rough in surface texture due to granular surface particles. The angularity of RAS particles reduces to semi-round to round as the particle size is reduced.

To stabilize RAS, a sample of self-cementing fly ash was obtained from Columbia Power Plant near Portage, Wisconsin. The compositional properties of the fly ash include 6.0% loss on ignition (LOI), minimum 50% of  $\text{SiO}_2$ ,  $\text{Al}_2\text{O}_3$ , and  $\text{Fe}_2\text{O}_3$ , and minimum 75% of strength activity at 7 days. The specific gravity of class C fly ash is 2.70 (Edil et al. 2006). This fly ash is classified as Class C fly ash in accordance to ASTM C618. Although a class C fly ash is investigated, other self-cementing fly ashes that do not meet class C specification, thus not suitable for concrete production and class F fly ashes activated with lime or cement may also provide the necessary stabilization to RAS.

An alternative to fly ash stabilization is to add granular materials to RAS to reduce its compressibility. Since the majority of RAS particles are plate-like in shape, addition of granular materials to RAS is expected to result in better packing of the particles, producing a mixture with lower compressibility and higher shear strength. This approach without stabilization is presented by Soleimanbeigi et al. (2011). Here a mixture of RAS and a granular additive stabilized with fly ash is also considered. Bottom ash (BA) was selected as the granular industrial byproduct additive to RAS. Fig. 1 (b) shows a light microphotograph of BA particles. The particles are internally porous, angular and rough in surface texture. Some pores of the particles are filled with dust. To compare engineering properties of stabilized RAS with those of a natural granular structural fill, mechanical tests were also conducted on a sample of Wisconsin glacial outwash sand (GOS) as a reference material. The light microphotograph of outwash sand particles is shown in Fig. 1 (c). The particles of GOS are smooth in surface, semi-round to round and free of dust.

Fig. 2 shows the particle size distribution curves of RAS, BA and GOS samples tested according to ASTM D 422. The majority of particles in each sample are sand size (between 0.075 mm and 4.75 mm) according to the Unified Soil Classification System (USCS). Table 1 summarizes the grain size indices and material classification according to the USCS.

The specific gravity ( $G_s$ ) of RAS measured in accordance with ASTM D854 (method B) is 1.74, which is a positive attribute for use as a light-weight fill material. The low  $G_s$  of RAS is attributed to asphalt cement content and cellulose fiber content, which together comprise from 18 to 50% of RAS. The typical  $G_s$  of asphalt cement is between 1.02 and 1.05 (Roberts et al. 1996) and that of cellulose fiber is between 1.3 and 1.5 (Klyosov 2007). Bottom ash has a  $G_s$  of 2.67, which is comparable to  $G_s$  of GOS (2.71).

## **Methods**

The engineering properties of RAS and stabilized RAS with 10%, 20% and 50% Class C fly ash content were obtained following the standard guide for use of coal combustion by-products in structural fills (ASTM E 1861-97).

### *Compaction*

Standard Proctor compaction tests following ASTM D 698 (method B) were conducted on different RAS:FA mixtures. Typically, a 1-h delay time between wetting/mixing and compaction was specified to simulate construction delays (ACAA 2003). Delay time causes density and strength of the stabilized soil be reduced because a portion of the compactive energy must be used to overcome the bonding of the soil particles by cementation; therefore, a portion of the cementation potential is lost (ACAA 2003). RAS:FA mixtures with 10%, 20% and 50% self-sementing fly ash content were compacted 1 h after wetting. The compaction test was also conducted on a sample of RAS:BA:FA mixture with 40%:40%:20% ratio as a potential mixture.

### *Hydraulic Conductivity*

Hydraulic conductivity tests with flexible-wall permeameters were conducted on compacted RAS and stabilized RAS specimens following ASTM D 5084-03 test procedure to evaluate the effect of confining stress ( $\sigma'_c$ ) on hydraulic conductivity. Each moistened RAS:FA mixture was compacted to 95% of standard  $\gamma_{dmax}$  at optimum water content ( $w_{opt}$ ). The compacted mixture was cured at 25°C and 100% relative humidity for 7 days. The hydraulic conductivity tests were conducted immediately after 7-day curing period. Each sample mixture was consolidated to the

desired effective stress ( $\sigma'_c=35$  kPa, 70 kPa and 140 kPa) for 24 h after the end of primary consolidation. The time for the end of consolidation is established when no further volume change is observed in the backpressure burette during consolidation. After consolidation phase, the hydraulic conductivity was measured according to the falling head rising tail method.

### *One-dimensional Compression*

Settlement of an embankment with large lateral extension can be considered one-dimensional and estimated from the results of one-dimensional consolidation tests. To evaluate compressibility of RAS and stabilized RAS, one-dimensional compression tests were performed on compacted stabilized RAS with different Class C fly ash content, the stabilized RAS:BA mixture with 20% Class C fly ash content, and GOS following ASTM D 2435-96. The standard consolidometer ring with 64 mm diameter and 25 mm height was used for the tests. Each specimen was compacted at the  $w_{opt}$  and relative compaction level of 95% inside the consolidometer ring in three lifts of equal thickness by a manual hammer. The specimens were then cured for 7 days in 100% humidity room. Pore pressure transducers were connected to the base of the specimens in the consolidometer cells to measure any generated excess pore water pressures ( $\Delta u$ ) during consolidation test. Drainage was allowed from the top. The specimens were loaded incrementally from 12.5 kPa with load increment ratio (LIR) of 1.0 and load increment duration (LID) of 24 h until the maximum vertical stress ( $\sigma'_v$ ) level of 1600 kPa. The specimen deformations were measured by a LVDT placed on the loading plate. The LABVIEW software (National Instruments, Austin, TX) and a data acquisition card (UPC601-U) were used for automated incremental loading and recording of vertical deformation.

### *Triaxial Strength Tests*

Consolidated drained (CD) triaxial compression tests were performed on RAS and stabilized RAS to evaluate shear strength and volumetric behavior. For each mixture three tests were performed under  $\sigma'_c$  of 35 kPa, 70 kPa and 140 kPa. The confining pressures were selected to represent typical effective stresses in highway embankments or retaining wall backfills. Each moistened RAS:FA mixture was compacted in a split mold using a standard Proctor compaction hammer. The split mold had a diameter of 73 mm and a height of 145 mm height. For each mixture the number of tamps per layer was determined by trials to obtain a density corresponding to the compaction level of 95%. After compaction the specimen was carefully removed from the split mold, wrapped using shrink wrap and cured for 7 days in a 100% humidity room. After curing, each specimen was placed in the triaxial cell chamber and backpressure-saturated according to ASTM D4767 so that a B value greater than 95% was attained. The specimen was subsequently isotropically consolidated under a given  $\sigma'_c$ . The specimen volume change during consolidation phase was monitored in the backpressure burette until no significant change in volume was observed. The shearing of each specimen in CD condition was performed under constant strain rate. The shearing rate of 0.1 mm/min was selected based on the time for primary consolidation and the ultimate strain of the specimen at failure as suggested by Bishop and Henkel (1962). The pore water pressure was monitored during shearing to ensure no  $\Delta u$  is generated. The volume change of each specimen during shearing was recorded from the volume change of water in backpressure burette.

### *K<sub>o</sub>-Consolidation Tests*

To evaluate coefficient of lateral earth pressure at rest ( $K_o$ ) of RAS and stabilized RAS, a specifically developed  $K_o$ -Consolidation cell by Edil and Wang (2000) was used. Fig. 3 shows the schematic of the apparatus. The cell has the diameter of a conventional consolidation ring (64 mm) and consists of a hollowed chamber with an inner ring thickness of 1 mm instrumented with strain gages. During application of  $\sigma'_v$  to the sample, the air pressure is applied into the lateral chamber around the inner ring to maintain the lateral displacement of the ring to a minimum.  $K_o$  is calculated by measuring the lateral air pressure,  $\sigma'_h$ , upon application of  $\sigma'_v$  on the sample,  $K_o = \sigma'_h / \sigma'_v$ . The standard consolidation test procedure with LID of 24 h was followed for the  $K_o$  tests. A program was written in LABVIEW to automate the test and acquire the data.

## **Results and Discussions**

### *Compaction behavior*

Fig. 4 shows the variation of dry unit weight ( $\gamma_d$ ) versus water content ( $w$ ) for RAS, different RAS:FA mixtures and a mixture of RAS:BA:FA. RAS and RAS:FA mixtures have well-defined compaction curves with  $\gamma_{dmax}$  varying from 11.3 kN/m<sup>3</sup> for RAS to 15.9 kN/m<sup>3</sup> for RAS:FA mixture with 50% Class C fly ash content. The  $\gamma_{dmax}$  of different RAS:FA mixtures are lower than  $\gamma_{dmax}$  of typical compacted sandy soils which typically ranges between 17 and 20 kN/m<sup>3</sup> (18.30 kN/m<sup>3</sup> for the Wisconsin GOS sample). The  $w_{opt}$  ranges from 8.6% for RAS to 13.2% for the RAS:BA:FA mixture indicating that the materials are not overly sensitive to compaction moisture content, which is an advantage in wet climates. The low  $\gamma_{dmax}$  of stabilized RAS makes it a favorable alternative to compacted sandy soils for construction of highway embankments over weak subgrade.

### *Hydraulic conductivity*

The hydraulic conductivity of RAS and stabilized RAS at different  $\sigma'_c$  is shown in Fig. 5. Compared to GOS, RAS and stabilized RAS have lower the hydraulic conductivity. The hydraulic conductivity also reduces with increasing  $\sigma'_c$ . Possible reason is the compressibility of RAS particles which facilitates densification of the specimen at higher  $\sigma'_c$  which consequently results in lower hydraulic conductivity. The hydraulic conductivity of stabilized RAS also decreases with increasing fly ash content. Addition of silt-size fly ash increases the fines content of the sample and consequently reduces the hydraulic conductivity. The hydraulic conductivities of RAS and stabilized RAS generally vary, depending on confining pressure, between  $2 \times 10^{-4}$  cm/s and  $9 \times 10^{-6}$  cm/s which is equivalent to hydraulic conductivity of very fine sand, silty sand, and silty clay soil (USBR 1987). The drainage capacity of different materials is also classified according to USBR (1987) and accordingly marked on Fig. 5. “Good Drainage” represents drainage capacity of clean gravel and sand while “Poor Drainage” represents drainage capacity of very fine sand, silty sand and silty clay soil. Drainage capacity of RAS and RAS:FA straddles good to poor depending on FA content and confining pressure.

### *Compressibility*

Fig. 6 shows the compression curves of RAS and stabilized RAS in terms of vertical strain,  $\epsilon_v$ , versus logarithm of vertical stress,  $\sigma'_v$ . Compared to outwash sand, pure RAS is highly compressible for structural fill applications. Under a  $\sigma'_v$  of 200 kPa, which is a typical overburden pressure in highway embankments, the  $\epsilon_v$  of GOS is only 2.0% whereas RAS exhibits a  $\epsilon_v$  of 17.5%. High compressibility of RAS is attributed to three mechanisms: (1) the

cellulose felt within RAS particles creates voids in the particles. Under increasing  $\sigma'_v$ , the voids in cellulose felt tend to close rapidly. The voids between the plate-like RAS particles also tend to close due to the flexibility of RAS particles; (2) the sand particles either on RAS particle surface or separated from RAS particles, penetrate into asphalt coating of other RAS particles under increasing  $\sigma'_v$ ; and (3) the smaller spherical RAS particles in the matrix [see Fig. 1(a)], tends to deform under  $\sigma'_v$  due to viscous asphalt cement. Asphalt cement and cellulose felt components together constitute between 35 to 50% by weight of RAS particles.

The compressibility of the stabilized RAS is systematically reduced with increasing self-cementing fly ash content. For  $\sigma'_v$  up to 200 kPa, compressibilities of GOS and stabilized RAS with 20% Class C fly ash are comparable. At higher  $\sigma'_v$ , the compressibility of the stabilized RAS increases possibly because of the breakage of bonding between RAS particles created by fly ash cementation. Further increase of the fly ash content to 50%, although considered to be very high, reduces the compressibility of the stabilized RAS to levels comparable to those of the GOS specimen under  $\sigma'_v$  even greater than 200 kPa. The compressibility of stabilized RAS:BA mixture is also shown in Fig. 6. The  $\epsilon_v$  of RAS:BA mixture stabilized with 20% Class C fly ash content is lower than  $\epsilon_v$  of RAS stabilized with 20% fly ash for  $\sigma'_v$  larger than 200 kPa but comparable up to  $\sigma'_v = 200$  kPa. This is attributed to more competent BA particles replacing some of the compressible RAS particles.

Settlement of a laterally wide earth structure is usually calculated using compressibility parameters obtained from the results of one-dimensional compression tests. The compressibility parameters for granular material obtained from the result of one-dimensional compression test include effective yield stress,  $\sigma'_y$ , pre-yield modified compression index,  $C_{pry} = \Delta\epsilon/\Delta \log \sigma'_v$ , post-yield modified compression index,  $C_{psy} = \Delta\epsilon/\Delta \log \sigma'_v$ , and secondary compression ratio,

$C_{\alpha\varepsilon} = \Delta\varepsilon/\Delta \log t$ . The  $\sigma'_y$  corresponds to the stress that divides the soil compression curve into a region of small and elastic deformation called pre-yield curve and a region of plastic deformation called post-yield compression curve. The values of  $\sigma'_y$ ,  $C_{pry}$ , and  $C_{psy}$  were obtained from the  $\varepsilon_v$  versus  $\log \sigma'_v$  curves of RAS and stabilized RAS according to the graphical construction of Casagrande (Casagrande 1936b). Fig. 7 shows variation of compressibility parameters of stabilized RAS with fly ash content. The increase in fly ash content increases  $\sigma'_y$  while reducing  $C_{pry}$  and  $C_{psy}$ . The  $C_{pry}$  of stabilized RAS with fly ash content more than 20% is reduced to lower than  $C_{pry}$  of GOS. Coduto (1999) classified the compressibility of soils based on  $C_{pry}$  and  $C_{psy}$  as summarized in Table 2. Accordingly, the stabilized RAS is classified as *very slightly compressible* to *slightly compressible* when the  $\sigma'_v$  is in the pre-yield range ( $\sigma'_v < \sigma'_y$ ). For  $\sigma'_v$  in the post-yield range ( $\sigma'_v > \sigma'_y$ ), the material is classified as *moderately compressible* to *highly compressible*.

Fig. 8 shows the variation of  $\varepsilon_v$  with logarithm of time for RAS and stabilized RAS under  $\sigma'_v = 100$  kPa. The time for complete dissipation of  $\Delta u$  under the applied  $\sigma'_v$  is marked as the end of primary consolidation ( $t_p$ ) on Fig. 8. As indicated, the primary consolidation accounts for a negligible compression of RAS and stabilized RAS; and the majority of settlement is due to secondary compression. The  $\varepsilon_v$  of RAS nonlinearly increases with logarithm of time after  $t_p$  and follows a constant rate after the standard LID of 24 h. Stabilization of RAS using Class C fly ash reduces the  $C_{\alpha\varepsilon}$ . Fig. 9 shows the variation of  $C_{\alpha\varepsilon}$  with fly ash content calculated for one log cycle after the standard LID under different  $\sigma'_v$ . The increase in fly ash content to more than 10% reduces the  $C_{\alpha\varepsilon}$  significantly. Under  $\sigma'_v$  of 200 kPa, which is a typical stress level for highway embankments, the  $C_{\alpha\varepsilon}$  is reduced from 0.041 for unstabilized RAS to 0.005 for stabilized RAS with 20% fly ash content.

Fig. 10 (a) shows the effect of secondary compression on  $\sigma'_y$  of unstabilized and stabilized RAS, i.e., the effect of aging. The LID under  $\sigma'_v$  of 100 kPa was extended from 24 h to 150 days during one-dimensional consolidation test. After the 150-day loading period, the test continued with standard LID of 24 h. The long-term compression increased the  $\sigma'_y$  of RAS from 65 kPa to 250 kPa and of stabilized RAS with 20% fly ash from 300 kPa to 420 kPa. The effect of secondary compression on  $\sigma'_y$  is more significant on RAS than on stabilized RAS possibly due to greater reduction in void ratio in RAS. The  $C_{pry}$  of RAS decreases from 0.07 to 0.03 as a result of this aging effect. The long-term compression under a constant  $\sigma'_v$  i.e., aging also affects the secondary compression rate at subsequent  $\sigma'_v$ . Fig. 10 (b) shows the variation of  $\varepsilon_v$  with time under  $\sigma'_v$  of 200 kPa for unstabilized and stabilized RAS before and after aging for 150 days. The  $C_{\alpha\varepsilon}$  of RAS decreased from 0.0249 to 0.0020 and of RAS stabilized with 20% Class C fly ash decreased from 0.0066 to 0.0009 after a 150-day compression period under  $\sigma'_v$  of 100 kPa. The results indicate that, aging not only reduces the secondary compression of both unstabilized and stabilized RAS, also is an effective alternative to stabilization for reducing compressibility of RAS. In this respect, RAS behaves like some clay soils.

### *Shear strength*

The stress-strain and volumetric behavior of unstabilized and stabilized RAS in consolidated drained triaxial compression tests are shown in Fig.11 along with that of GOS for comparison. Unstabilized RAS exhibits a stress-strain and volumetric behavior similar to that of loose sand. There is no peak on stress-strain curve and the volume change is contractive at different  $\sigma'_c$ . RAS has comparable peak shear strength to GOS but unlike GOS, the peak shear strength occurs at larger axial strain. Stabilization of RAS with self-cementing fly ash increases the shear

strength and the peak point on the stress-strain curves develops at smaller axial strain resembling the stress-strain behavior of dense sand. The volume change of stabilized RAS tends to be more dilative. Stabilization has more prominent effect on stress-strain and volume change of RAS at smaller  $\sigma'_c$ . At  $\sigma'_c=35$  kPa, stabilization of RAS with 20% fly ash increased the shear strength from 170 kPa to 420 kPa (reflecting a 150% increase) and changed the volumetric behavior from contractive to dilative whereas at  $\sigma'_c=140$  kPa with the same fly ash content, the shear strength increased from 440 kPa to 630 kPa (reflecting a 43% increase) and the volume change remained contractive.

The deviator stress at failure was selected as either the peak deviator stress or the deviator stress corresponding to 15% axial strain whichever is reached earlier (ASTM D4767). Fig. 12 shows the effective friction angle and cohesion of unstabilized and stabilized RAS. The friction angle of unstabilized RAS is  $36^\circ$  which is comparable to the friction angle of GOS. Pure RAS also exhibited an apparent cohesion ( $c'$ ) of 20 kPa possibly due to slight binding of RAS particles together during compaction. This apparent cohesion can be neglected for practical purposes. The friction angle decreases and cohesion increases with increasing fly ash content of stabilized RAS indicating diminishing contribution of confining stress to strength development and increasing contribution of cementation.

### *Coefficient of lateral earth pressure*

Fig. 13 shows the variation of  $K_o$  with  $\sigma'_v$  of unstabilized and stabilized RAS along with GOS for comparison. The  $K_o$  of RAS nonlinearly decreases with increasing  $\sigma'_v$  from about 1.0 at  $\sigma'_v$  lower than 100 kPa to 0.36 at  $\sigma'_v$  higher than 500 kPa. On the other hand, stabilization of RAS with 20% Class C fly ash significantly reduces  $K_o$  to less than 0.1 under  $\sigma'_v$  smaller than 400 kPa. The

stronger interlock and higher friction between particles generally tend to reduce  $K_o$  (Jáky 1944; Ladd et al. 1977; Mesri and Hayat, 1993). Under higher  $\sigma'_v$ ,  $K_o$  increases to 0.2 presumably due to breakage of cementation of the bonds between the RAS particles. The  $K_o$  of GOS sample nonlinearly decreases from 0.6 under  $\sigma'_v$  of 25 kPa and approaches to 0.4 under  $\sigma'_v$  higher than 400 kPa. The  $K_o$  of normally consolidated soils typically ranges from 0.35 to 0.7 (Coduto 1998; Holtz and Kovacs 2004). With  $\gamma_{dmax}$  of 13.8 kN/m<sup>3</sup> and  $K_o$  less than 0.1, stabilized RAS exhibits remarkably smaller lateral earth pressure than typical compacted soils, which is highly beneficial behind retaining structures and expected to result in significant reduction in the dimensions of retaining walls.

## **Practical Implication**

The total or differential settlement that can be tolerated by a pavement is rarely specified except in the case of bridge approaches for which the tolerable settlement is commonly specified as 12 mm to 25 mm. For roadway embankments the allowable settlement after paving depends on the length of the fill and rate at which settlement develops. If the variations in settlement are uniformly distributed along the length of the embankment, settlement of 150-mm to 300-mm can be tolerated in long embankments (NCHRP Synthesis of Highway Practice 8). Although the maximum settlement of highway embankments are allowed between 300-mm and 600-mm (NCHRP Synthesis of Highway Practice 29 and Stark et al. (2004), 300-mm is a more widely accepted limit and is adopted here.

To illustrate the performance of embankment fill constructed with stabilized RAS and preloaded RAS, example calculations were made on embankments 12 m wide at the top and 2, 5, 10, and 15 m high constructed on a 10 m thick sand deposit. Since compacted RAS and

stabilized RAS have comparable shear strength to typical compacted sand, emphasis was made on evaluation of embankment settlements during the life-time period rather than side slope stability. Settlements were evaluated using the following relationship:

$$s = \sum_{i=1}^n s_i = \sum_{i=1}^n h_i C_{\alpha\varepsilon,i} \log \left( \frac{t}{t_o} \right)$$

where  $s$  is the embankment settlement,  $s_i$  is the settlement of a layer with thickness  $h_i$  ( $h_i$  was selected 0.5 m in the calculations),  $n$  is the number of layers to which the embankment height  $H$  was divided ( $H=nh_i$ ),  $t$  is time, and  $t_o$  is an arbitrary reference time that for the calculations herein was taken 1 d after completion of construction. The material properties for the settlement calculations are summarized in Table 3.

Fig. 14 shows the variation of settlement of an embankment 10 m high, constructed with RAS, stabilized RAS, preloaded RAS and sand during 40 years after construction. The majority of settlements occur within 1 year after completion of the construction. The total settlement of the embankment constructed with RAS is about 1025 mm, which is far more than the allowable settlement. Aging by preloading of RAS reduces the total settlement to 83 mm which reflects 92% reduction in settlement. Stabilization of RAS with 10% fly ash reduces the total embankment settlement to 300 mm reflecting 70% reduction. Increase of fly ash content to 20% results in negligible total settlement during the 40-year lifetime. The average height of the embankments constructed in the U.S. is 4.5 m (Wright 1996). Having identical subgrade soil conditions, shorter embankments exhibit smaller settlement than those plotted in Fig. 14. Fig. 15(a) shows the variation of settlement with time and height of the embankments which preloading technique is used to reduce compressibility of RAS. The total settlement of the preloaded RAS fill with 5 m high in average is 30 mm. Fig. 15(b) plots the variation of settlement with time of RAS fill stabilized with 10% fly ash. The total settlement of an average

fill constructed with the stabilized RAS is 70 mm. Fig. 16(c) indicates that total settlement of embankment fills with preloaded RAS or stabilized RAS up to 15 m high during the 40-year lifetime is within the allowable settlement limit. The variation of total settlement with percent fly ash is illustrated in Fig. 16(d). Stabilization of RAS with 10% fly ash significantly reduces the total settlement. The settlement reduction is more noticeable in embankments with lower height. Increase of fly ash content to 20% results in negligible total settlement for embankments with different height. The fly ash content between 10 to 15%, which is also the typically used fly ash content with soils and base course materials (ACAA 2003), is recommended to reduce compressibility of RAS as structural fill to an acceptable limit while maintaining adequate drainage capacity (Fig. 5).

## **Conclusions**

In this research the geotechnical properties of recycled asphalt shingles (RAS) stabilized with a self-cementing fly ash were evaluated for potential reuse as structural fill in highway embankments or backfill behind retaining structures. Compaction, hydraulic conductivity, compressibility, shear strength and coefficient of lateral earth pressure at rest characteristics of RAS stabilized with self-cementing fly ash were evaluated in a systematic manner. The following observations are made:

1. The maximum dry unit weight of RAS and stabilized RAS is lower than that of typical compacted soils. The maximum dry unit weight of the stabilized RAS increases with increase in fly ash content. The lower maximum dry unit weight of RAS and stabilized RAS makes them a favorable lightweight fill material over weak soils.

2. The hydraulic conductivity of unstabilized and stabilized RAS is comparable to that of silty sands. The hydraulic conductivity is reduced with increasing confining pressure due to compressibility of RAS particles. The hydraulic conductivity is also reduced with increase in fly ash content. Due to significant reduction in drainage capacity, maximum fly ash content in stabilized RAS is recommended to be limited to 20%.
3. RAS alone is too compressible as a structural fill material. Stabilization of RAS significantly reduces short-term and long-term compressibility of the material. RAS stabilized with 10 to 20% Class C fly ash under low to moderate  $\sigma'_v$  (i.e., 25 to 200 kPa) has the compressibility comparable to that of compacted sandy soil. Stabilization of RAS mixed with a granular material like bottom ash results even lower compressibility compared to the stabilization of pure RAS. Aging by preloading for a specific time such as 150 days is an alternative method to reduce long-term compressibility of RAS. The effect of preloading on reducing the compressibility is more significant for unstabilized RAS than for stabilized RAS.
4. The stress-strain and volumetric behavior of RAS resemble those of loose sandy soils. RAS alone exhibits sufficient shear strength as a structural fill material. Stabilization of RAS further increases the shear strength and changes the volumetric behavior from compressive to dilative.
5. Stabilization of RAS significantly reduces the  $K_o$  of RAS. Lower maximum dry unit weight and  $K_o$  of stabilized RAS than those of typical compacted sandy soils make the stabilized RAS a favorable backfill material behind retaining walls with potential to greatly reduce the dimensions of the walls.

Based on the results of this research, stabilized RAS is considered to be a viable material for use as structural fill in highway embankments and backfill behind retaining walls. Structural fill is an alternative application to use in hot mix asphalt, which is likely to allow use of large volume of waste asphalt shingles and help to save landfill space, reduce disposal costs, energy consumption, and green house gas emissions due to mining and production of virgin aggregates. Additionally, stabilized RAS offer certain superior fill material characteristics compared to conventional materials such as light weight and reduced lateral pressures. However, RAS samples obtained from different sources and with different particle sizes may have different mechanical behavior and need to be tested for specific applications. Further studies need to be made to generalize use of stabilized RAS in structural fills and to evaluate the potential effect of high ground temperatures in certain climatic regions.

## **Acknowledgement**

Support for this study was provided by the Recycled Materials Resource Center, which is supported by the Federal Highway Administration. The opinions, findings, conclusions, or recommendations expressed herein are those of the author(s) and do not necessarily represent the views of the sponsors.

## **References**

- American Coal Ash Association (ACAA). (2009). Coal Combustion Product (CCP) Production & Use Survey Results. Aurora, CO. September 15, 2009 [online].
- American Coal Ash Association (ACAA). (2003). *Fly Ash Facts for Highway Engineers*. Washington, DC.
- American Society for Testing and Materials (ASTM). (1997). "Standard guide for use of coal combustion by-products in structural fills." *Designation E 1861-97*, PA.

- American Society for Testing and Materials (ASTM). (1963). "Standard test method for particle-size analysis of soils." *Designation D 422-63*, PA.
- American Society for Testing and Materials (ASTM). (2000). "Standard test methods for specific gravity of soil solids by water pycnometer." *Designation D 854-00*, PA.
- American Society for Testing and Materials (ASTM). (2000). "Standard test methods for laboratory compaction characteristics of soil using standard effort [[12,400 ft lbf/ ft<sup>3</sup> (600 kN m/m<sup>3</sup>)]." *Designation D 698-00a*, PA.
- American Society for Testing and Materials (ASTM). (1995). "Standard test methods for measurement of hydraulic conductivity of saturated porous materials using a flexible wall permeameter." *Designation D 5084-03*, PA.
- American Society for Testing and Materials (ASTM). (1996). "Standard test method for one-dimensional consolidation properties of soils." *Designation D 2435-96*, PA.
- Bin-Shafique, M. S., Senol, A., Edil, T. B., and Benson, C. H. (2004). "Incorporating Fly Ash Stabilized Subbase into Pavement Design-Case Study." *Geotechnical Engineering*, Institute of Civil Engineers, United Kingdom, 157(GE4), 239-249.
- Bishop, A.W. and Henkel, D.J. (1962). *The Measurement of Soil Properties in the Triaxial Test*. 2<sup>nd</sup> ed., London, Edward Arnold.
- Button, J. W., Williams D., and Scherocman, J.A. (1995). "Roofing Shingles and Toner in Asphalt Pavements." Research Report 1344-2F, Texas Transportation Institute, College Station, Texas.
- Casagrande, A. (1936a). "The determination of the pre-consolidation load and its practical significance." Discussion D-34, *Proc. First Int. Conf. Soil Mech. Found. Engr.*, Cambridge, Vol. 3, 60-64.
- Cetin, B., Aydilek, A. H. and Li, L. (2012). "Manganese and chromium leaching from high carbon fly ash stabilized highway base layers." *GeoCongress 2012*, Geo Institute, American Society of Civil Engineers, Oakland, Ca. CD-ROM.
- Coduto, D. P. (1999). *Geotechnical Engineering Principles and Practices*. Prentice Hall.
- DiGioia, A. M., McLaren, R. J., Burns, D. L., Miller, D. E., (1986). "Fly Ash Design Manual for Road and Site Application." Vol. 1: Dry or Conditioned Placement, Manual Prepared for EPRI, Interim Report, CS-4419, Electric Power Research Institute, Palo Alto, CA.
- Edil, T. B. (2006). "Green Highways: Strategy for Recycling Materials for Sustainable Construction Practices." *Proceedings of the Seventh International Congress on Advances in Civil Engineering*, 2006, Yildiz Technical University, Istanbul, Turkey, 91-112.

- Edil, T. B., and Wang, X. (2000). "Shear strength and  $K_o$  of peats and organic soils." *Geotechnics of High Water Content Materials, ASTM Special Technical Publication*, pp. 209-225.
- Ferguson, G. (1989). "Use of Coal Ash in Highway Construction: Kansas Demonstration Project." *GS-6460, Research Project 2422-15, Electric Power Research Institute*, Palo Alto, CA.
- Ferguson, G., Levorson, S. M. (1999). "Soil and Pavement Base Stabilization with Self-Cementing Coal Fly Ash." American Coal Ash Association, Alexandria, VA.
- Grodinsky, C., Plunkett, N., and Surwilo, J. (2002). "Performance of Recycled Asphalt Shingles for Road Applications." *Final Report*, State of Vermont's Agency of Natural Resources.
- Hooper, F., and Marr, W. (2004). "Effects of Reclaimed Asphalt Shingles on Engineering Properties of Soils." *Recycled Materials in Geotechnics, Geotechnical Special Publication*, No. 127, ASCE, 137-149.
- Jáky, J. (1948). "Earth pressure in soils." *Proceedings of the Second International Conference on Soil Mechanics and Foundation Engineering*, Rotterdam, Vol. 1, 103-107.
- Kim, B. and Prezzi, M. (2008). "Evaluation of the mechanical properties of class-F fly ash." *Waste Management*, Vol. 28, 649-659.
- Krivit, D. (2007). Recycling of Tear-Off Shingles: Best Practices Guide. Final report prepared for the Construction Materials Recycling Association (CMRA).
- Klyosov A.A. (2007). *Wood-plastic composites*. John Wiley & Sons, Inc. Hoboken, NJ.
- Kosson, D. S., van der Sloot, H. A., and Eighmy, T. T. (1996). "An approach for estimation of contaminant release during utilization and disposal of municipal waste combustion residues." *Journal of Hazardous Materials*, 47(1-3), 43-75.
- Kosson, D. S., Van Der Sloot, H. A., Sanchez, F., and Garrabrants, A. C. (2002). "An integrated framework for evaluating leaching in waste management and utilization of secondary materials." *Environmental Engineering Science*, 19(3), 159-204.
- Holtz, D. R. and Kovacs, W. D. (2004). *An introduction to geotechnical engineering*. Pearson Education Taiwan Ltd.
- Komonweeraket, K. Benson, C.H., Edil, T.B., and Bleam, W.F.(2010). "Leaching Behavior and Mechanisms Controlling the Release of Elements from Soil Stabilized with Fly Ash." *Geo-Frontiers 20111*, Dallas, TX, CD-ROM.
- Ladd, C.C., Foote, R., Ishihara, K., Schlosser, F., and Poulos, H.G. (1977). "Stress-Deformation and Strength Characteristics." State-of-the-Art Report, *Proceedings of the Ninth*

*International Conference on Soil Mechanics and Foundation Engineering*, Tokyo, Vol. 2, 421-494.

- Lee, J. C., Edil, T. B., Tinjum, J. M. and Benson, C. H. (2010). "Quantitative Assessment of Environmental and Economic Benefits of Using Recycled Construction Materials in Highway Construction." *Journal of the Transportation Research Board*, No. 2158 Paper 10-2505, National Research Council, Washington D. C., 2010, 138-142.
- Li, L., Benson, C. H., Edil, T. B. and Hatipoglu, B. (2006). "WiscLEACH: A Model for Predicting Ground Water Impacts from Fly-Ash Stabilized Layers in Roadways." *GeoCongress 2006*, Atlanta, GE, ASCE, CD-ROM.
- Li, L., Benson, C. H., Edil, T. B. and Hatipoglu, B. (2008). "Sustainable Construction Case History: Fly Ash Stabilization of Recycled Asphalt Pavement Material." *Geotechnical and Geological Engineering*, 26(2), 177-188.
- Li, L., Edil, T. B., and Benson, C. H. (2009). "Mechanical Performance of Pavement Geomaterials Stabilized with Fly Ash in Field Applications." *Coal Combustion and Gasification Products* 1, pp. 43-49, doi: 10.4177/CCGP-D-09-00018.1
- Marks, V. J., and Petermeier, G. (1997). "Let Me Shingle Your Roadway." *Research Project HR-2079, Iowa Department of Transportation*, Ames, Iowa
- Mesri, G., and Hayat, T. M. (1993). "The coefficient of earth pressure at rest." *Canadian Geotechnical Journal*, 30(4), 647-666.
- McLaren, R.J., DiGioia, A.M. (1987). "The Typical Engineering Properties of Fly Ash." *Geotechnical Practice for Waste Disposal '87, Geotechnical Special Publication*, No. 13, 683-697.
- Misra, A. (2000). "Utilization of western coal fly ash in construction of highways in the Midwest." Mid-America Transportation Center, MATC project No. MATC UMC 96-2, Lincoln, NE.
- Patelunas, G. M. (1986). "High Volume Fly Ash Utilization Projects in the United States and Canada." *Electric Power Research Institute*, Report No. CS-4446, Palo Alto, CA.
- Srivastava, L. and Collins, R. J. (1989). "Ash Utilization in Highways: Delaware Demonstration Project." Interim Report, GS-6481, Research Project 2422-3, Electric Power Research Institute, Palo Alto, CA.
- Soleimanbeigi, A., Edil, T., and Benson, C. (2010). "Recycled asphalt shingles mixed with granular byproducts as structural fill." *Journal of ASTM International*, 9(1).

- Townsend, T., Powell, J., and Xu, C. (2007). "Environmental issues associated with asphalt shingle recycling." *Construction Materials Recycling Association, US EPA Innovations Workgroup*.
- Turley, W. (2010). Personal Communication. *Construction Materials Recycling Association, Eola, IL*.
- U.S. Bureau of Reclamation (USBR). (1987). *Design of small dams*. Denver, CO.
- Warner, J. D. (2007). "The beneficial reuse of asphalt shingles in roadway construction." *MSc thesis, Department of Civil and Environmental Engineering, University of Wisconsin-Madison*.
- Wen, H. and Edil, T. B. (2009). "Sustainable Reconstruction of Highways with In-Situ Reclamation of Materials Stabilized for Heavier Loads." *BCR2A Conference, Proc. 2nd Int. Conf. on Bearing Capacity of Roads, Railways and Airfields 2009, Champaign, IL, CD-ROM, 1011-1017*.
- Wen, H., Warner, J. D., Edil, T. B. and Wang, G. (2010). "Laboratory Comparison of Crushed Aggregate and Recycled Pavement Material With and Without High Carbon Fly Ash" *Geotechnical and Geological Engineering, 28(4), 405-411*.
- Wright, P. H. (1996). *Highway Engineering*. John Wiley & Sons, Inc.
- Zickell, A. J. (2003). "Asbestos Analysis of Post Consumer Asphalt Shingles." *Technical Report #41. Chelsea Center for Recycling and Economic Development, Technical Research Program*.

Table 1-Grain size indices and USCS classifications RAS, bottom ash and outwash sand

Material	d <sub>10</sub> (mm)	d <sub>50</sub> (mm)	C <sub>u</sub>	C <sub>c</sub>	% fines	USCS symbol	USCS name
RAS	0.17	1.1	7.6	1.6	3.8	SW	Well graded sand
Bottom ash	0.19	0.9	6.3	0.8	1.9	SP	Poorly graded sand
Glacial outwash sand	0.21	0.5	3.1	0.8	0.0	SP	Poorly graded sand

d<sub>10</sub>: effective particle size (particle size for which 10% of the sample is finer than d<sub>10</sub>); d<sub>50</sub>: average particle size (particle size for which 50% of the sample is finer than d<sub>50</sub>); C<sub>u</sub>: coefficient of uniformity (d<sub>60</sub>/d<sub>10</sub>); C<sub>c</sub>: coefficient of curvature ( $C_{30}^2 / (C_{10} \times C_{60})$ ); G<sub>s</sub>: specific gravity; USCS: Unified Soil Classification System

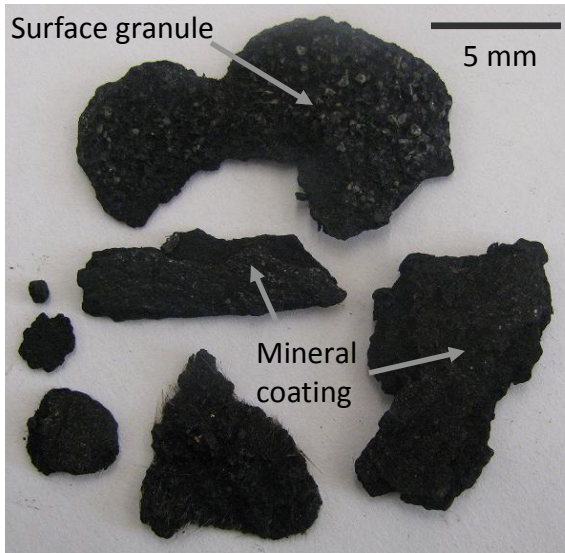
Table 2-Classification for material compressibility (after Coduto 1998)

<i>Modified Compression Index</i>	Compressibility Classification
0-0.05	Very Slightly compressible
0.05-0.10	Slightly compressible
0.10-0.20	Moderately compressible
0.20-0.35	Highly compressible
> 0.35	Very Highly compressible

Table 3-Material properties for settlement evaluation

Properties	Sand	RAS	Preloaded RAS*	RAS:FA (90:10)	RAS:FA (80:20)
$\gamma_d$ (kN/m <sup>3</sup> )	18.3	11.3	11.8	12.5	13.8
$\sigma'_y$ (kPa)	340	65	250	190	310
$C_u$ 0-5 m	0.0002	0.0117	0.0020	0.0045	0.0012
5-10 m	0.0005	0.0157	0.0020	0.0061	0.0022
10-15 m	0.0007	0.0195	0.0020	0.0095	0.0044

\* After aging with a preload surcharge



(a)



(b)



(c)

FIG. 1- (a) Photograph of RAS, (b) light microscope photomicrographs of bottom ash, and (c) Wisconsin glacial outwash sand

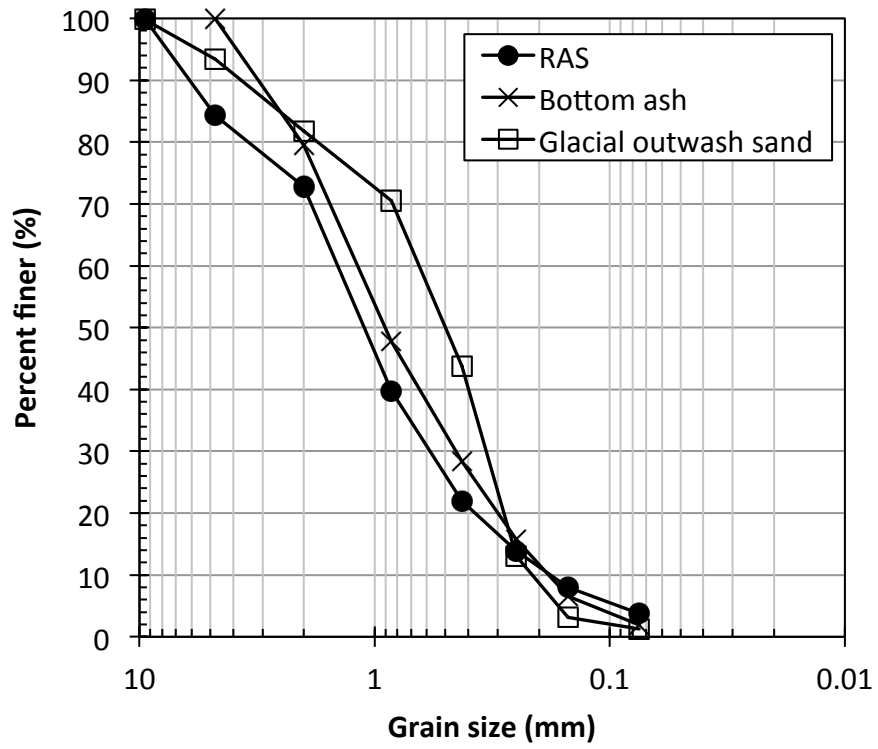


FIG. 2- Grain size distribution of RAS, bottom ash, and Wisconsin glacial outwash sand

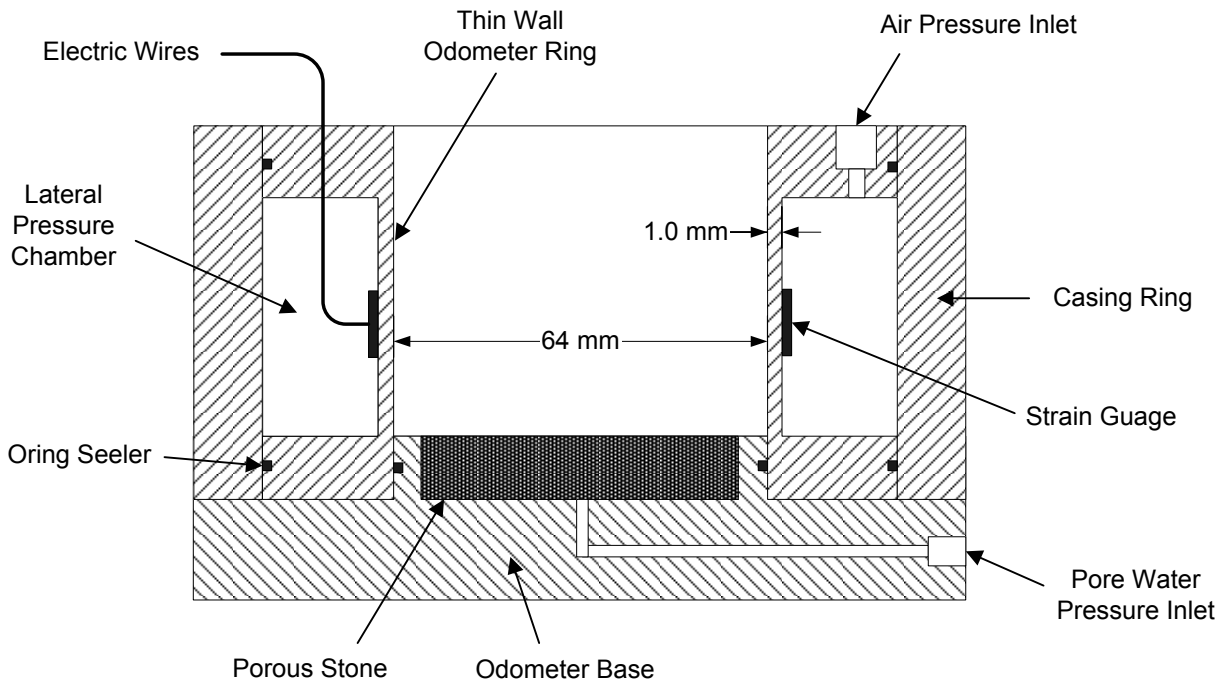


FIG. 3- $K_0$ -Consolidation cell (after Edil and Wang 2000)

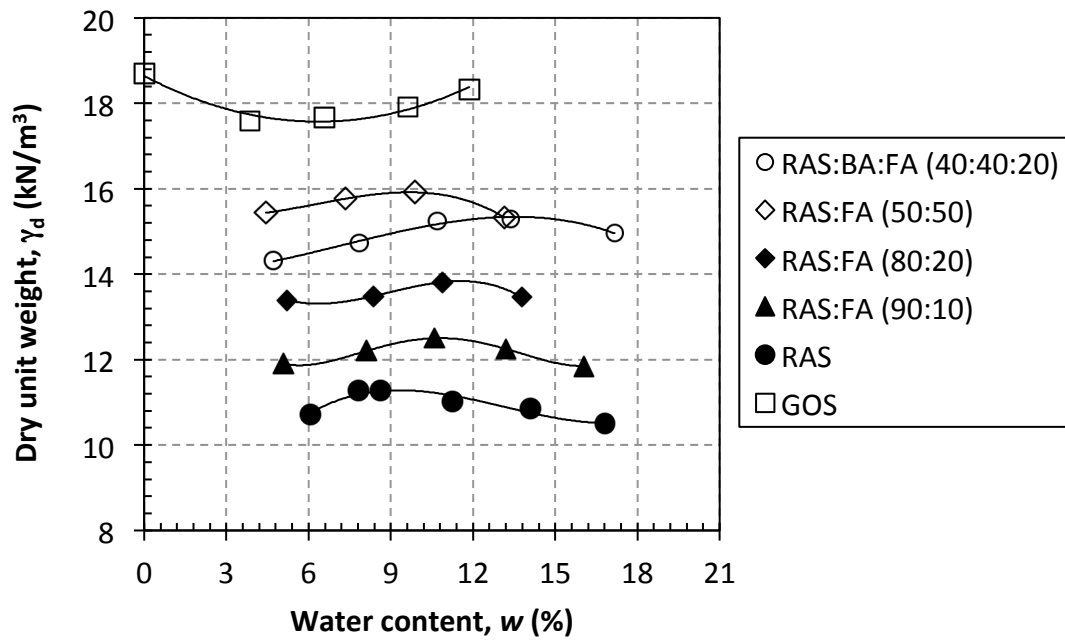


FIG. 4- Dry unit weight versus water content of RAS (:BA):FA mixtures

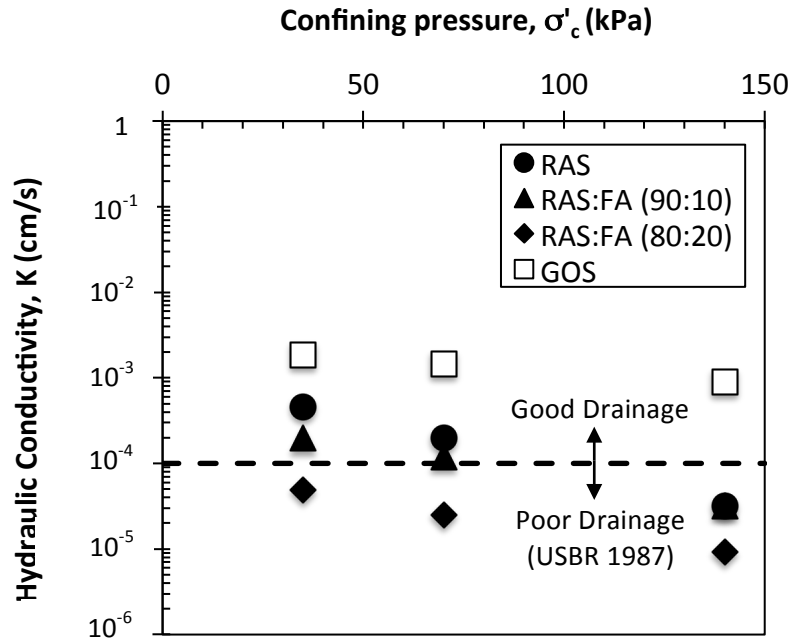


FIG. 5-Hydraulic conductivity of pure and stabilized RAS versus effective confining pressure

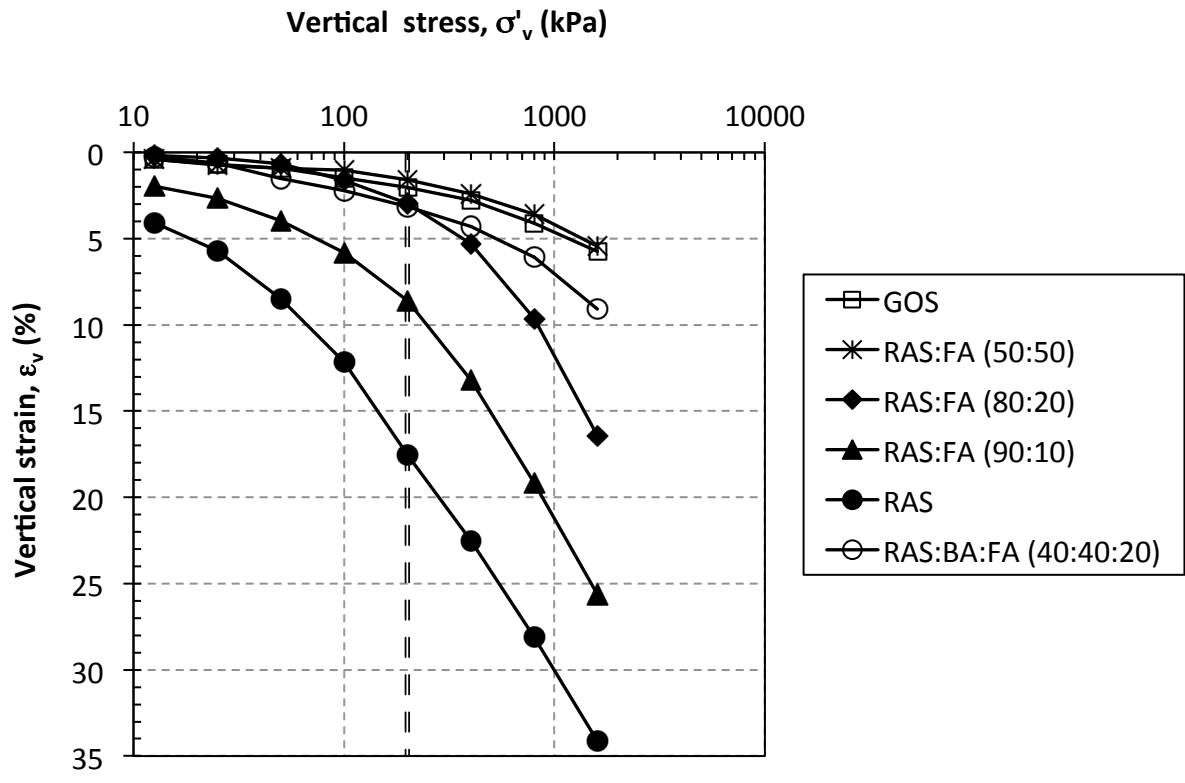


FIG. 6- One-dimensional compression curves

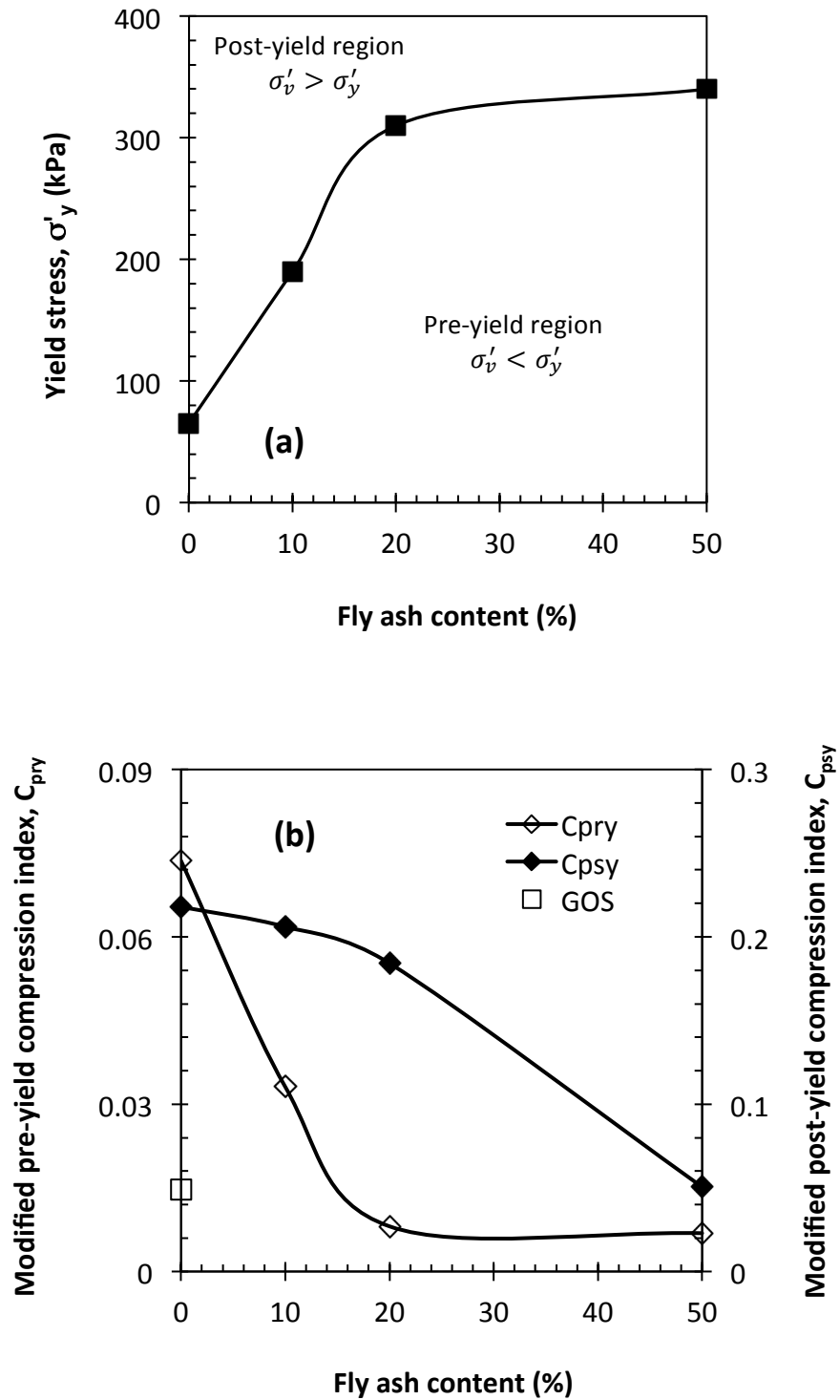


FIG. 7-Compressibility parameters: (a) variation of  $\sigma'_y$ , and (b)  $C_{pry}$  and  $C_{psy}$  of stabilized RAS with Class C fly ash content

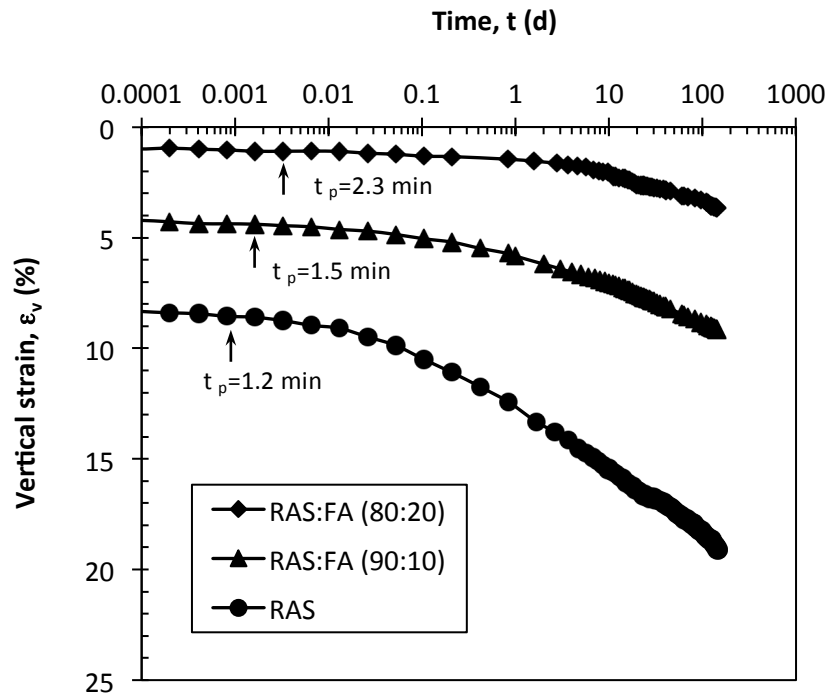


FIG. 8-Variation of  $\epsilon_v$  with time for RAS and stabilized RAS for  $\sigma'_v=100$  kPa

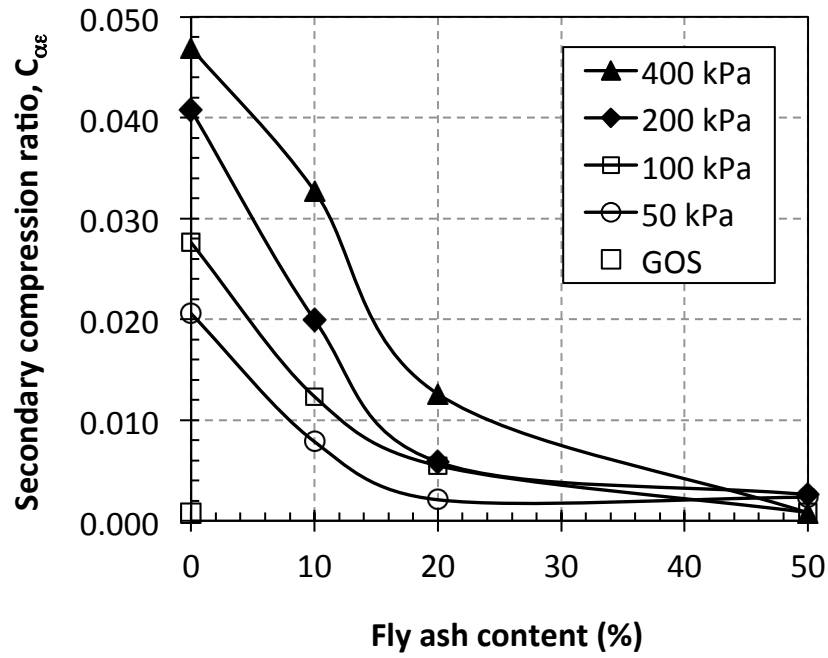


FIG 9- Variation of long term compression of stabilized RAS with fly ash content

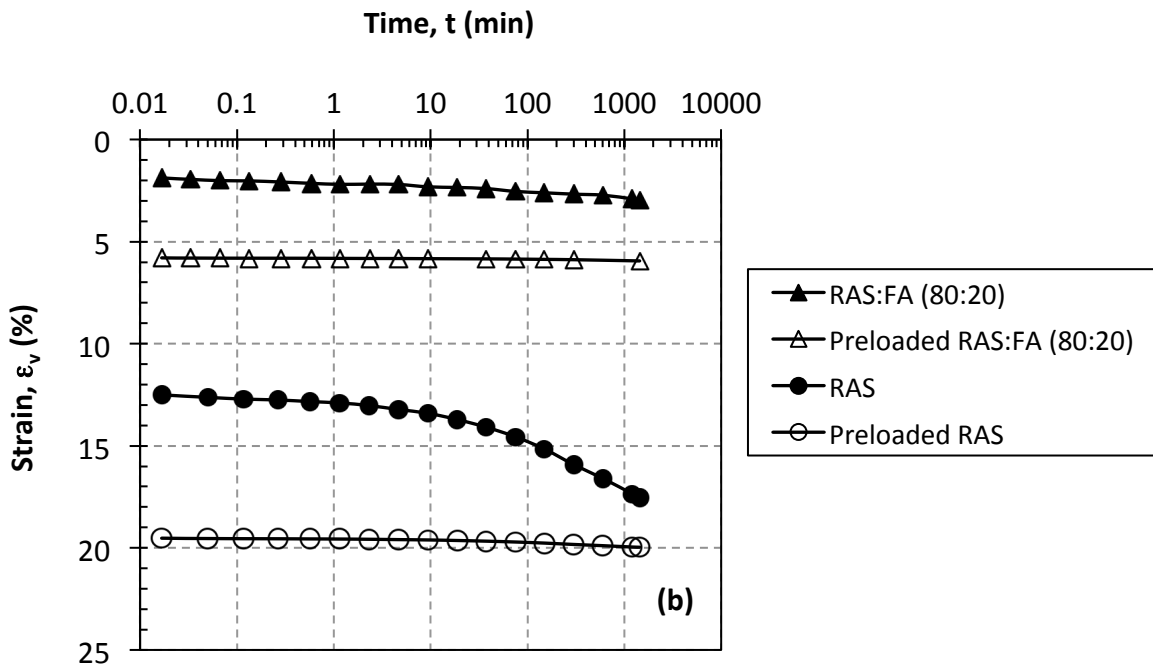
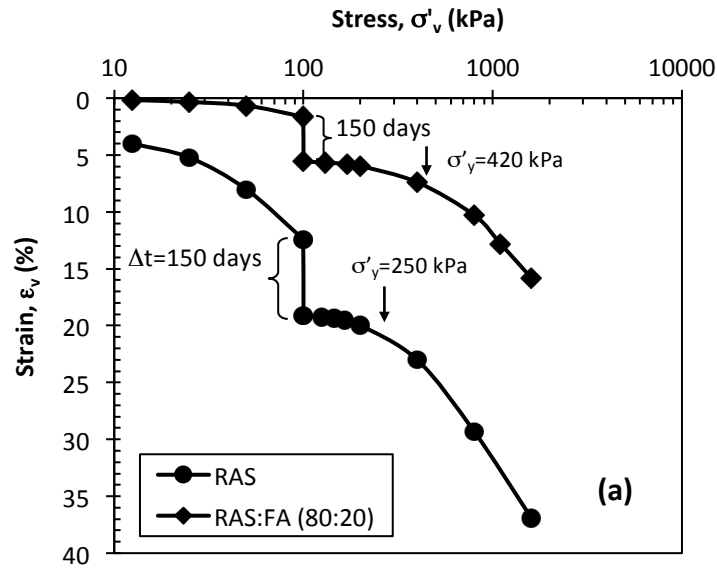


FIG 10- (a) Yield pressure of pure and stabilized RAS resulting from secondary compression, (b) effect of secondary compression on compression rate

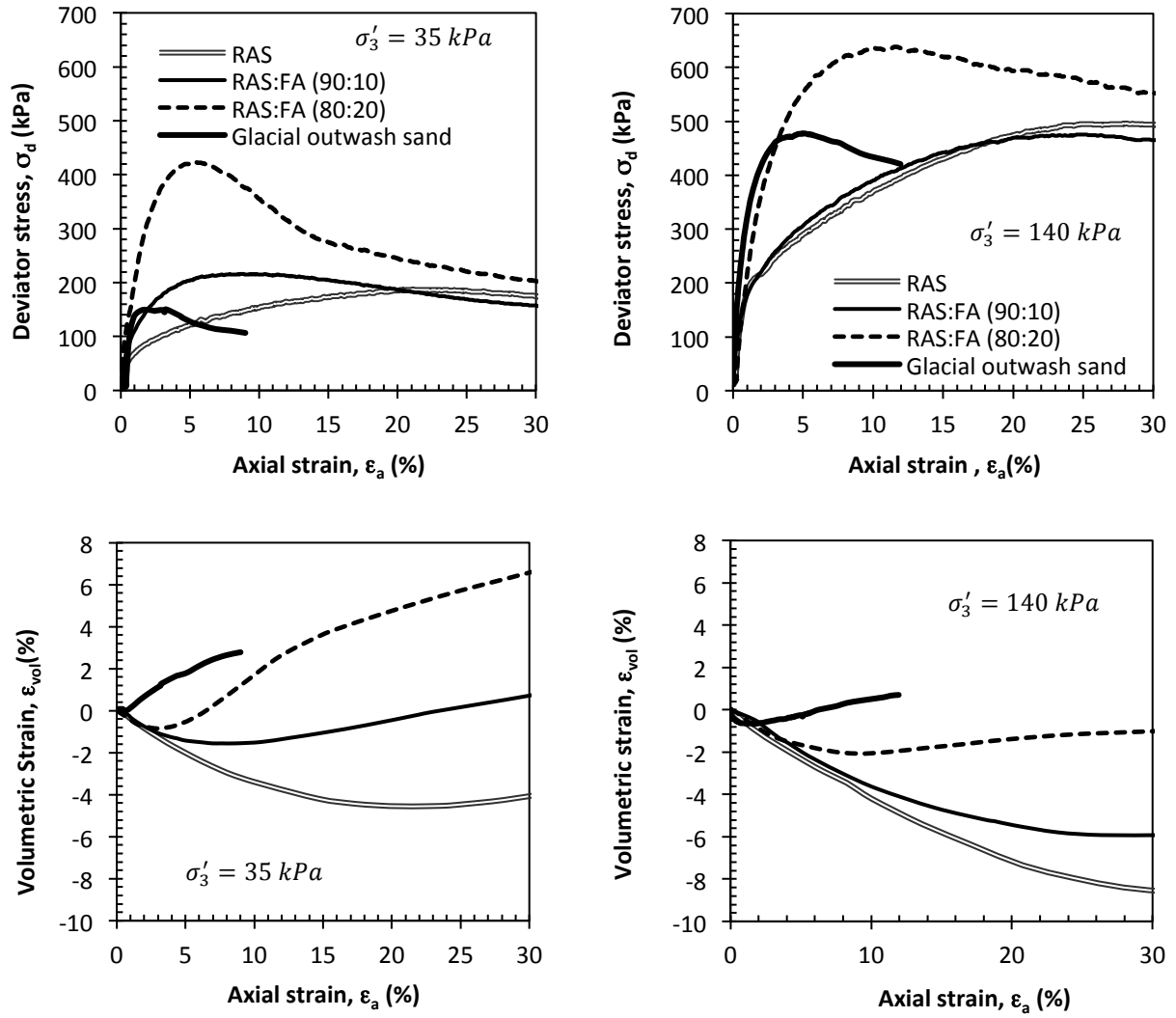


FIG 11. Stress-strain and volumetric behavior of pure and stabilized RAS

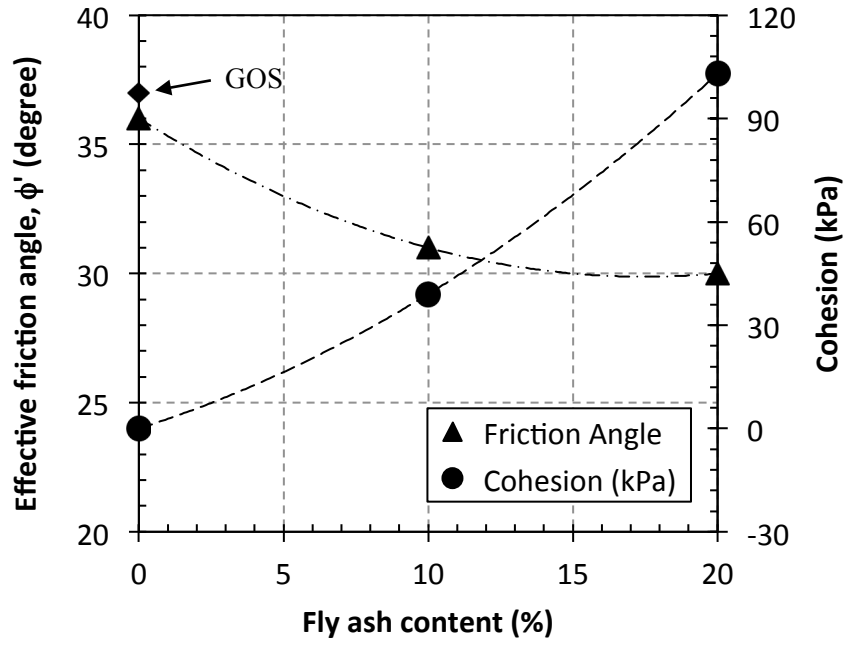


FIG. 12- Effective friction angle and cohesion of pure and stabilized RAS

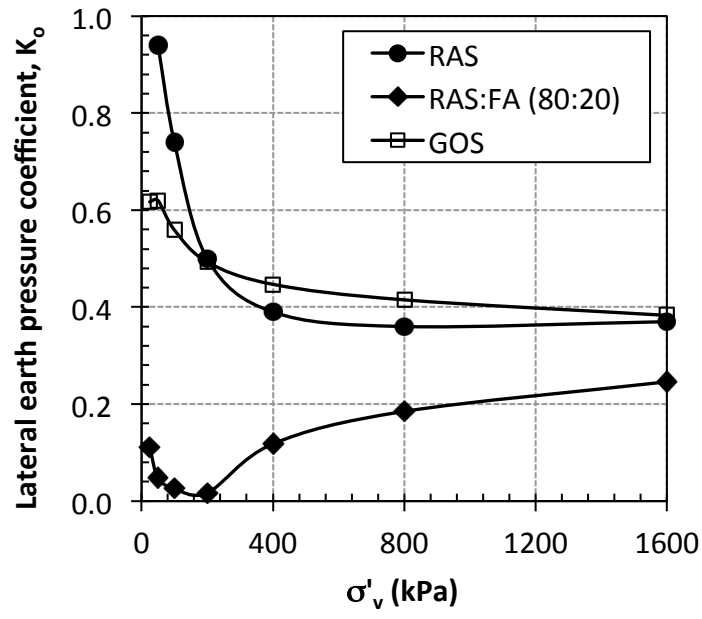


FIG. 13-Variation of  $K_o$  of pure and stabilized RAS with  $\sigma'_v$

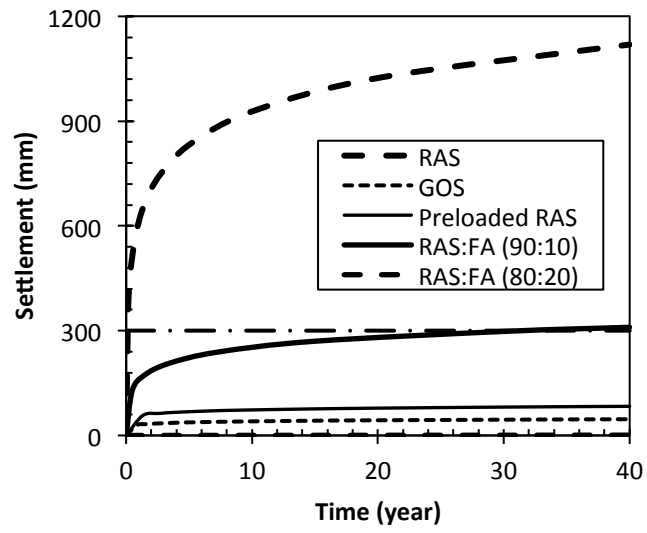


FIG. 14- Variation of embankment settlement with time

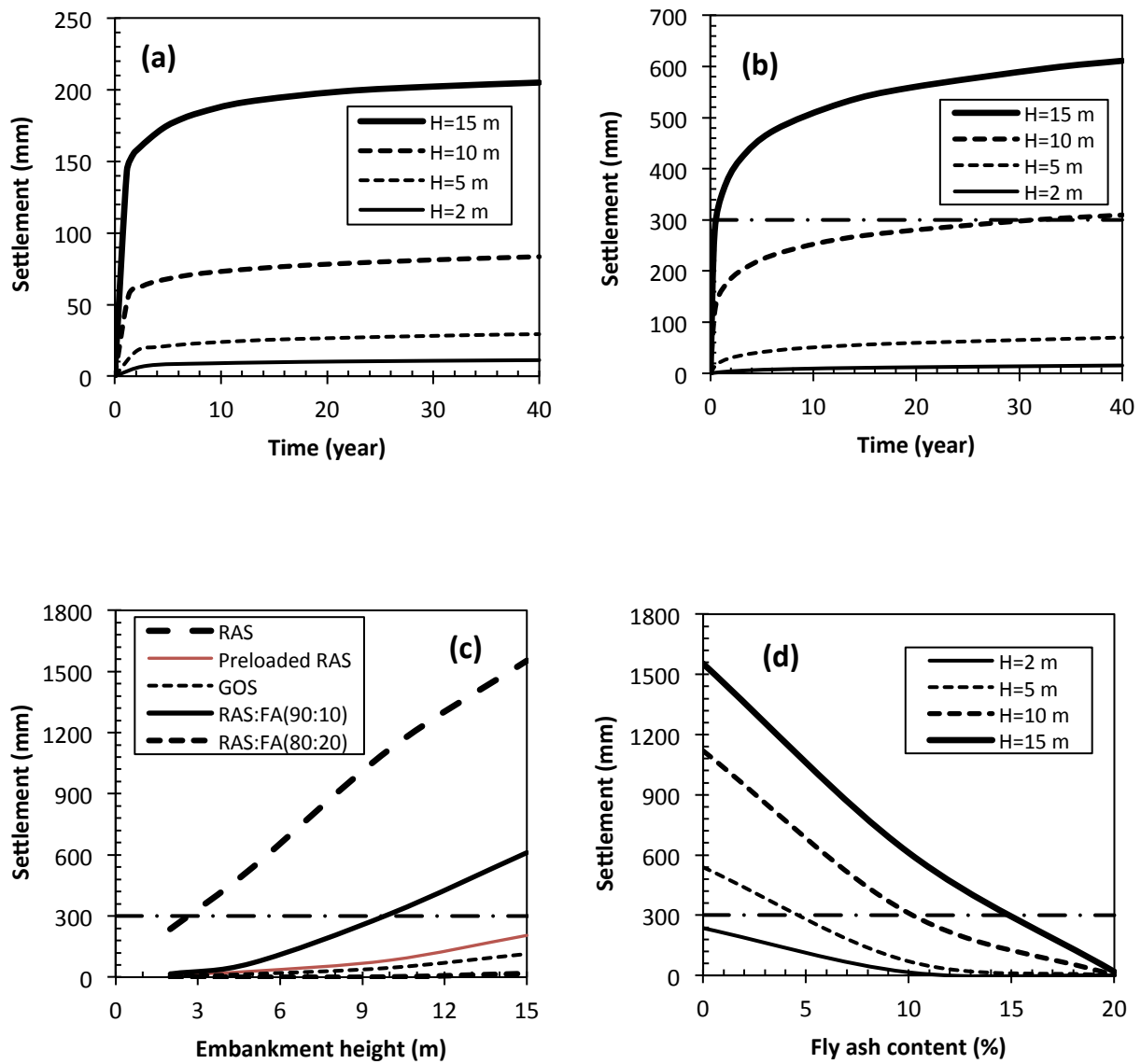


FIG 15- Variation of settlement of preloaded RAS (a) and RAS stabilized with 10 % fly ash (b) with time and embankment height; variation of settlement with embankment height (c) and fly ash content in RAS (d)

## Chapter 4

# Effect of Temperature on Geotechnical Properties of Recycled Asphalt Shingles Mixtures

**Abstract:** The effect of seasonal field temperature variations on engineering properties of recycled asphalt shingles used as structural fill material was investigated using a thermo-mechanical system. The thermo-mechanical system includes temperature-controlled triaxial cell, consolidometer, and permeameter. Shear strength, compressibility and hydraulic conductivity of RAS improved by mixing with bottom ash (BA) or stabilized with self-cementing fly ash were evaluated in a systematic manner at temperatures ranging from 5°C to 35°C. The results indicate that increase in temperature reduces the shear strength, increases the compressibility and hydraulic conductivity of RAS:BA mixture and stabilized RAS significantly and the temperature effects should be taken into consideration in design. The friction angle of RAS:BA mixtures and stabilize RAS, however, remains within a range suitable for stability of embankment fill. The secondary compression ratio, on the other hand, exponentially increases with temperature. Thermal cycling induces thermal preloading to the RAS:BA mixture, which, in turn, reduces compressibility and increases shear strength. Based on these results, to achieve the optimum behavior, construction of embankments made with RAS:BA mixture or fly ash stabilized RAS is recommended to be made during warm seasons.

**KEYWORDS:** Recycled asphalt shingle, bottom ash, fly ash, thermo-mechanical testing, temperature, structural fill, induced thermal effect.

## **Introduction**

Thermal geomechanics has gained increasing attention as a result of new types of applications. Testing soil samples in the laboratory at temperatures different from those in the field may lead to erroneous predictions of mechanical properties of soil (Viridi and Keedwell 1988, Bruyn and Thimus 1996; Graham et al. 2003; Laloui 2001). Thermo-mechanical behavior of soil has been investigated in connection with the disposal of high-level radioactive waste (Gera et al. 1996), oil and gas pipelines (Slegel and Davis, 1977), geothermal structures (Laloui et al. 2003), zones around buried high voltage cables (Abdel-Hadi and Mitchell, 1981; Mitchell et al. 1982), and problems related to the effect of temperature change during sampling, storage and testing (Demars and Charles, 1982). The majority of the investigations focused on saturated clays as temperature change has significant impact on the volume change during drained loading or excess pore pressure generation during undrained loading due to thermal expansion of clay particles and adsorbed water (e.g., Mitchell 1969, Baldi et al. 1988, Delage et al. 1998; Cekerevac and Laloui 2004). Therefore temperature change affects the compressibility and shear strength of clay (e.g., Campanella and Mitchell 1968, Houston et al. 1985; Leroueil and Marques 1996; Abuel-Naga et al. 2007). Fox and Edil (1995) demonstrated the increase in the rate of secondary compression of peat. Temperature changes can be expected to influence the mechanical behavior of new types of geomaterials such as recycled asphalt shingles (RAS) and recycled asphalt pavement (RAP), which contain primarily non-clay soils but contain a temperature-sensitive component such as asphalt binder. Thus, the significance of thermal

impacts on the mechanical properties of these materials needs to be assessed prior to field applications in structural fills.

Approximately 11 million Mg of waste asphalt roofing shingles are generated per year in the U.S. of which 10 million Mg are tear-off roofing shingles and 1 million Mg is factory scraps (Townsend et al. 2007). Reuse of recycled asphalt shingles (RAS) has been identified by the U.S. Environmental Protection Agency (EPA) as a top priority. Only between 10 to 20 % of the total asphalt shingle waste is beneficially used in hot mix asphalt and most of it landfilled (Turley, 2010). Therefore, there is an urgent need to find high-volume applications for RAS. Another potential application, which could use large volume of asphalt shingle waste, is structural fill including highway embankment fills or backfill behind retaining walls. Preliminary compression tests showed that pure RAS is too compressible for use as structural fill. Soleimanbeigi et al. (2012) evaluated engineering properties of stabilized RAS and RAS mixed with bottom ash (BA) at room temperature and verified that compacted RAS:BA mixtures and stabilized RAS are potential favorable lightweight material with acceptable compressibility in structural fill applications including highway embankment fill and backfill behind retaining structures.

RAS has 16 to 35% asphalt cement content as well as 2-15 % cellulose felt, 20-38 % mineral granule/aggregates and 8-40% mineral filler/stabilizer (Krivit, 2007). The temperature change has significant effect on viscosity of asphaltic concrete (Roberts et al. 1996), which may similarly affect mechanical properties of RAS:BA or RAS:FS mixtures when used as unbound fill materials in the field. In this paper, development of a new thermo-mechanical system to investigate the effect of seasonal temperature change on engineering properties of the compacted

RAS:BA mixtures and stabilized RAS is presented. The test procedures were devised and the experimental results were explained.

## **Temperature Variation in Structural Fills**

The type of application determines the temperature range for which the mechanical properties of the geo-materials are investigated. For accurate characterization of mechanical properties of the compacted RAS:BA mixtures or stabilized RAS, the laboratory mechanical property tests were conducted at temperatures close to those expected in the field. The temperature range for thermo-mechanical behavior of structural fills depends on the mean annual earth temperature and the seasonal ground temperature of the locality. The earth temperature is relatively constant at depths greater than 9 m below the ground surface, and corresponds roughly to the water temperature measured in groundwater wells 9 m to 15 m deep. This temperature is referred to as mean earth temperature;  $T_m$ . Fig. 1 shows the  $T_m$  contours across the United States. The  $T_m$  varies between 3 °C in north of Minnesota to 25 °C in south of Florida. In Wisconsin where this study is conducted, the  $T_m$  varies from about 4.5 °C in Superior (north) to 10 °C in Beloit (south). The seasonal soil temperature change on either side of  $T_m$  depends on the type of soil and depth below the ground surface. Deeper soil experiences less seasonal variation in temperature than the soil in shallower depths and lags behind the seasonal changes in overlaying air temperature. At a particular location, the seasonal soil temperature change adds from -10 to +10 °C to the range of  $T_m$  as shown in Fig. 2. The temperature to which the compacted RAS:BA mixtures and stabilized RAS in embankment fills in the U.S. could be subjected ranges from -5 °C to 35 °C. In this study, however, the practical lowest test temperature is set conservatively at 5 °C.

## Materials

RAS samples were obtained from B.R. Amons & Sons Company in Elkhorn, Wisconsin. Visual inspection indicated that RAS samples were free of impurities such as wood chips, plastics, and nails. Warner (2007) concluded that RAS particles with maximum size ( $d_{max}$ ) of 10-mm, result in higher dry unit weight and higher stiffness and strength. Therefore, in this study, the RAS supply was screened to limit the  $d_{max}$  to 10-mm. Bottom ash and self-cementing (Class C) fly ash samples were obtained from Columbia Power Station in Wisconsin. Fig. 3 shows the particle size distribution curves of RAS, BA and GOS samples tested according to ASTM D 422. The majority of particles in each sample are sand size (between 0.075 mm and 4.75 mm) according to the Unified Soil Classification System (USCS). Table 1 summarizes the grain size indices and material classification according to the USCS. RAS and BA particles have almost similar grain size distributions; therefore, grain size distribution of different RAS:BA mixtures will fall within a narrow range. The specific gravity ( $G_s$ ) of RAS measured in accordance with ASTM D854 (method B) is 1.74, which is a positive attribute as a light-weight fill material. The low  $G_s$  of RAS is attributed to asphalt cement content and cellulose fiber content, which together comprise from 18 to 50% of RAS. The typical  $G_s$  of asphalt cement is between 1.02 and 1.05 (Roberts et al. 1996) and that of cellulose fiber is between 1.3 and 1.5 (Klyosov 2007). Bottom ash has the  $G_s$  of 2.67, which is comparable to  $G_s$  of outwash sand sample (2.71).

RAS particles are plate-like, irregular in shape, highly angular and have rough surface texture. The angularity of RAS particles reduces to semi-round to round as the particle size decreases. BA particles are angular to highly angular, internally porous and have rough surface texture. Some pores of the particles are filled with dust. On the other hand, particles of outwash sand are solid, semi-round to round and have smooth surface texture. Particle surfaces are clean,

shiny and free of dust (Soleimanbeigi et al. 2012). Pure RAS has a well-defined compaction curve with the maximum dry unit weight ( $\gamma_{dmax}$ ) of 11.3 kN/m<sup>3</sup> and optimum water content ( $w_{opt}$ ) of 8% (Fig. 4). The  $\gamma_d$  of the compacted RAS:BA mixture increases with increasing BA content. Although BA and outwash sand have comparable specific gravities, the high porosity of BA particles reduces the  $\gamma_{dmax}$  to 15 kN/m<sup>3</sup> which is lower than  $\gamma_{dmax}$  of typical compacted sand. As the BA content increases the  $\gamma_d$  of the mixture becomes less susceptible to water content.

## **Methods**

### ***Thermo-Mechanical Testing System***

Temperature-controlled triaxial compression, one-dimensional (1D) compression, and flexible-wall hydraulic conductivity tests were conducted. The test cells consisted of conventional cells equipped with a heating and cooling system. To uniformly change the temperature of the specimen in the triaxial compression and the hydraulic conductivity tests, a copper coil tubing (with 6 mm outside diameter) was spiraled around the specimen to circulate heated or cooled water. There is a 3.0 cm distance between the copper coil and the specimen to avoid contact during shearing in the triaxial compression tests whereas the coil was spiraled with 1.0 cm distance outside the consolidometer ring in the 1D compression tests. The heating and cooling system was designed to induce the temperature range of 5 °C to 35 °C on the specimens. The 1D compression cell consists of a 8-mm thick stainless steel consolidometer ring placed inside a polyvinyl chloride (PVC) cylinder. The consolidometer ring is 102-mm in diameter and 47-mm in height. The PVC cylinder helps minimize heat transfer from or into the specimen.

### **Heating System**

The water is heated inside a heating bath using a 250 W heater. A 12 V compact mini circulating pump, which is placed outside of the heating bath, circulates the warm water from the heating bath into the spiraled copper coil inside the test cells. Tygon plastic tubes were used to minimize temperature loss during water circulation. Temperatures in the heating bath ( $T_b$ ), in the cell chamber ( $T_c$ ), and inside the specimen ( $T_s$ ) were measured using three K-type thermocouples. To control and maintain the target temperature of the specimen, a LabView program was written to regulate the electrical power to the heater by means of a relay installed in the electrical circuit. A temperature tolerance of  $\pm 0.5$  °C was allowed. Fig. 5 illustrates the schematic of the heating system. To avoid disturbance of the specimens due to insertion of thermocouples inside them, a correlation between the temperature inside the specimen and inside the cell chamber was obtained. The required time to bring the specimen temperature,  $T_s$ , to the target temperature (i.e. 35°C) is approximately 100 min in the triaxial and one-dimensional compression tests and 240-min in the hydraulic conductivity tests due to larger diameter specimens. The target temperature of the specimen for the subsequent tests is controlled by the temperature inside the cell (see Appendix A, Fig. A-1 for the variation of  $T_b$ ,  $T_c$ , and  $T_s$ ).

### **Cooling System**

The minimum temperature considered in this study is 5 °C. The cooling bath is a PVC box filled with ice in equilibrium with water shown in Fig. 5. The target temperature of the specimen for temperatures cooler than the room temperature (i.e., 4 to 20 °C) is controlled by regulating the power supply to the circulating pump using a program written in LabView. The circulating pump is switched off if  $T_c$  is below the target temperature. A tolerance of  $\pm 0.5$  °C was allowed for  $T_c$  to reduce the number of turn-on/off of the pump. Fig. A-1 in Appendix A illustrates that the

approximate required time to bring the specimen temperature down to 5°C is 100-min in triaxial and 1D compression cells and 300-min in the permeameter.

### ***Specimen Preparation***

The specimens prepared for thermo-mechanical tests include RAS:BA mixtures and stabilized RAS with self-cementing fly ash. Table 1 summarized the testing program for all of the tests. For triaxial compression tests, each sample was compacted in five layers in a split mold with 74 mm diameter and 148 mm height at  $w_{opt}$  and 95% of standard Proctor maximum dry unit weight ( $\gamma_{dmax}$ ). The number of tamps per layer using a standard Proctor hammer was determined such that the same compaction energy as in the standard compaction effort (592 kN.m/m<sup>3</sup>) is applied to each sample mixture. Hydraulic conductivity samples were compacted in a split mold with 150 mm diameter and 116 mm height following the ASTM D 5084. For consolidation tests, each sample was compacted in three layers in the consolidometer ring at  $w_{opt}$  and 95% of  $\gamma_{dmax}$  obtained from standard Proctor compaction test. Similarly, the number of tamps per layer using a standard Proctor hammer was determined such that the same compaction energy as in the standard compaction effort is applied to each sample.

The compacted RAS:FA mixture specimens were carefully removed from their molds, wrapped using shrink wrap and cured in a 100% humidity room. Since the hydration rate of fly ash is temperature dependent, and it is intended to evaluate the effect of temperature change on mechanical behavior of stabilized RAS at considerable time after construction of structural fill, a 28-d curing period was considered to achieve the majority of hydration of the stabilized RAS specimen, conducting the mechanical tests.

## ***Test Procedure***

### **Triaxial Compression**

After assembling the temperature controlled triaxial system, each specimen was backpressure-saturated according to ASTM D4767 so that a B-value greater than 95% was attained. Following the saturation, each specimen was consolidated for 24 h under the chosen effective confining pressure (i.e.,  $\sigma'_3=35$  kPa, 70 kPa and 140 kPa) at room temperature. Due to relatively high hydraulic conductivity of both RAS:BA and stabilized RAS specimens, pore water pressure quickly dissipated when  $\sigma'_3$  was applied. The specimen volume change during consolidation phase was monitored in the backpressure burette until no significant volume change was observed. After 24-h consolidation period, the temperature of the specimen was brought to the target temperature (i.e., 5 °C or 35 °C) over 100 min. Axial loading was then carried out at an axial strain rate of 3.0%/h, which is considered to provide drained condition during loading based on comparison with similar soils as well as computations made using the pore water expulsion rate during the consolidation stage. The volume change of each specimen during shearing was recorded from the volume change of water in backpressure tubing.

To evaluate the effect of temperature change history on the stress-strain behavior, thermal cycle was also applied to each specimen. For thermal cycling tests, after consolidation for 24 h at room temperature, the temperature of each specimen was increased to 35 °C, kept constant for 48 h and then decreased to room temperature for another 24 h before shearing. The volume change of each specimen during consolidation, temperature change and shearing was also recorded.

### **One-Dimensional Compression**

The compacted RAS:BA mixtures or stabilized RAS were tested under three  $\sigma'_v$  (50 kPa, 100 kPa and 200 kPa) which represent the typical road embankment overburden pressures. The compressibility of each specimen under a given  $\sigma'_v$  was evaluated at three different temperatures, i.e. 5 °C, 20 °C and 35 °C. The loading of each specimen started from 12.5 kPa and increased at room temperature with the load increment ratio (LIR) of 1 up to the target  $\sigma'_v$  after which the temperature changed to target temperature and  $\sigma'_v$  was maintained constant for at least 10 d. The effect of thermal cycling on compressibility of the compacted RAS:BA mixtures or stabilized RAS was also evaluated. After compression at 35 °C for 10 d, the test continued for one month at room temperature and the compressibility was evaluated. To evaluate the effect of compaction and construction at warm seasons, a RAS:BA mixture was compacted at 35 °C inside the consolidometer ring and incrementally loaded (LID=1, LIR=1) from 12.5 kPa to  $\sigma'_v$  at 35 °C and then the compression test continued at room temperature.

### **Hydraulic Conductivity**

The specimens for hydraulic conductivity tests were consolidated at three levels of confining pressure (i.e.,  $\sigma'_3=35, 70,$  and 140 kPa). The specimens were backpressure-saturated using the B-test procedure according to ASTM 5084-03. To saturate the specimen, the cell pressure and backpressure were increased incrementally until the B-value over 95% was attained. Each specimen was consolidated for 24 h at room temperature after saturation. The excess pore water pressure in the compacted RAS:BA mixtures or stabilized RAS dissipates shortly after the confining pressure is applied. The volume change of each specimen was obtained by measurement of water elevation in the backpressure burette. The hydraulic gradients of 0.5 and

2.0 were respectively applied to the compacted RAS:BA mixture and stabilized RAS specimens following the recommendations per ASTM 5084-03.

## **Results and Discussion**

### ***Shear Strength***

#### **RAS Mixed with Bottom Ash**

Temperature change has negligible effect on the stress-strain and volumetric change behavior of the compacted BA. However, when the RAS content increases to 25%, the stress-strain and volumetric change behavior of the compacted RAS:BA mixture becomes sensitive to temperature change. As the specimen temperature increases from room temperature to 35 °C, the peak deviator stress,  $\sigma'_{dmax}$ , reduces and the volumetric behavior becomes more compressive. The stress-strain and volumetric change behavior of the sample sheared at 35 °C resemble those of sandy soil in loose state. The axial strain corresponding to  $\sigma'_{dmax}$  increases at increased temperature. There is no clear failure plane and the specimen bulges during shearing. On the other hand, the  $\sigma'_{dmax}$  increases and the volumetric behavior changes to dilative when the specimen temperature reduces to 5 °C. The stress-strain and volumetric change behavior resemble those of compacted sand in dense state. The shearing of the specimen occurs along a clear failure plane. The details can be viewed in Appendix A Fig. A-2 to Fig. A-4.

Fig. 6 shows the variation of normalized strength,  $\sigma'_{dft}$ , (i.e. deviatoric stress at failure normalized with respect to that at 20 °C) of RAS:BA mixtures with temperature. The sensitivity of  $\sigma'_{dft}$  with respect to temperature change is higher at lower temperatures than room temperature. The sensitivity of  $\sigma'_{dft}$  with temperature change also increases with increasing RAS content in the mixture as expected. However, the variation of  $\sigma'_{dft}$  with temperature does not

seem to follow a clear trend with stress level. As temperature rises from 20 °C to 35 °C, the  $\sigma'_{\text{eff}}$  is reduced, on average, by 10% for the RAS:BA mixture with 25% RAS content, and by 20% for RAS:BA mixture containing 50% RAS. The effective friction angle ( $\phi'$ ) of the RAS:BA mixtures at different temperatures were obtained from the Mohr-Coulomb failure envelope and presented in Fig. 7 (a) along with the friction angle of BA not mixed with RAS. These mixtures did not have a cohesion intercept. The  $\phi'$  of the compacted RAS:BA mixtures decreases with temperature. While the  $\phi'$  of bottom ash is almost insensitive to temperature change, the  $\phi'$  of the mixture containing 25% RAS is reduced from 41° to 36° and of the mixture containing 50% RAS is reduced from 41° to 29° when the temperature rises from 5 °C to 35 °C. To obtain a design graph for practical use, the  $\phi'$  at different temperatures were interpolated from Fig. 7 (a) and presented in Fig. 7 (b). The increase of RAS content makes the  $\phi'$  of the mixture more sensitive to temperature change. As the temperature increases, the variation of  $\phi'$  with RAS content becomes more pronounced. At T=35 °C, when the RAS content increases from 0 to 50%, the  $\phi'$  of the RAS:BA mixture reduces from 44° to 29° reflecting 27% reduction while at T=5°C the  $\phi'$  of the mixture reduces from 44° to 41° which reflects only 7% reduction. In general, reduction in  $\phi'$  of compacted RAS:BA mixtures due to seasonal temperature change in the U.S. does not appear to endanger stability of the typical highway embankments containing RAS.

Change in stress-strain, volumetric, and strength behavior of RAS:BA mixture at different temperatures is attributed to change of viscosity of asphalt binder in RAS particles. The viscosity of asphalt binder in RAS reduces with increasing temperature (Frigio et al. 2011; ASTM D2493). Consequently, the deformability of the asphalt binder on the contact surfaces between individual RAS particles and also between RAS and BA particles increases resulting in higher shearing at the contact surface under a given deviatoric stress increment. Reduction of

viscosity of asphalt binder also increases compressibility of individual RAS particles. Increased deformability of the particles and larger shear strain at the contact surface between RAS and BA particles reduces tendency of the particles to roll over each other during shearing and therefore the volumetric change tends to exhibit contractive behavior. On the other hand, the viscosity of asphalt binder in RAS particles increases when the temperature is reduced. Consequently, the deformability of RAS particles as well as the shear strain along the contact surface between RAS and BA particles decreases when the specimen undergoes shear stress. With increased stiffness of the RAS particles at reduced temperature, the particles tend to roll over each other during shearing, exhibiting a dilative behavior.

### **RAS Stabilized with Fly Ash**

The effect of temperature change on  $\phi'$  and cohesion intercept ( $c'$ ) of stabilized RAS with 20% self-cementing fly ash is illustrated in Fig. 8 (a). The  $\phi'$  noticeably reduces from  $46^\circ$  to  $26^\circ$  (43%) when the temperature increases from  $5^\circ\text{C}$  to  $35^\circ\text{C}$ , however, the  $c'$  increases from 44 kPa to 71 kPa. The reduction in  $\phi'$  is attributed to reduction in  $\sigma'_{df}$  due to increased deformability of RAS component in the stabilized RAS specimen at increased temperature as illustrated in Appendix A Fig. A-5. The increase of  $c'$  is possibly due to accelerated hydration of self-cementing fly in the compacted RAS:FA mixture which creates stronger bond between the RAS particles at higher temperature. The acceleration of hydration process of self cementing fly ash at elevated temperature was verified elsewhere (ASTM C 593).

During drained shear failure of each compacted RAS:BA or stabilized RAS specimen in triaxial cell, no pore water pressure was developed and the  $\sigma'_3$  is constant . Therefore, the

compressive strength of the compacted RAS:BA mixtures or stabilized RAS may be obtained from the Mohr-Coulomb failure criterion as:

$$\sigma'_{df} = \frac{2c' \cos \phi' + 2\sigma'_3 \sin \phi'}{1 - \sin \phi'} \quad (1)$$

In which  $\phi'$  for the compacted RAS:BA mixtures is obtained from Fig. 7 (b) and  $c'$  and  $\phi'$  for the stabilized RAS is obtained from Fig. 8 (a). Fig. 8 (a) also compares the compressive strength ( $\sigma'_{df}$ ) of stabilized RAS with that of a natural granular material (in this study glacial outwash sand) at different temperatures at  $\sigma'_3=70$  kPa. Although the  $\sigma'_{df}$  of the stabilized RAS exhibits 40% reduction from 580 kPa to 340 kPa due to increasing temperature from 5 °C to 35 °C, the  $\sigma'_{df}$  remains consistently higher than that of the sand. The variation of  $\sigma'_{df}$  with temperature of glacial sand is almost negligible. The reduction in  $\phi'$  due to temperature rise, reduces  $\sigma'_{df}$  more noticeably at higher stress level ( $\sigma'_3=140$  kPa) than lower stress level ( $\sigma'_3=35$  kPa) as shown on Fig. 8 (b) as the variation of  $\sigma'_{ndf}$  ( $\sigma'_{df}$  of stabilized RAS normalized to  $\sigma'_{df}$  of outwash sand) with temperature. The  $\sigma'_{ndf}$  linearly reduces with temperature at the same rate under different stress levels. The shear strength of stabilized RAS is therefore sufficient for application in typical structural fill at different climate in North America.

### **Effect of Thermal Cycle on the Stress-Strain Behavior**

The reduction of viscosity of asphalt binder in RAS particles was considered the main contributing factor to increased deformation of compacted RAS:BA mixture when the temperature increased. As shown in Appendix A Fig. A-2, the volumetric change behavior of

compacted RAS:BA mixture at increased temperature is compressive. Therefore, the compacted RAS:BA material experiencing an increase in temperature should have lower void ratio under applied compressive stresses resulting in higher shear strength and stiffness when the temperature is reduced to room temperature compared to a specimen compressed in isothermal condition. Fig. 9 (a) shows the permanent volume reduction of a specimen isotropically compressed at 35 °C for 48 hours. The reduction in void ratio resulted in an increased stiffness and strength ( $\sigma'_{df}$ ) of the specimen compared to those of the specimen compressed at constant room temperature [Fig. 9 (b)]. The practical implication of this behavior is that the RAS:BA embankment fill compacted and came to equilibrium with the operating stresses at warm temperatures will exhibit higher shear strength and stiffness during mild and cold seasons. In this respect, construction of embankments containing RAS during cold seasons of the year is not recommended because it will lead to greater changes in stiffness and strength as the temperature rises.

### **Modeling of Stress-Strain Behavior**

The nonlinear stress-strain curves of both clay and sand have been successfully approximated with a high degree of accuracy by a simplified and practical hyperbolic model (Kondner and Zelasko 1963; Duncan and Chang 1970). The hyperbolic relationship between the deviatoric stress and axial strain is represented by:

$$\frac{\varepsilon_a}{\sigma'_d} = \frac{1}{E_i} + \frac{\varepsilon_a}{\sigma'_{d,ult}} \quad (2)$$

where  $\sigma'_{d,ult}$  is the asymptotic value of  $\sigma'_d$  which is related to  $\sigma'_{df}$  by means of a factor  $R_f$  defined as:

$$R_f = \sigma'_{df} / \sigma'_{d,ult} \quad (3)$$

and  $E_i$  is the initial stress dependent tangent modulus of soil expressed as:

$$E_i = \kappa p_a \left( \frac{\sigma_3}{p_a} \right)^\eta \quad (4)$$

where  $\kappa$  is the modulus number,  $\eta$  is the modulus exponent and  $p_a$  is the atmospheric pressure.

To characterize Eq. (4),  $\varepsilon_a / \sigma'_d$  is plotted versus  $\varepsilon_a$ . The  $E_i$  and  $\sigma'_{d,ult}$  are obtained from the intercept and slope of the best fitted line to the data points. Parameters  $\kappa$  and  $\eta$  are readily obtained by plotting the values of  $E_i$  against  $\sigma'_c$  on log-log scale and fitting a straight line to the data. The hyperbolic model parameters of RAS:BA mixtures are given in Appendix A Table A-1. The hyperbolic model allows the prediction of expected systematic change in  $E_i$  and  $\sigma'_{df}$  with temperature change and can be used in numerical analyses of embankments constructed of RAS containing materials. Fig. 10 (a) shows the linear variation of  $E_i$  obtained from hyperbolic model with  $\sigma'_3$  in a log-log scale. The slope of the line ( $\eta$ ) increases and the intercept of the line with  $\sigma'_3$  of unity ( $\kappa$ ) decreases with increasing RAS content indicating that  $E_i$  decreases and becomes more sensitive to  $\sigma'_3$  when RAS content increases. Fig. 10 (b) shows the variation of  $\kappa$  and  $\eta$  with temperature. Similarly,  $\eta$  increases and  $\kappa$  decreases with increasing temperature indicating that  $E_i$  of the mixture reduces and becomes more sensitive to  $\sigma'_3$  with increasing temperature. The hyperbolic model parameters were used to predict the experimental stress-strain data [Fig. 10 (c) and Fig. A-5]. The hyperbolic model represents the stress-strain data of the compacted RAS:BA mixtures and stabilized RAS reasonably well up to the  $\sigma'_{dmax}$ . To predict the compressive strength using the hyperbolic model, the axial strain at failure,  $\varepsilon_f$ , for each specimen compressed at a given  $\sigma'_3$  and sheared at different temperatures were measured and presented in Fig. A-6. As illustrated, the  $\varepsilon_f$  increases with increasing RAS content,  $\sigma'_3$  and temperature.

Having  $\varepsilon_f$ , the compressive strength (i.e.  $\sigma'_{df}$ ) of compacted RAS:BA mixture is obtained from Eq. (2) and the effective friction angle is obtained from Eq. (1).

## ***One-Dimensional Compression***

### **RAS Mixed with Bottom Ash**

Fig. 11 presents the variation of vertical strain ( $\varepsilon_v$ ) with time of the compacted RAS:BA mixtures compressed under  $\sigma'_v = 200$  kPa at different temperatures. After 24 h compression at room temperature, the specimen heated to 35 °C, exhibits higher vertical strain and strain rate than the replicate specimen compressed at room temperature (22 °C). The increase of  $\varepsilon_v$  with time significantly slows down when the temperature of the specimen is reduced 5 °C. As mentioned in the triaxial compression test section, change of viscosity of asphalt binder in RAS particles with temperature is considered to be the major controlling factor in deformational behavior of RAS:BA mixtures at elevated temperatures.

Fig. 12 shows that logarithm of vertical strain rate ( $\dot{\varepsilon}_v$ ) linearly varies with temperature for compacted RAS:BA specimens. The slope of the line is independent of stress level and elapsed time after the start of temperature change as illustrated in Figs. 12 (a) and (b). The slope of the line is defined as thermal coefficient of compression and denoted as  $C_{T\varepsilon}$ . The unit of  $C_{T\varepsilon}$  is one per second-degree Celsius [ $1/t$  °C]. Since  $C_{T\varepsilon}$  is independent of time and stress level, it may be regarded as an inherent property of the material. Fig. 12 (c) shows that  $C_{T\varepsilon}$  varies with RAS content in the mixture and increases with increasing RAS content. The equation of the fitting line is therefore given by:

$$\frac{d\varepsilon}{dt} = \dot{\varepsilon} = Ae^{C_{T\varepsilon}T} \quad [5]$$

$$\text{or } \frac{d \ln \dot{\varepsilon}}{dT} = C_{T\varepsilon} \quad [6]$$

The modified secondary compression index is most commonly defined as:

$$C_{\alpha\varepsilon} = \frac{d\varepsilon}{d \log t} \quad [7]$$

where  $t$  is the elapsed time. From Eq. (7), the strain rate is obtained as:

$$\dot{\varepsilon} = \frac{C_{\alpha\varepsilon} \ln 10}{t} \quad [8]$$

By substitution of Eq. (8) into eq. (6):

$$\frac{\Delta \ln \frac{C_{\alpha\varepsilon} \ln 10}{t}}{\Delta T} = C_{T\varepsilon} \rightarrow \ln \frac{C_{\alpha\varepsilon} \ln 10}{t} \Big|_T - \ln \frac{C_{\alpha\varepsilon} \ln 10}{t} \Big|_{T_0} = C_{T\varepsilon} \Delta T \rightarrow \ln \left( \frac{C_{\alpha\varepsilon, T}}{C_{\alpha\varepsilon, T_0}} \right) = C_{T\varepsilon} \Delta T$$

Therefore:

$$C_{\alpha\varepsilon, T} = \frac{d\varepsilon}{d \log t} \Big|_{T_0} e^{C_{T\varepsilon} \Delta T} \quad [9]$$

Eq. (9) indicates that secondary compression ratio ( $C_{\alpha\varepsilon}$ ) of RAS:BA mixture is an exponential function of temperature change. To assess how well Eq. (9) captures the experimental data, the measured  $C_{\alpha\varepsilon}$  for RAS:BA mixtures compressed at elevated temperatures along with  $C_{\alpha\varepsilon}$  calculated from Eq. (9) are plotted in Fig. 13. There is good agreement between measured and calculated  $C_{\alpha\varepsilon}$ .

The modified secondary compression indices for compacted RAS:BA mixtures compressed at elevated temperatures were calculated for over 10 days following the 24 h compression period under a given  $\sigma'_v$ . Fig. 14 illustrates the variation of  $C_{\alpha\varepsilon}$  with temperature for RAS:BA specimens compressed under different  $\sigma'_v$ . The response is consistent with the exponential function of temperature given in Eq. (9). Under a given temperature, the  $C_{\alpha\varepsilon}$  increases with increasing  $\sigma'_v$ . It appears that increasing  $\sigma'_v$  increases the micro shear stresses along the contact surface between RAS and BA particles, which in turn accelerates the shear

strain along the surface, resulting in increasing  $C_{\alpha\varepsilon}$ . To obtain a practical graph for design purpose,  $C_{\alpha\varepsilon}$  at intermediate temperatures were interpolated from the  $C_{\alpha\varepsilon}$ -T curves given in Fig. 14 and plotted in Fig. 15. The graphs in Fig. 15 may be used in design practice to determine the required RAS content in the RAS:BA mixture corresponding to a desired  $C_{\alpha\varepsilon}$  and an elevated temperature.

Fig. 16 shows the compression curve of a RAS:BA specimen with 20% RAS, compacted at 35 °C in the consolidometer ring and incrementally loaded to  $\sigma'_v=200$  kPa at 35 °C. After compression for 24 h under  $\sigma'_v=200$  kPa, the temperature was reduced to room temperature and compression continued. The measured  $C_{\alpha\varepsilon}$  is 0.0004 which is significantly lower than the corresponding  $C_{\alpha\varepsilon}$  of an identical specimen compressed at room temperature throughout the test. As shown in Fig. 16, under each incremental  $\sigma'_v$ , the specimen compressed at higher temperature exhibits higher vertical strain than the specimen compressed at room temperature. Therefore the specimen compressed at higher temperature has lower void ratio compared to the specimen compressed at room temperature. The temperature rise induced thermal preloading to the compacted RAS:BA mixture and reduced the  $C_{\alpha\varepsilon}$  to as low as that for Wisconsin outwash sand (Table 2). The practical implication of this behavior is in compaction and construction of RAS containing embankments in warm seasons of the year. During construction at higher temperature, the void ratio of the RAS containing fill reduces at higher rate and therefore negligible settlement is expected during the following seasons.

### **RAS Stabilized with Fly Ash**

Three stabilized RAS specimens were first compressed at room temperature for 24 h under  $\sigma'_v=200$  kPa. The compression of the specimens then continued at three different temperatures,

i.e. 5, 22, and 35 °C for 10 days. Fig. 17 (a) shows the compression curves. The vertical strain at 5 °C and 22 °C is fairly constant with logarithm of time after 24 h. However, at 35 °C the vertical strain rapidly increases when the temperature increases and eventually becomes constant. Unlike the compacted RAS:BA mixture for which the  $\log(\epsilon)$ -T relationship was linear at different time, the variation of  $\log(\epsilon)$ -T for fly ash stabilized RAS is only linear for the  $\epsilon$  immediately after temperature change as indicated in Fig. 18 (b). The coefficient of thermal creep,  $C_{T\epsilon}$ , is 0.168. The  $C_{\alpha\epsilon}$  calculated using Eq. (9) with this  $C_{T\epsilon}$  agrees well with the experimental data at time immediately after temperature change.

To evaluate possible thermal preconsolidation on stabilized RAS, the compression of the specimens after 10 days of compression at 22 °C and 35 °C were continued at 22 °C for another 5 weeks. The  $C_{\alpha\epsilon}$  of the specimen which experienced temperature rise, reduced to 0.0002 which reflects 8 times reduction compared to  $C_{\alpha\epsilon}$  of the specimen compressed at constant room temperature during the test. The temperature rise induced thermal preloading to the compacted stabilized RAS and reduced the  $C_{\alpha\epsilon}$  to as low as that for Wisconsin outwash sand (Table 2).

### ***Hydraulic Conductivity***

Fig. 18 shows that the hydraulic conductivity of the compacted RAS:BA mixture and stabilized RAS generally increases with temperature. The hydraulic conductivity of the compacted RAS:BA mixture compressed at  $\sigma'_3=70$  kPa increases from  $9 \times 10^{-4}$  cm/s to  $1.3 \times 10^{-3}$  cm/s which reflects 40% increase while the hydraulic conductivity of stabilized RAS increases from  $2.6 \times 10^{-4}$  cm/s to  $4.8 \times 10^{-4}$  cm/s reflecting 85% increase. Two mechanisms are assumed to be involved. First, the change in viscosity of circulating water with temperature and second, the change in

void ratio of the specimen due to deformability of RAS particles containing viscous asphalt binder.

The hydraulic conductivity of a porous medium is separated into the product of two multiples, one reflecting property of the porous medium and one reflecting fluid properties:

$$K = k \frac{\rho g}{\mu} \quad (10)$$

Where  $K$  is the hydraulic conductivity of the porous medium,  $k$  is the intrinsic permeability of the porous medium,  $\rho$  is density of water,  $\mu$  is the viscosity of water and  $g$  is the gravitational acceleration. To verify the first assumption, variation of water density and viscosity with temperature is considered in the range of 5 °C to 35 °C. Water density is reduced slightly (0.8%) while water viscosity is reduced by 50% (see Appendix A Fig. 9). Assuming there is no change in intrinsic permeability with temperature, the ratio of hydraulic conductivity at elevated temperature to the hydraulic conductivity at room temperature ( $K_o$ ) is obtained from:

$$\frac{K}{K_o} = \frac{\rho}{\rho_o} \cdot \frac{\mu_o}{\mu} \quad (11)$$

where  $\rho_o$  is the water density and  $\mu_o$  is the water viscosity at room temperature. The normalized measured hydraulic conductivity of RAS:BA specimens along with Eq. (11) are plotted in Fig. 19. The deviation of data points from the curve reflects the effect of change in void ratio on the hydraulic conductivity due to temperature change. Fig. 19 At temperatures higher than the room temperature the reduction in void ratio has a decreasing effect on the hydraulic conductivity while at temperatures lower than the room temperature the increase in void ratio has increasing effect. The intrinsic permeability is generally related to porosity and average pore or particle diameter. Fig. 20 shows that the volumetric strain (or void ratio) of each specimen decreases with increasing temperature. However, since the hydraulic conductivity generally increases with

temperature, the reduction in void ratio, shown in Fig. 20, is not a dominant factor in variation of hydraulic conductivity of RAS:BA or stabilized RAS with temperature. Therefore, the reduction of viscosity of permeating water is the major contributing factor to increased hydraulic conductivity of the compacted RAS:BA mixture or stabilized RAS.

## **Summary and Implication**

The effect of seasonal temperature change typically observed in the field on geotechnical properties of compacted RAS:BA mixture and stabilized RAS with Class C fly ash was evaluated. The range of temperature considered herein encompasses the extreme seasonal temperature change observed in North America.

The shear strength of both compacted RAS:BA mixture and stabilized RAS consistently decreases with increasing temperature. As the RAS content in the RAS:BA mixture increases the temperature change has more pronounced effect on the shear strength of the mixture. However, shear strength of the embankment fills constructed with the compacted RAS:BA mixtures (with RAS content no more than 50%) or stabilized RAS with 20% self-cementing fly ash remains within the range sufficient to provide stability of the typical road embankment fill in the climate ranges of North America (i.e., up to 35 °C fill temperatures).

Temperature change, on the other hand, has significant and limiting impact on compressibility of the compacted RAS:BA mixture and stabilized RAS with self-cementing fly ash. The secondary compression index increases exponentially with temperature. During the cold seasons (temperatures lower than 10 °C), the compression of the RAS:BA mixture or stabilized RAS is comparable to that of natural granular material and is practically negligible. However, the compressibility exponentially increases during warm seasons (when the temperature rises to 20

to 35 °C). This indicates that an embankment fill containing RAS or stabilized RAS constructed during the cold to mild seasons of the year may exhibit significant settlement during the warm season. In any region in North America, if the embankment is constructed during the warm season, the majority of the compression will occur during construction and negligible settlement can be expected in the seasons following the warm season. The design graphs were developed to predict subsequent settlement of an embankment constructed at a temperature around 20 °C as a function of RAS content, temperature and stress levels for RAS:BA mixtures. In using the design graph, one may meet the design specifications for the maximum allowable settlement of a road embankment (such as required by a state transportation agency).

The hydraulic conductivity of the RAS:BA mixture or stabilized RAS provides adequate drainage capacity for the embankment fill. The drainage capacity of the material increases with temperature due to reduction in water viscosity.

Previous research results showed that compressibility of the BA is greater than natural sand. The acceptable BA content of the compacted RAS:BA mixture can be safely replaced by natural granular material content and the results and design graphs obtained herein can be used conservatively for the compacted RAS mixtures with sands and gravels. The results obtain in this research is also specific to the type and maximum particle size of the recycled asphalt shingles used.

## **Conclusions**

On the premise that recycled asphalt shingles (RAS) are too compressible for use as structural fill material led to an investigation of mixing RAS with a less compressible materials such as bottom ash (BA) or stabilize with a self-cementing fly ash. Such improvement resulted in

acceptable structural fill behavior at moderate temperatures. The effect of temperature change on mechanical properties of these improved mixtures is evaluated herein. A thermo-mechanical system including temperature-controlled triaxial compression cell, temperature-controlled one-dimensional compression cell and temperature-controlled permeameter was developed and the test procedures were devised to closely simulate the field conditions in the laboratory. Based on the test results the following conclusions were made:

- 1- The shear strength of RAS:BA mix and stabilized RAS decreases with temperature. However, the reduction of shear strength due to seasonal temperature change in the U.S. does not endanger stability of typical highway embankments. The hyperbolic model represents the stress-strain data of RAS:BA mix and stabilized RAS well up to the maximum deviator stress.
- 2- The vertical strain and strain rate in one-dimensional compression increases with temperature. The coefficient of thermal compression, defined as the slope of the log of strain rate with temperature, is an inherent property of the material and is independent of time and stress level. Secondary compression index of RAS:BA mixture and FA stabilized RAS is an exponential function of temperature change. The design graphs indicating variation of secondary compression rate with RAS content, temperature and stress level were developed to select suitable RAS content in a mixture with a granular material like bottom ash under a given stress level and temperature.
- 3- Hydraulic conductivity of RAS:BA mixture and stabilized RAS increases with temperature. The increase of hydraulic conductivity is mostly due to reduction of water viscosity with temperature. However, there is no concern regarding drainage capacity of RAS:BA or FA stabilized RAS at elevated temperatures.

## Acknowledgment

Funding for this research was provided by the recycled material resource center (RMRC) and Solid Waste Research Program (SWRP) at the University of Wisconsin-Madison. Authors also greatly appreciate B.R. Amon & Sons, Inc. to provide samples of recycled asphalt shingles for this research.

## References

- Abdel-Hadi, O.N. and Mitchell, J.K. (1981). "Coupled Heat and Water Flows around Buried Cables." *Journal of Geotechnical Engineering, ASCE*, Vol. **107**, pp. 1461–1487.
- Abuel-Naga, H. M., Bergado, D. T., and Lim, B. F. (2007). "Effect of temperature on shear strength and yielding behavior of soft Bangkok clay", *Soils and Foundations*, Vol. 47, No. 3, pp. 423-436.
- Baldi, G., Hueckel, T., and Pellegrini, R. (1988). "Thermal volume change of the mineral-water system in low porosity clay soil.", *Canadian Geotechnical Journal*, Vol. 25, pp. 807-825.
- Bruyn, D.D. and Thimus, J. F. (1996). "The influence of temperature on the mechanical characteristics of Boom clay: The results of an initial laboratory program", *Engineering Geology*, Vol. 41, pp. 117-126.
- Campanella, R.D., and Mitchell, J. K. (1968). "Influence of temperature variations on soil behavior." *Journal of the Soil Mechanics and Foundations Division, ASCE*, Vol. 94, No. SM3, pp. 709-734.
- Delage, P., Sultan, N., and Cui, Y. J. (1999). "On the thermal consolidation of Boom clay", *Canadian Geotechnical Journal*, Vol. 37, pp. 343-354.
- Demars, K. R. and Charles, R. D. (1982). "Soil volume changes induced by temperature cycling", *Canadian Geotechnical Journal*, Vol. 19, pp. 188-194.
- Duncan J. M. and Chang, C. Y. (1970). "Nonlinear analysis of stress and strain in soils" *Journal of Soil Mechanics and Foundation Engineering Division*, Vol. 96, SM5, pp.1629-1651.

- Edil, T., Benson, C., Bin-Shafique, M., Tanyu, B., Kim, W., and Senol, A. (2002). "Field evaluation of construction alternatives for roadway over soft subgrade," *Transportation Research Record*, 1786, Transportation Research Board, National Research Council, Washington, DC, pp. 36-48.
- Frigio, F., Tabatabaee, N., and Bahia, H. (2011). "Estimating the effect of RAP, RAS, and warm mix additives on high temperature viscosity of blended binders." *Transportation Research Board* (Submitted).
- Fox, P. J. and Edil, T.B. (1996). "Effects of stress and temperature on secondary compression of peat." *Canadian Geotechnical Journal*, Vol. 33, pp. 405-415.
- Geo4VA (2011). Earth Temperature and Site Geology. Virginia Tech, <http://www.geo4va.vt.edu/A1/A1.htm>, Accessed February 2011.
- Gera, F., Hueckel, T. and Peano, A. (1996). "Critical issues in modeling of the long-term hydro-thermal performance of natural clay barriers." *Engineering Geology*, Vol. 41, pp. 17 – 33.
- Graham, J., Tanaka, N., Crilly, T., and Alfaro, M. (2001). "Modified Cam-Clay modeling on temperature effects in clay.", *Canadian Geotechnical Journal*, Vol. 38, pp. 608-621
- Houston, S. L., Houston, W. N. and Williams, N. D. (1985). "Thermo-mechanical behavior of seafloor sediments", *Journal of Geotechnical Engineering, ASCE*, Vol. 111, pp. 1249-1263.
- Huang, H. W. (1990). "The Use of Bottom Ash in Highway Embankments, Subgrade, and Subbases." *Joint Highway Research Project, Final Report*, FHWA/IN/JHRP-90/4, Purdue Univ., West Lafayette, IN.
- Klyosov A.A. (2007). *Wood-plastic composites*. John Wiley & Sons, Inc. Hoboken, NJ.
- Kondner R. L., Zelasko J. S. (1963). "A hyperbolic stress-strain formulation for sand." *2nd Pan-American Conference on Soil Mechanics and Foundation Engineering Division*, Brazil, pp. 289-324.
- Krivit, D. (2007). *Recycling of Tear-Off Shingles: Best Practices Guide*. Final report prepared for the Construction Materials Recycling Association (CMRA).
- Laloui L, Cekerevac C, and Vulliet L. (2001). "Thermo-mechanical modeling of the behaviour of MC clay." *In: Desai CD, editor. Computer methods and advances in geomechanics. Balkema*, pp. 829–35.
- Laloui, L. and Cekerevac, C. (2003). "Thermo-plasticity of clays: An isotropic yield mechanism", *Computers and Geotechnics*, Vol. 30, pp. 649-660.

- Mitchell, J. K. (1969). "Temperature effects on engineering properties and behavior of soils." *Highway Research Board*, Special Report No. 103, Washington, DC, pp. 9-28.
- Mitchell, J. K. and Soga, K. (2005). *Fundamentals of soil behavior*. John Wiley & Sons, Inc., New York.
- Mitchell, J. K., McMillan, J. C., Green, S. L., Sisson, R. C. (1982). "Field testing of cable backfill systems." In: *Boogs SA, et al., editors. Underground cable thermal backfill*. New York: Pergamon Press; pp. 19-33.
- Virdi, S.P.S. and Keedwell, M.J., (1988). "Some observed effects of temperature variation on soil behaviour." In: M. J. Keedwell (Editor), *International Conference on Rheology and Soil Mechanics*, Coventry, Elsevier Applied Science Publishers, London, pp. 336-354.
- Roberts, F. L., Kandhal, P. S., Brown, E. R., Lee, D. Y. and Kennedy, T. W. (1996). *Hot Mix Asphalt Materials, Mixture Design, and Construction*. National Asphalt Paving Association Education Foundation. Lanham, MD.
- Leroueil, S. and Marques, M.E.S. (1996). "State of the art; Importance of strain rate and temperature effects in Geotechnical Engineering", *Measuring and Modeling Time Dependent Soil Behavior, Geotechnical Special Publication No. 61, ASCE*, pp. 1-60.
- Soleimanbeigi, A., Edil, T., and Benson, C. (2011). "Recycled asphalt shingles mixed with granular byproducts as structural fill", *Journal of ASTM International*, Vol. 9, No. 1.
- Yoon, S., Balunaini, U., Yildirim, I. Z., Prezzi, M. and Siddiki, N. Z. (2009). "Construction of an embankment with a fly and bottom ash mixture: Field performance study." *Journal of Material in Civil Engineering, ASCE*, Vol. 21, No. 6, pp. 271-278.

Table 1-Thermal test program for mechanical properties of RAS:BA mixture and stabilized RAS

Type of test	Material	$\sigma'_3$ or $\sigma'_v$ (kPa)	T (°C)	# of tests
Triaxial Compression	RAS:BA (50:50)	35, 70, 140	5, 20, 35	12
	RAS:BA (25:75)	35, 70, 140	5, 20, 35	12
	RAS:BA (0:100)	35, 70, 140	5, 35	6
	RAS:FA (80:20)	35, 70, 140	5, 20, 36	12
1D Compression	RAS:BA (50:50)	50, 100, 200	5, 20, 35	9
	RAS:BA (25:75)	50, 100, 200	5, 20, 35	9
	RAS:BA (0:100)	50, 200	5, 35	4
	RAS:FA (80:20)	50, 200	5, 20, 35	6
Hydraulic Conductivity	RAS:BA (50:50)	50, 100, 200	5, 20, 35	9
	RAS:FA (80:20)	50, 100, 200	5, 20, 35	9

Table 2- Secondary compression ratio of different materials

Material	$C_{\alpha\alpha}$
Clay	0.01
Stabilized RAS	0.003
Stabilized RAS (thermally precompressed)	0.0002
Wisconsin outwash sand	0.0003

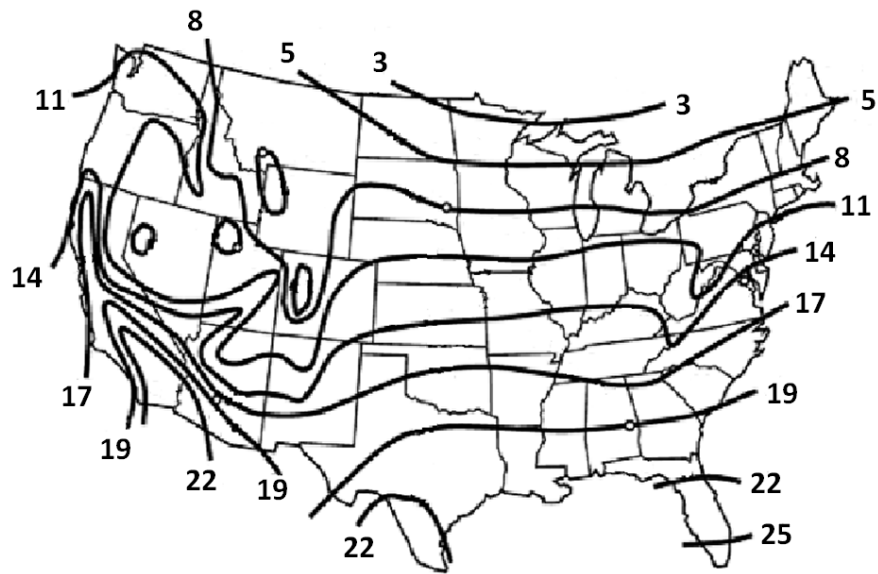


Fig. 1- Mean annual earth temperature observations [ $^{\circ}$ C] in U.S. (Geo4VA, 2011)

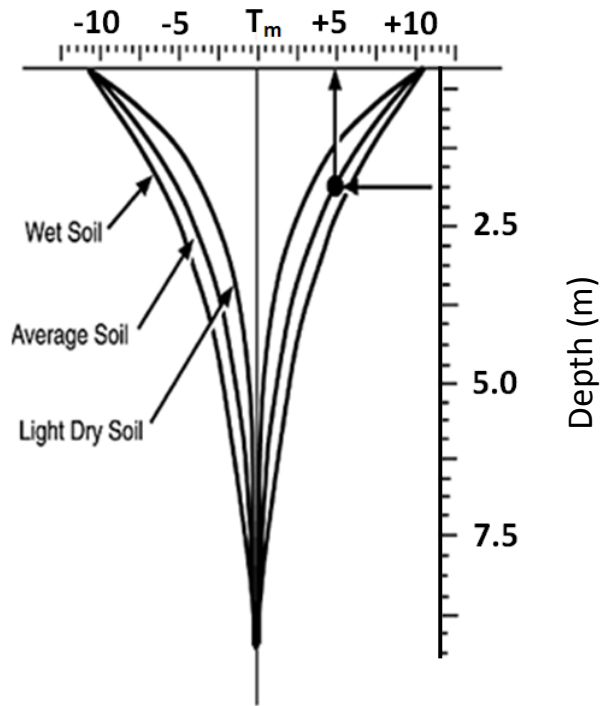


Fig. 2- Seasonal soil temperature change as a function of depth below ground surface (Geo4VA, 2011)

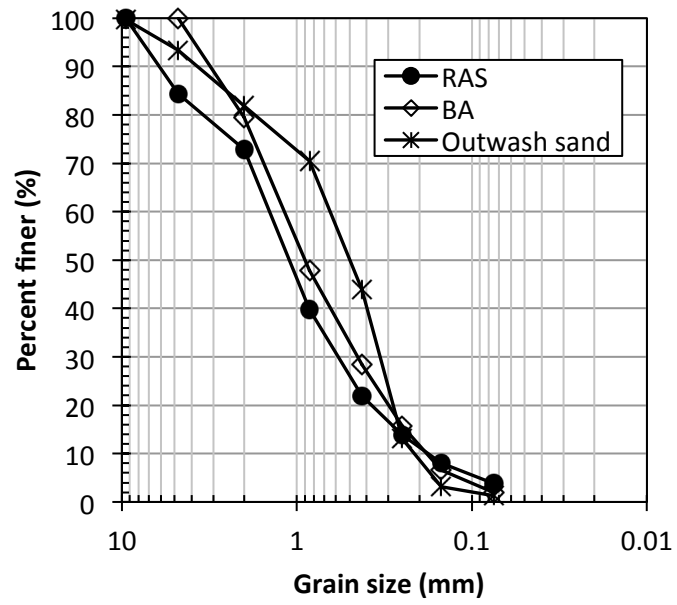


Fig. 3- Grain size distribution of RAS, BA and outwash sand

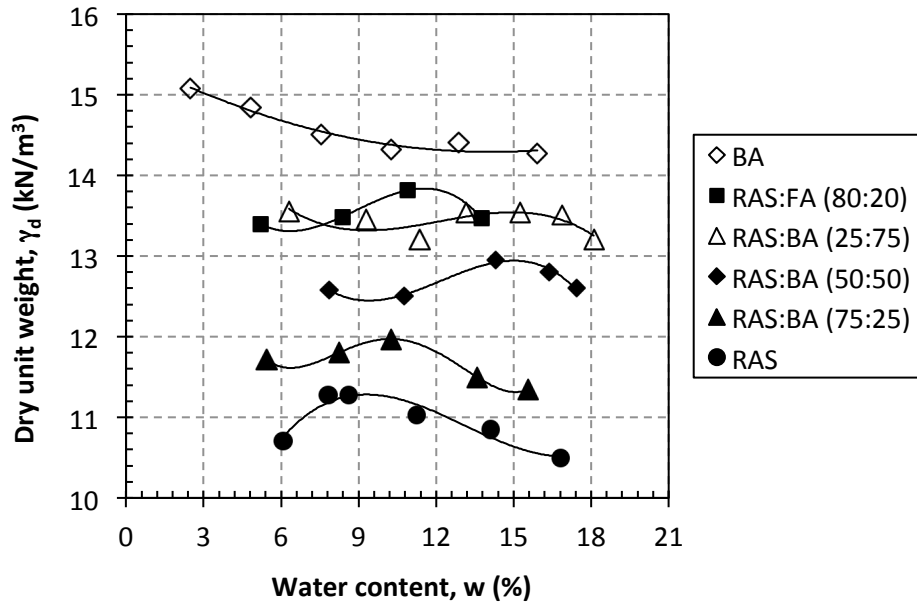


Fig. 4- Compaction curves of RAS:BA and stabilized RAS

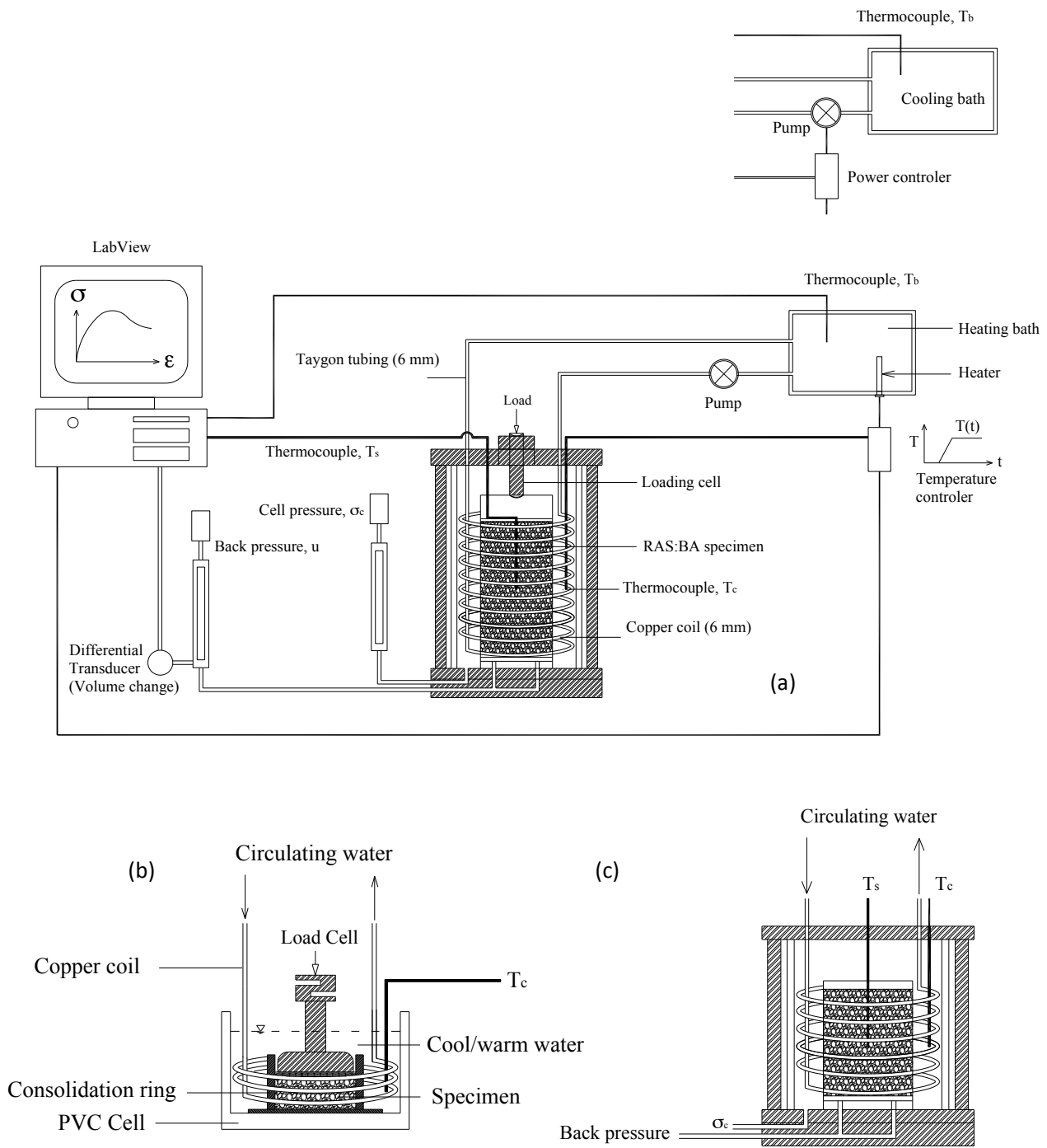


Fig. 5-Thermo-mechanical system: (a) temperature controlled triaxial cell (b) temperature controlled 1D compression cell and (c) temperature controlled permeameter

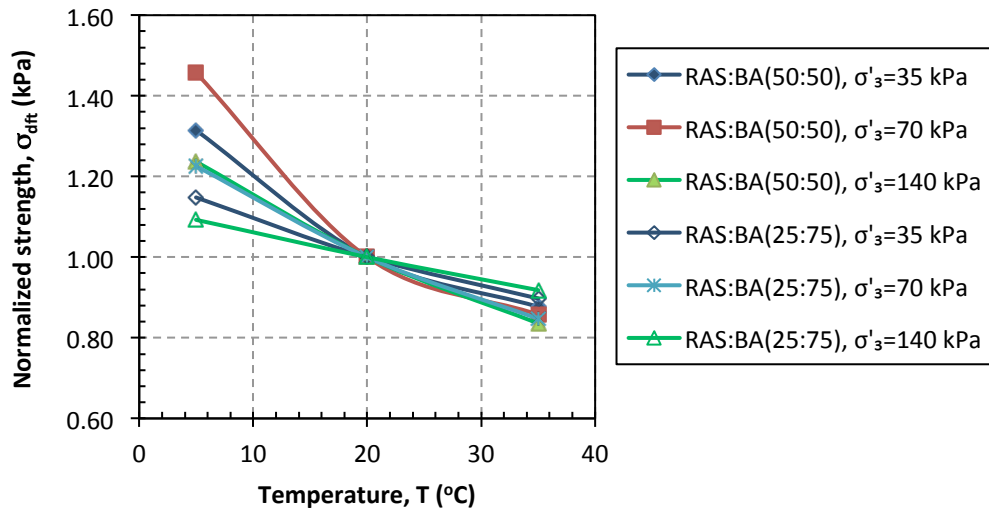


Fig. 6- Variation of normalized strength of RAS:BA mixtures at different temperatures

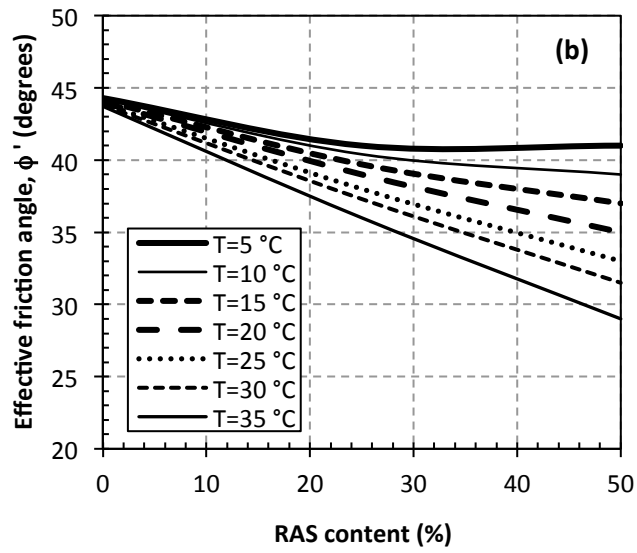
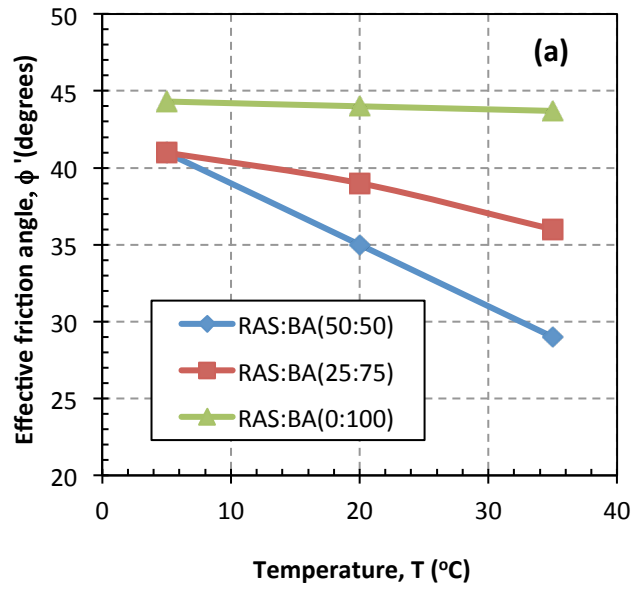


Fig. 7- Variation of effective friction angle with temperature (a) and with RAS content (b) of RAS:BA mixtures

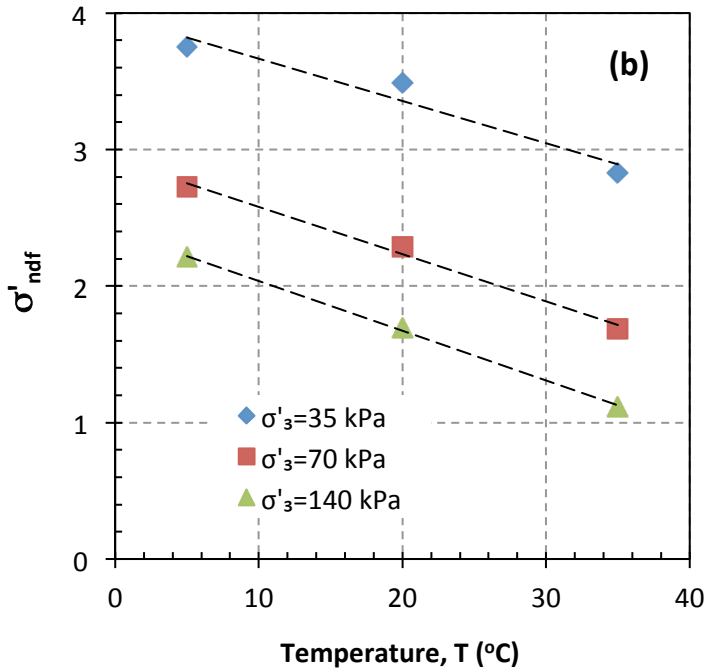
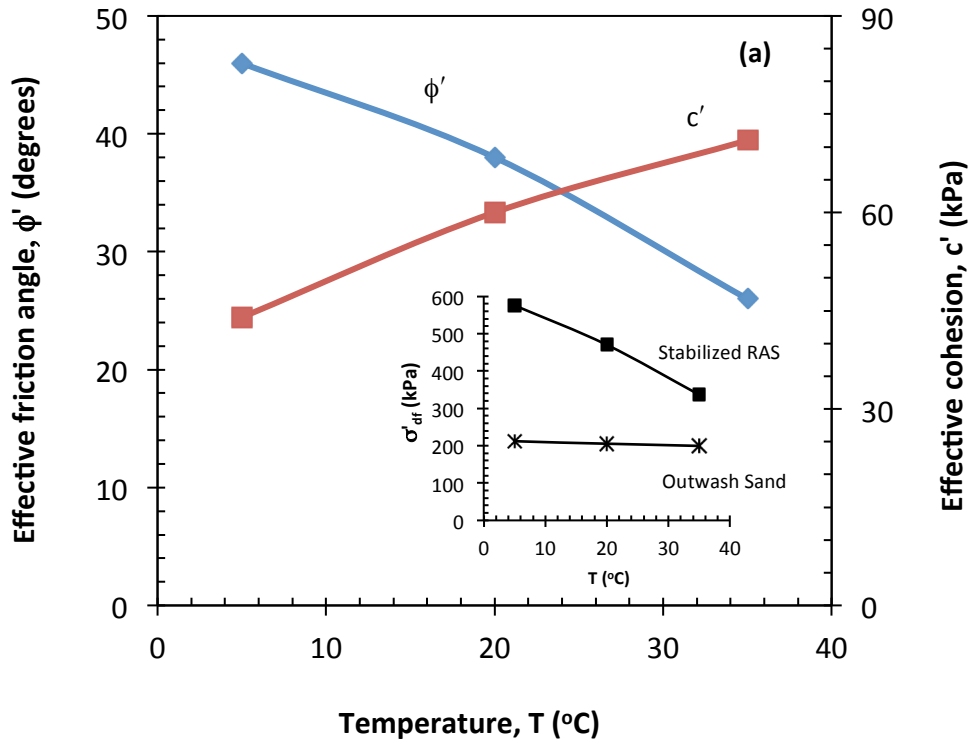


Fig. 8-Variation of (a) friction angle and cohesion of stabilized RAS and (b)  $\sigma'_{ndf}$  with temperature

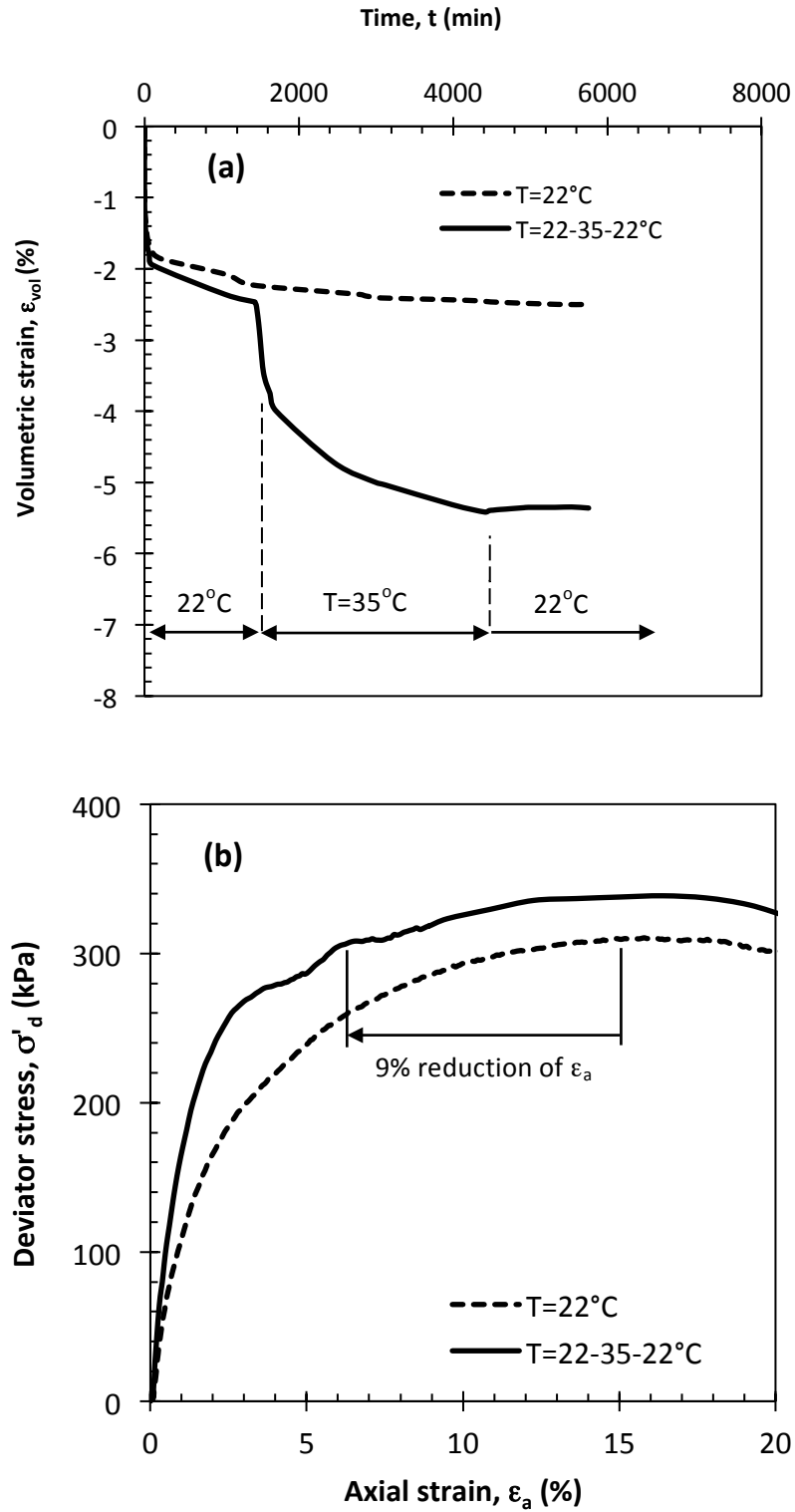


Fig. 9-Effect of thermal cycle on stress-strain behavior of RAS:BA mix

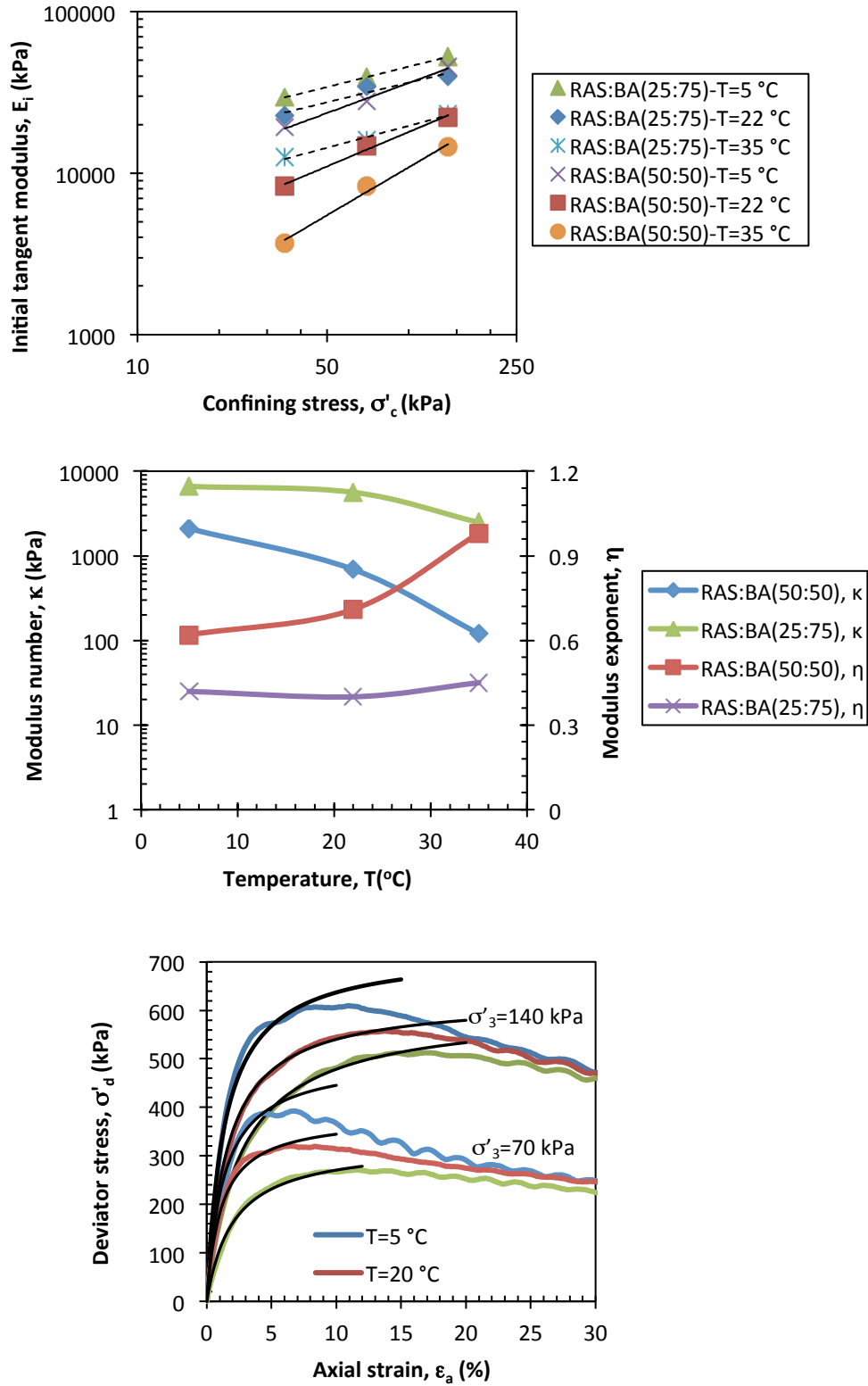


Fig. 10-Variation of  $E_i$  with  $\sigma'_3$  (a) and variation of  $\kappa$  and  $\eta$  of RAS:BA mixtures with temperature (b)

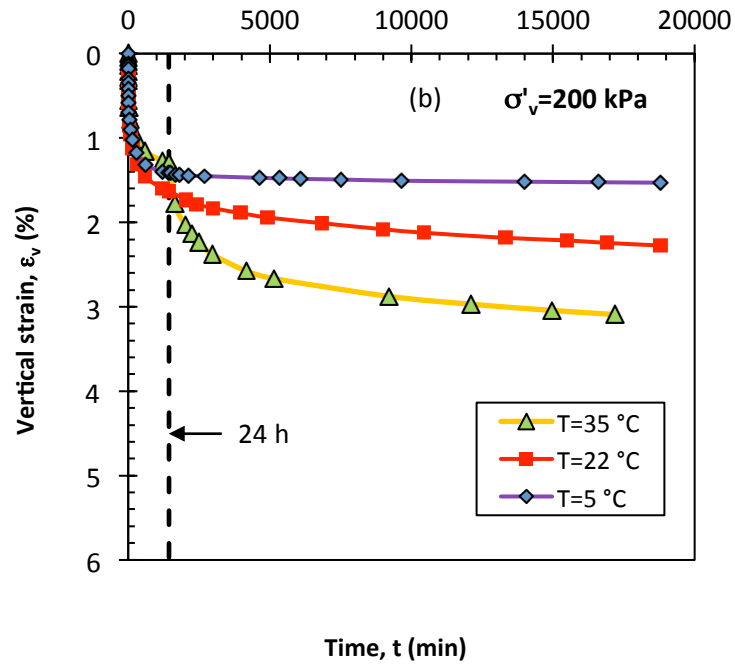
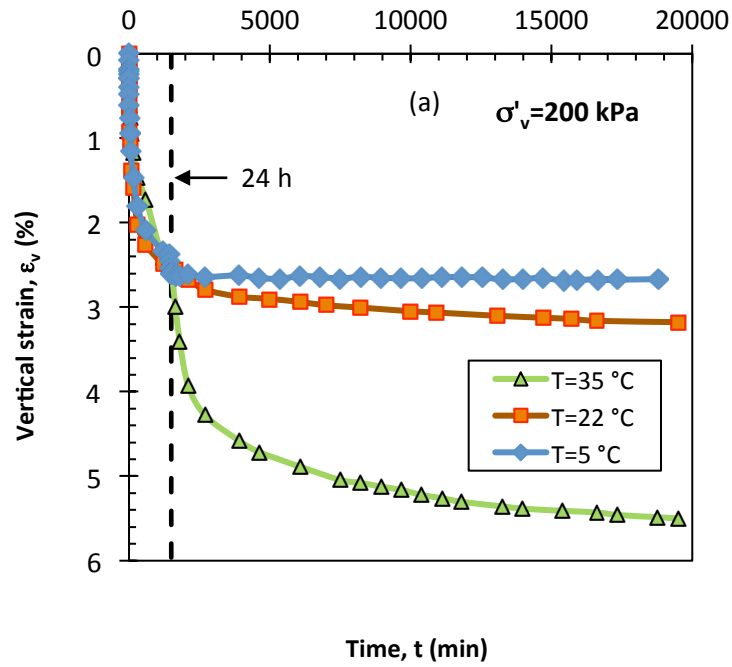


Fig. 11- Variation of  $\epsilon_v$  with time at different temperatures for (a) RAS:BA (50:50) and (b) RAS:BA (25:75)

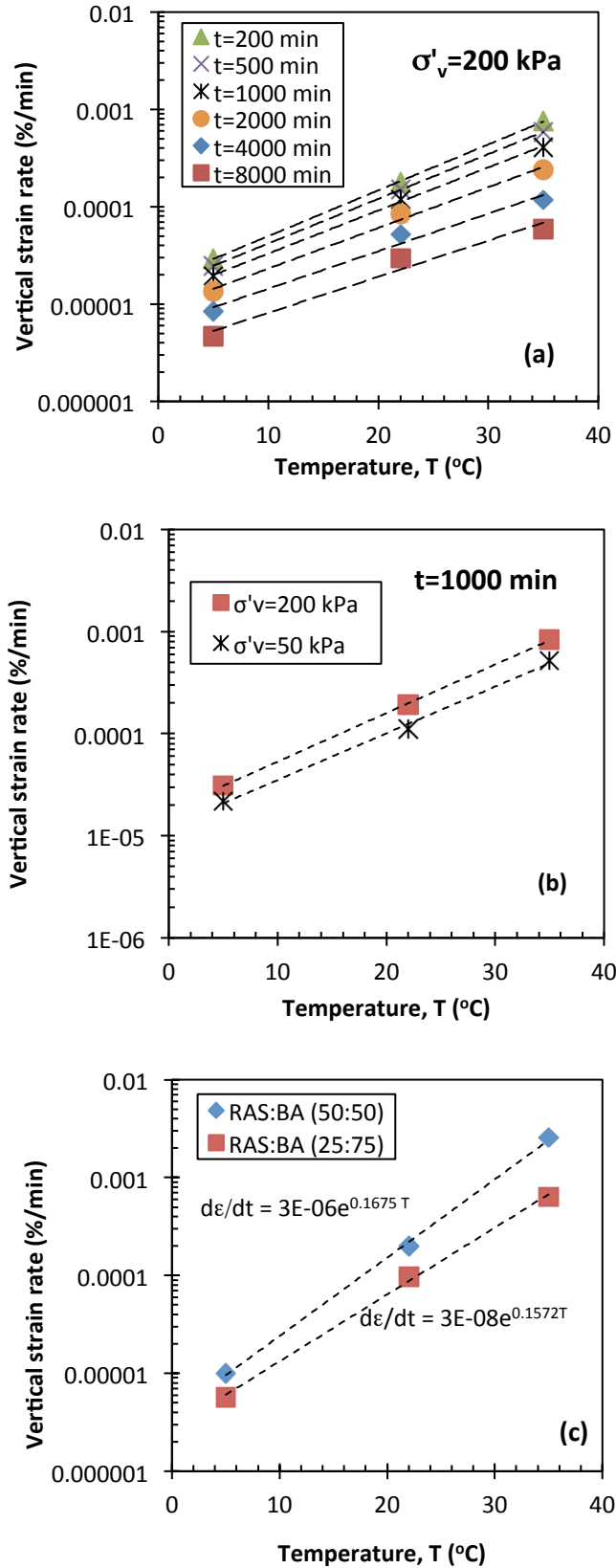


Fig. 12- Variation of strain rate of RAS:BA mixtures with temperature

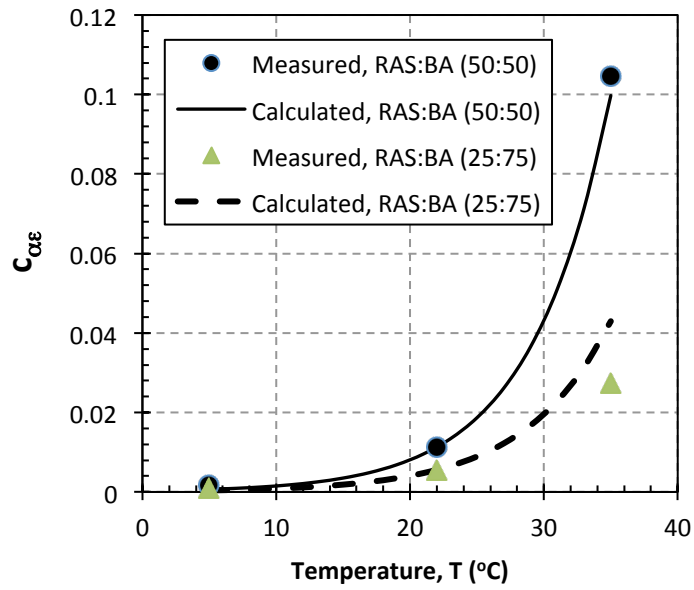


Fig. 13- Predicted versus measured secondary compression ratio of RAS:BA mixtures

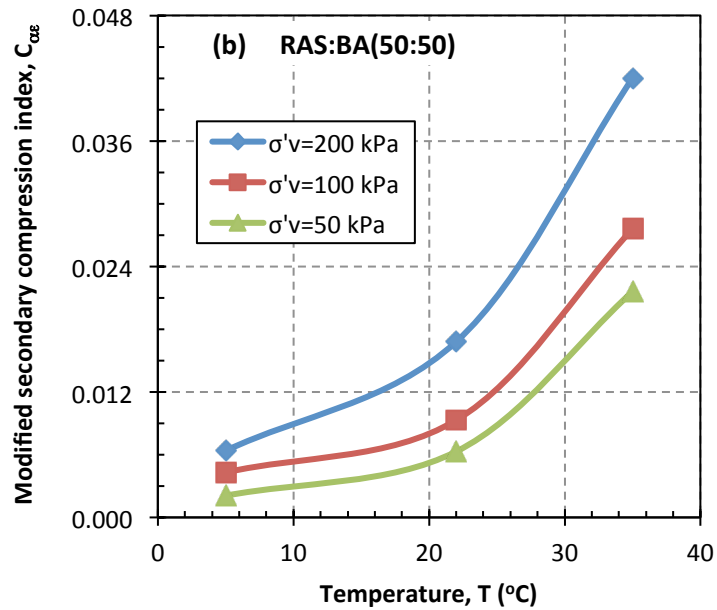
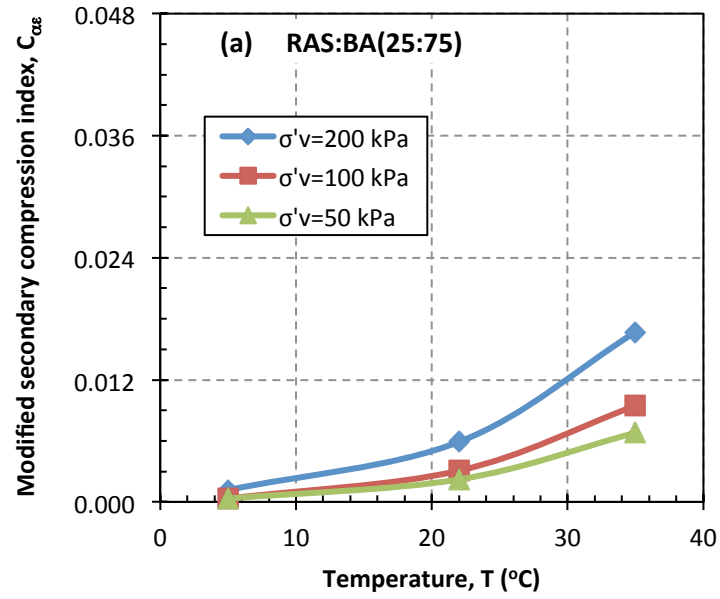


Fig. 14-Variation of  $c_{cs}$  with temperature of compacted RAS:BA mixtures compressed under different  $\sigma'_v$

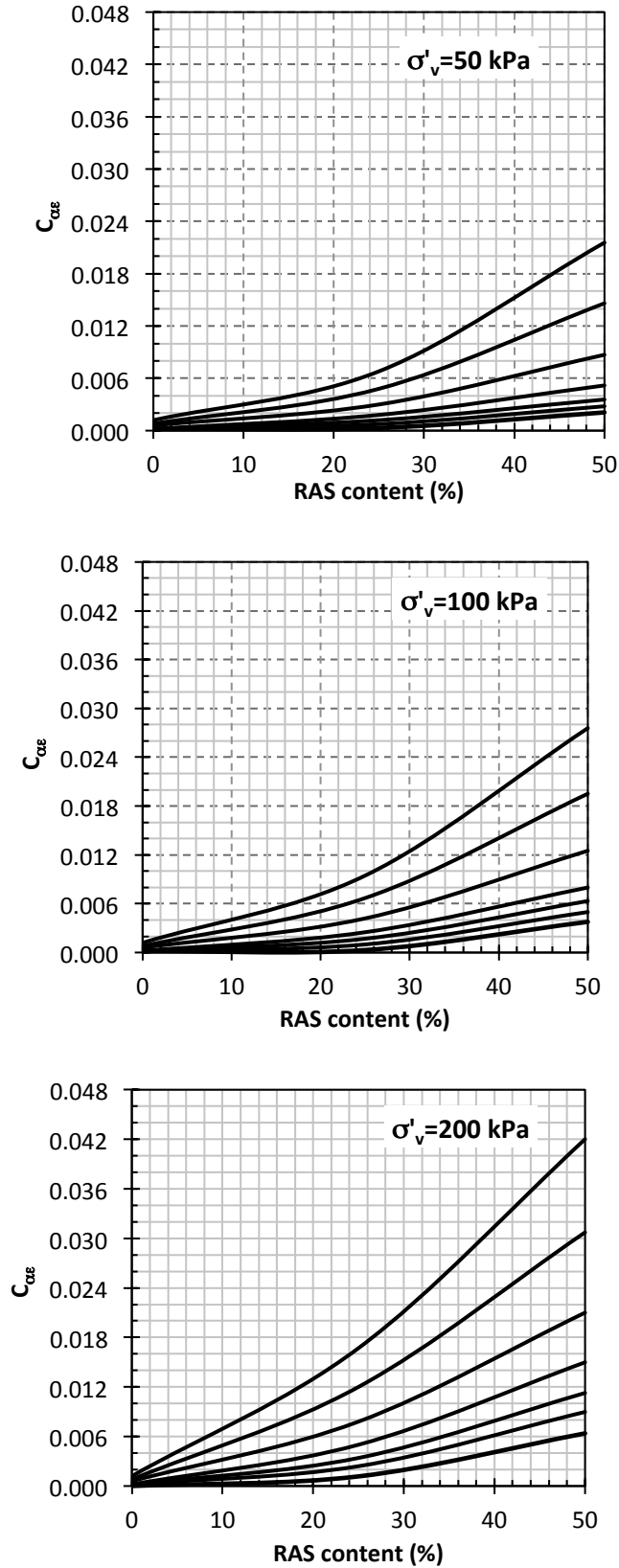


Fig. 15-Variation of  $c_{ce}$  with RAS content at different temperatures and  $\sigma'_v$

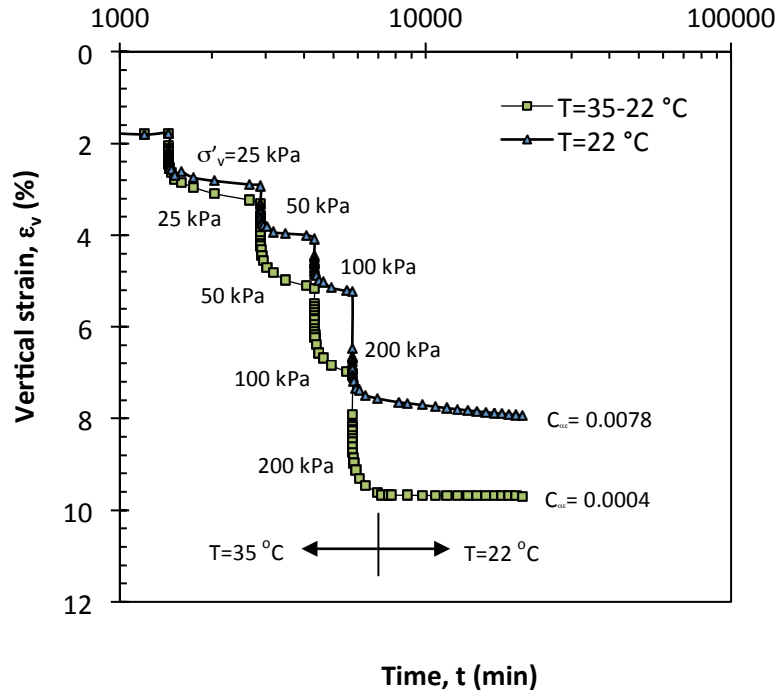


Fig. 16- Effect of construction at elevated temperature on compressibility of compacted RAS:BA mixture

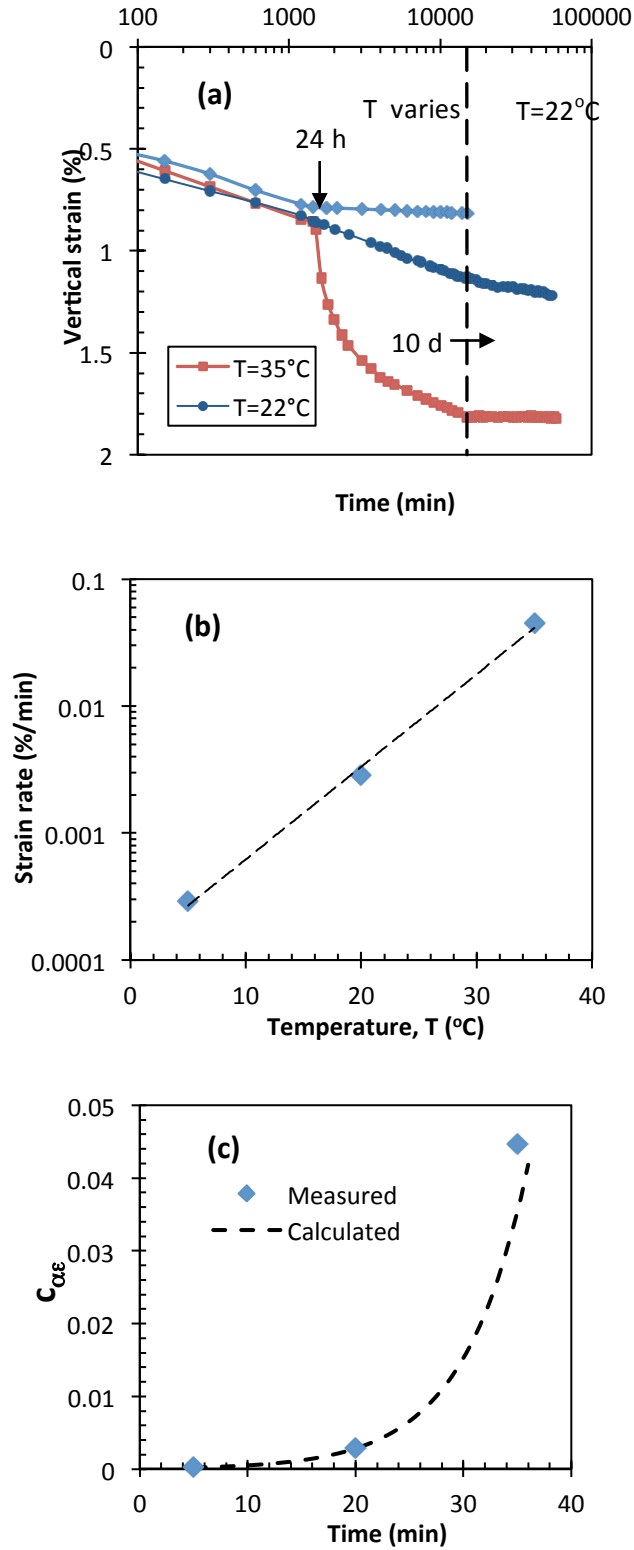


Fig. 17- (a) variation of vertical strain with time of stabilized RAS at different temperatures; (b) Strain rate with temperature; and (c)  $C_{\alpha\epsilon}$  with temperature

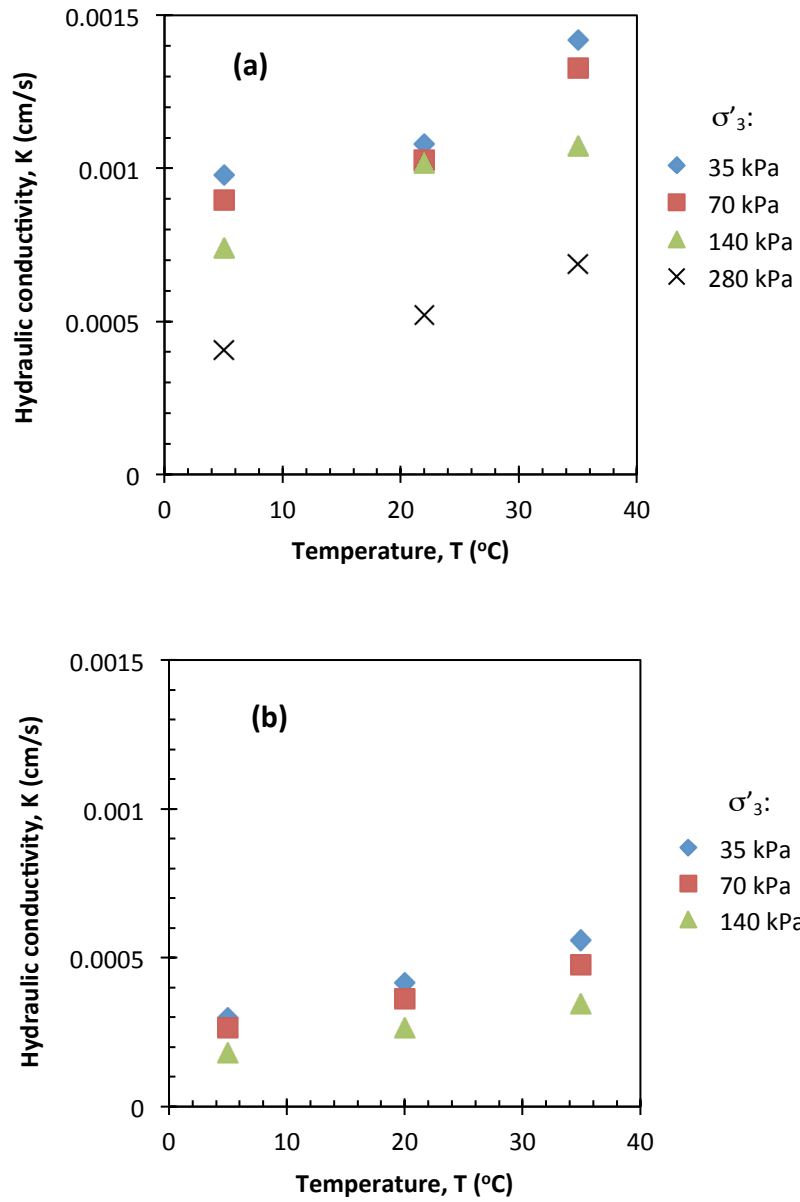


Fig. 18- Variation of hydraulic conductivity of (a) RAS:BA mixture; and (b) stabilized RAS with temperature

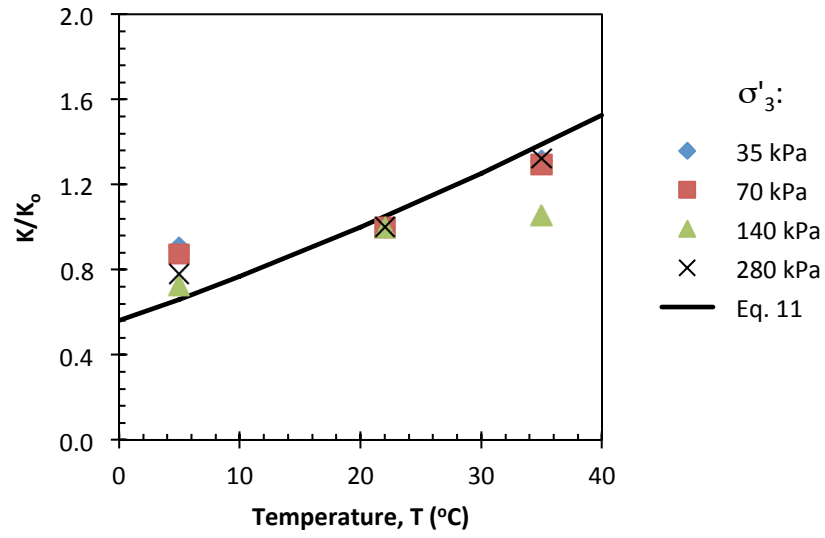


Fig. 19-Variation of normalized hydraulic conductivity of RAS:BA with temperature

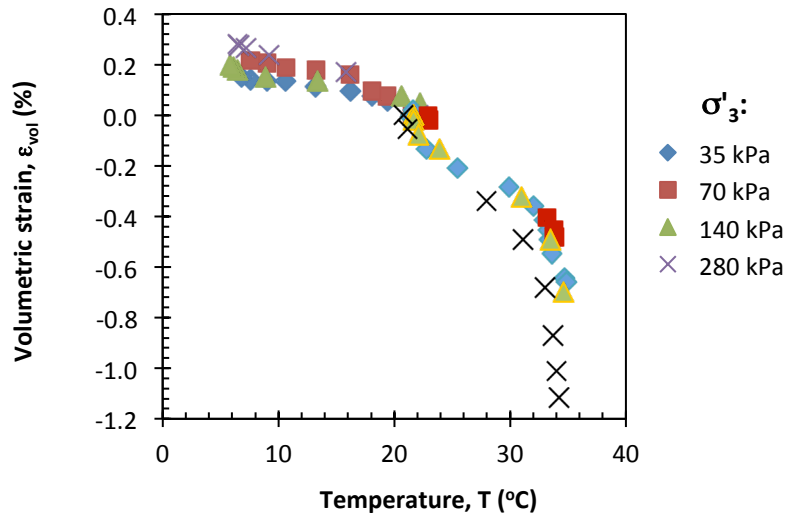


Fig. 20- Variation of volumetric strain of the specimen with temperature

# APPENDIX

Table A-1-Hyperbolic model parameters for stress-strain behavior of compacted RAS:BA mixtures

RAS (%)	$\sigma'_3$ (kPa)	35			70			140		
	T(°C)	5	20	35	5	20	35	5	20	35
25	$E_i$ (kPa)	29400	22700	12500	39200	34400	16000	52600	39800	23300
	$\sigma'_{d,ult}$	294	278	256	503	383	326	725	625	602
	$\sigma'_{df}$	239	208	187	392	320	271	610	558	512
	$R_f$	0.81	0.75	0.73	0.78	0.84	0.83	0.84	0.89	0.85
50	$E_i$ (kPa)	19300	8300	3700	27800	14700	8300	45500	22200	14500
	$\sigma'_{d,ult}$	263	227	233	556	362	360	714	526	323
	$\sigma'_{df}$	237	180	158	452	310	266	629	509	425
	$R_f$	0.90	0.79	0.68	0.81	0.86	0.74	0.88	0.97	1.32

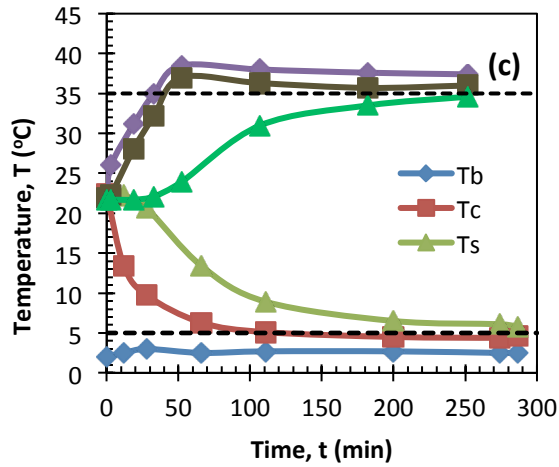
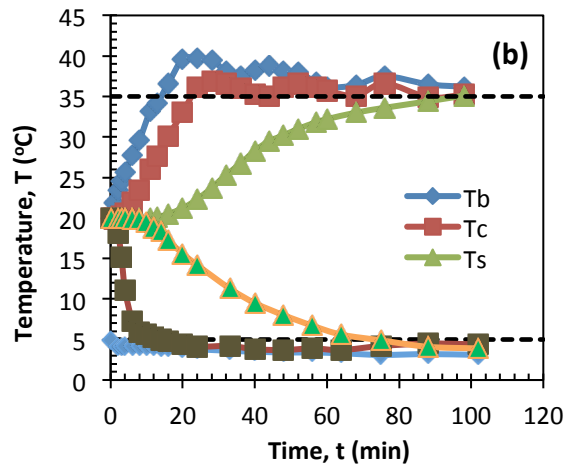
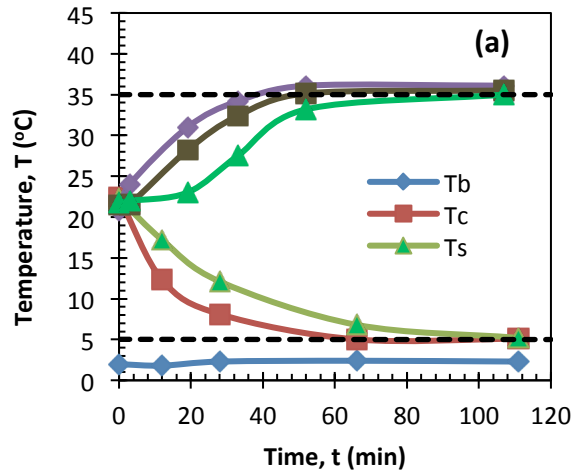


Fig. A-1- Calibration curves for temperature variation in heating/cooling bath, cell and specimen for (a) temperature controlled triaxial cell; (b) temperature controlled consolidometer; and (c) temperature controlled permeameter ( $T_b$ =bath temperature,  $T_c$ =cell temperature,  $T_s$ =specimen temperature)

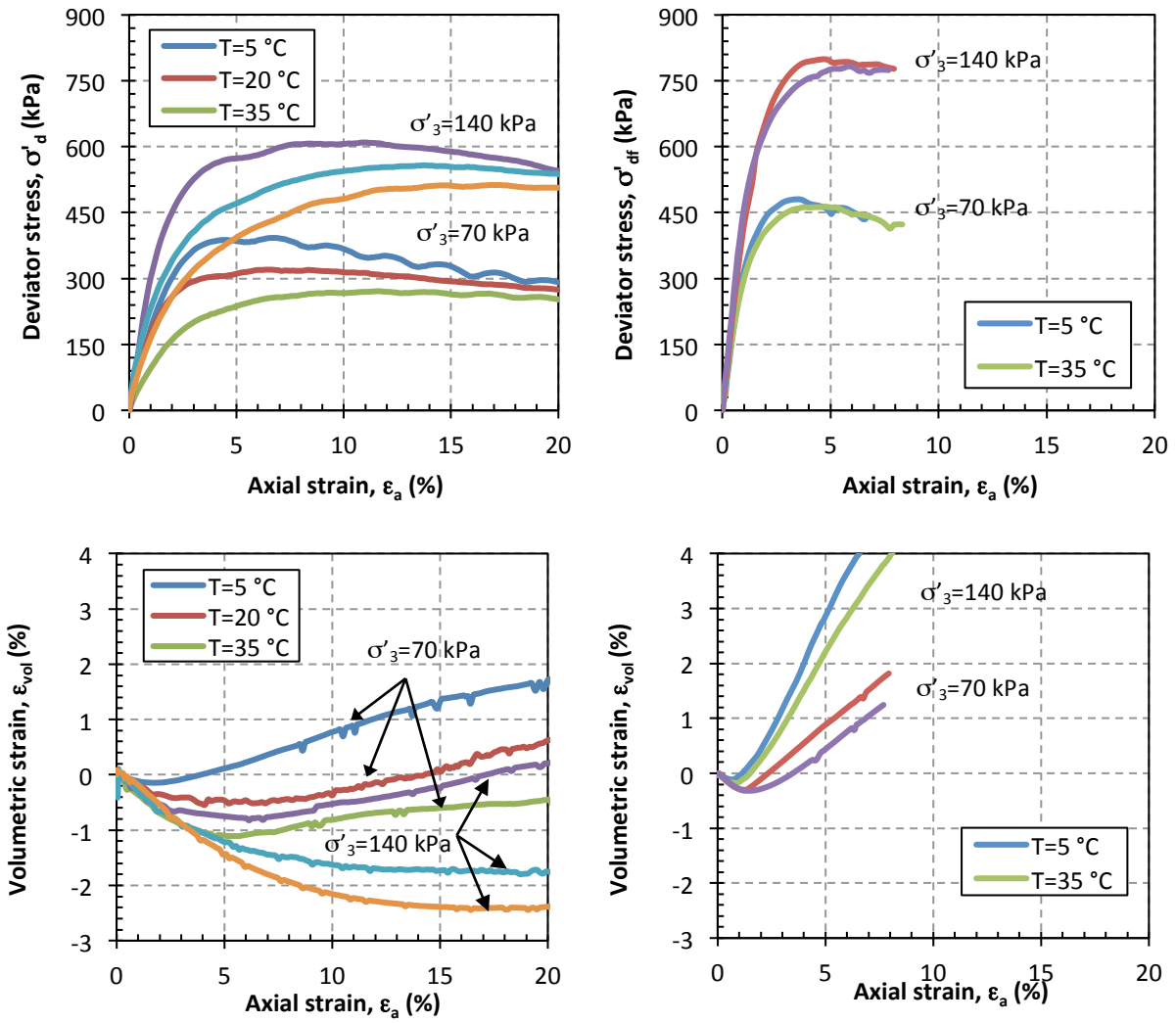


Fig. A-2-Effect of temperature on stress-strain and volumetric change behavior of RAS:BA mixture with 25% RAS



(a)  $T=22^{\circ}\text{C}, 35^{\circ}\text{C}$



(b)  $T=5^{\circ}\text{C}$

Fig. A-3- Modes of failure of RAS:BA mixture specimen at different temperatures

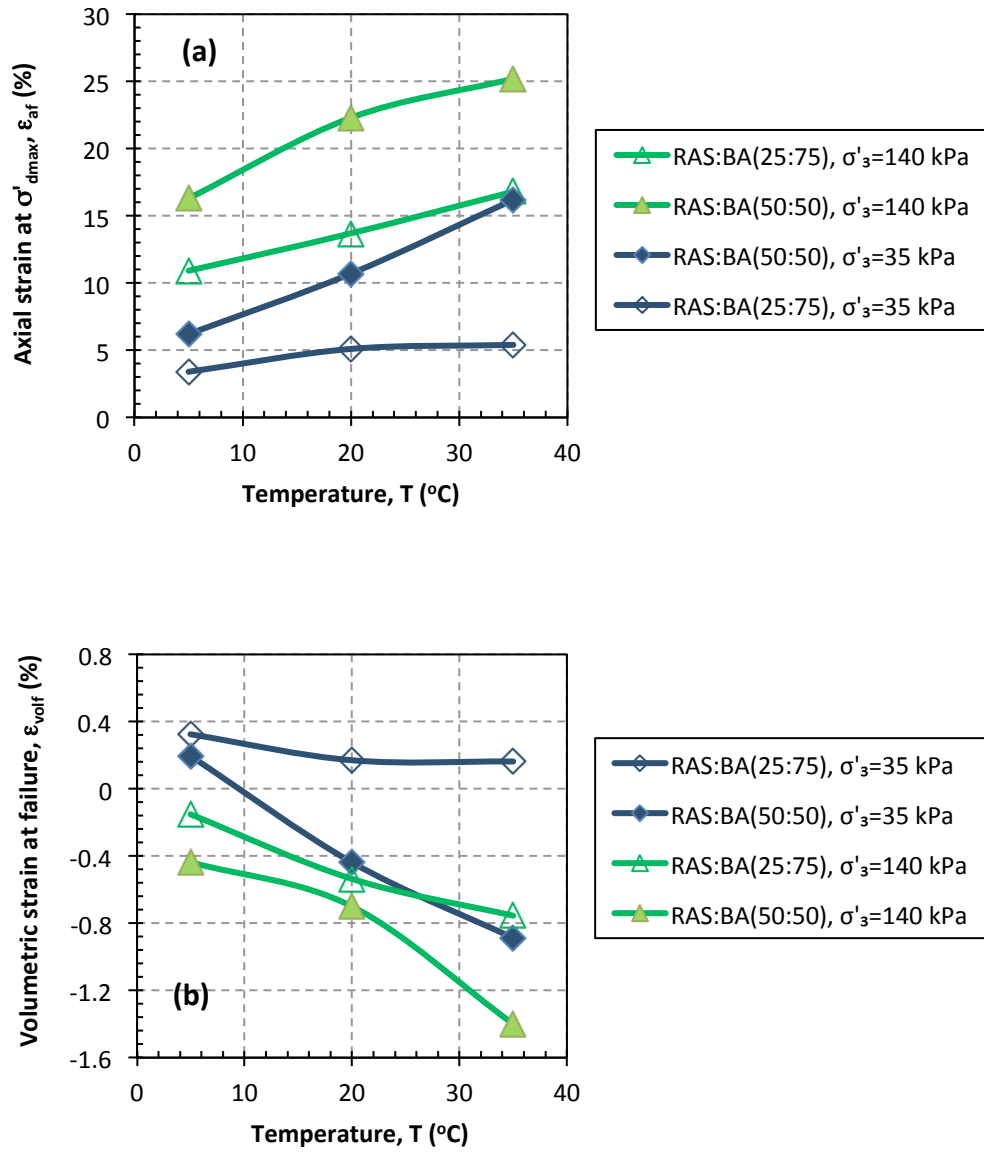


Fig. A-4-Variation of axial strain at  $\sigma'_{\text{max}}$  (a) and volumetric strain (b) of RAS:BA mixtures with temperature

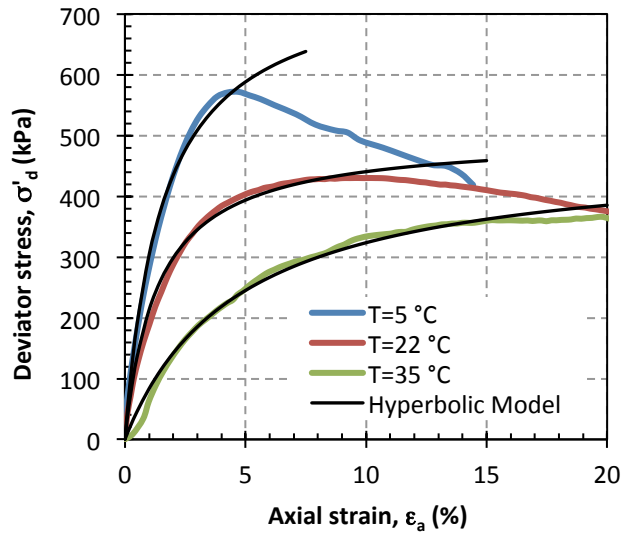


Fig. A-5- Stress-strain behavior and hyperbolic curve fit of stabilized RAS at different temperatures

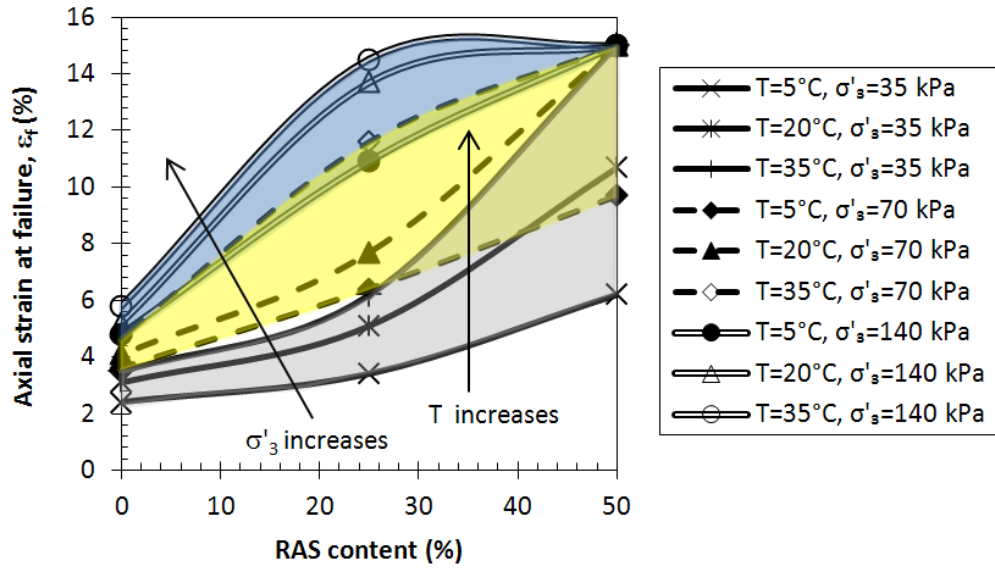


Fig. A-6-Variation of axial strain at failure with temperature and confining pressure

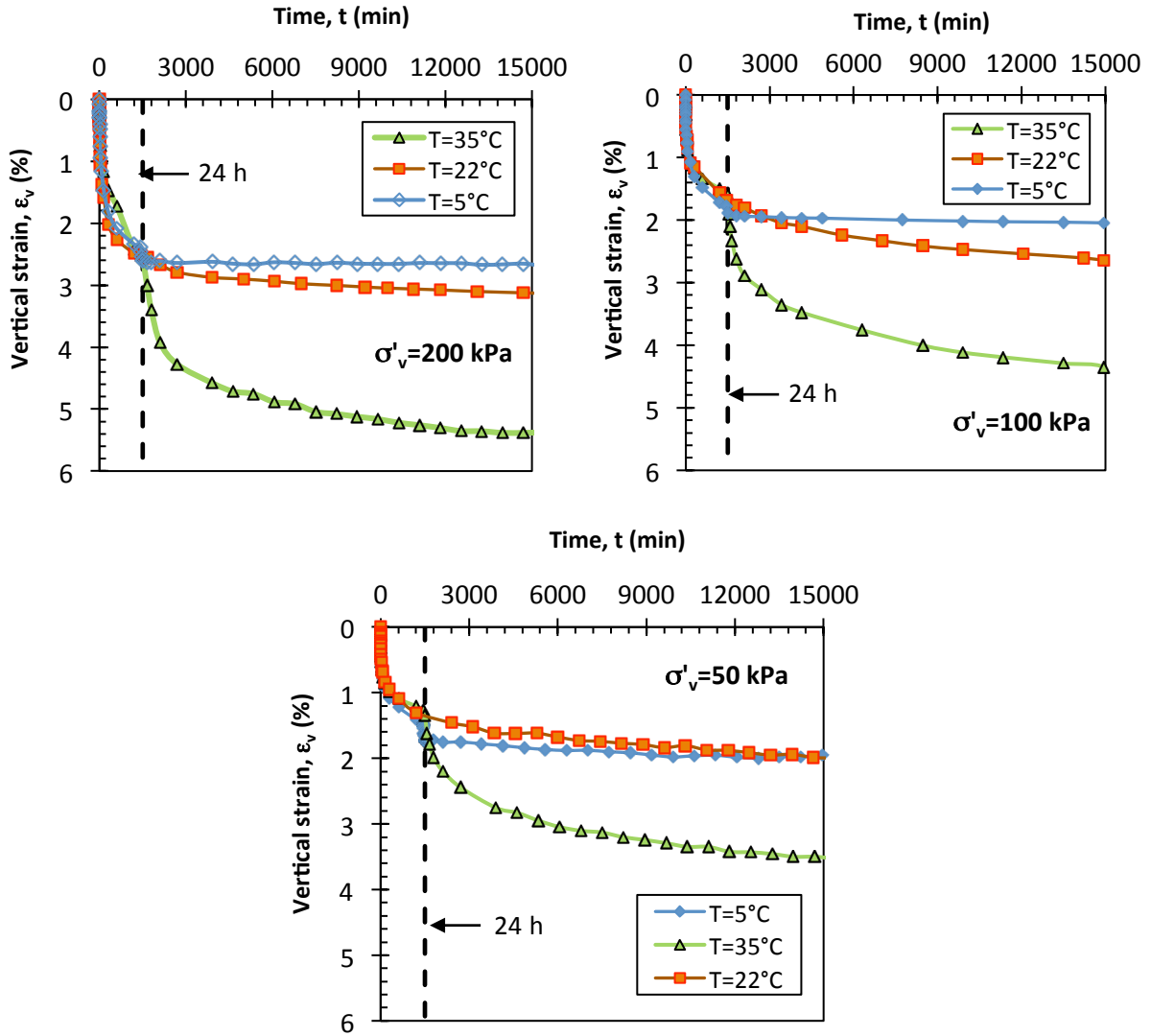


Fig. A-7- Variation of vertical strain with time at different temperatures for RAS:BA (50:50)

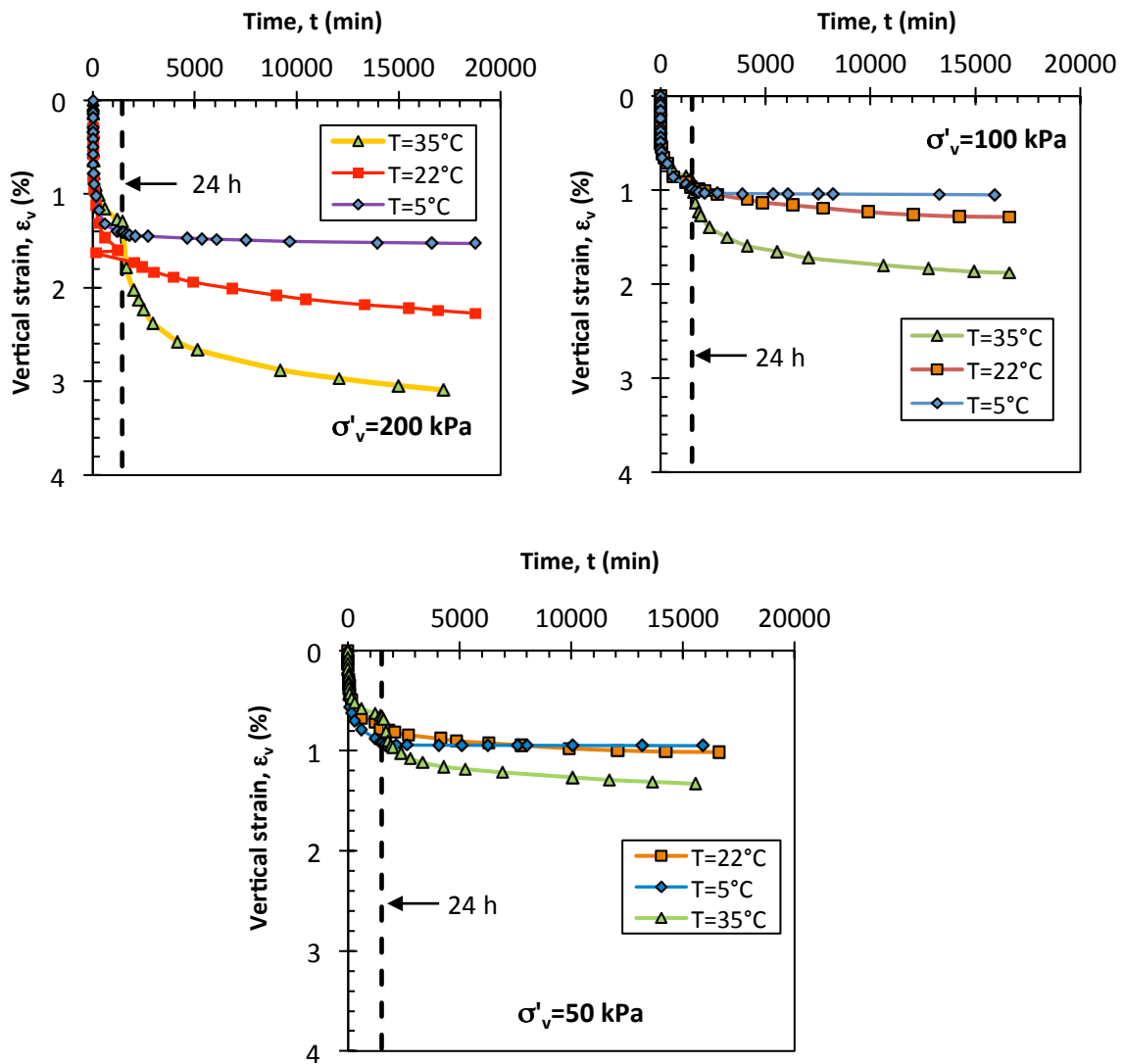


Fig. A-8- Variation of vertical strain with time at different temperatures for RAS:BA (25:75)

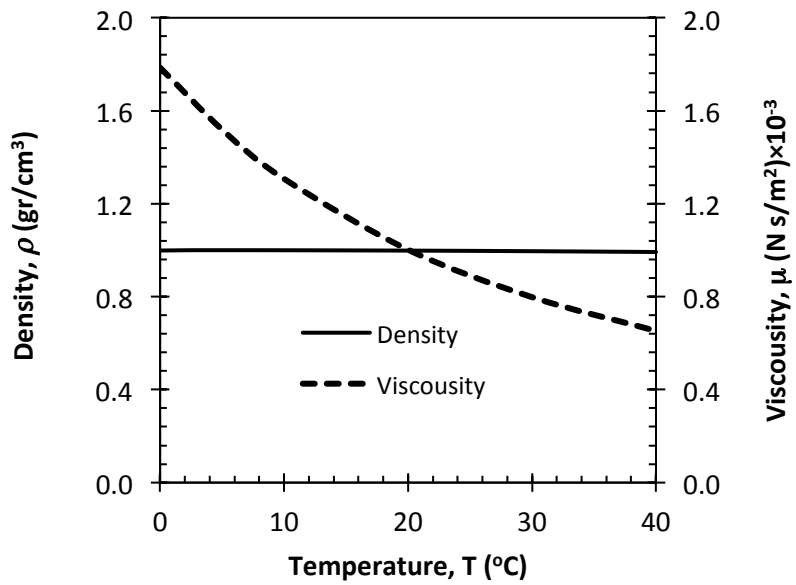


Fig. A-9- Variation of density and viscosity of pore water with temperature

# Chapter 5

## Summary and Conclusion

In this study, recycled asphalt shingles (RAS) were evaluated for potential use as structural fill in highway embankments or backfills behind retaining walls. To reduce compressibility of RAS, addition of granular materials as additives to RAS and stabilization using self cementing fly ash were considered. Geotechnical properties of compacted RAS:BA/FS mixtures and stabilized RAS including compaction behavior, hydraulic conductivity, shear strength, compressibility and coefficient of earth pressure at rest were evaluated in a systematic manner. Since RAS particles contains viscous asphalt binder, to evaluate possible seasonal temperature change on mechanical properties of RAS containing fills, a thermo-mechanical system was developed to investigate the effect of temperature change on geotechnical properties. The range of temperature considered herein encompasses the extreme seasonal temperature change observed in North America.

The following specific observations are made based on the test results:

### Compaction Behavior

RAS:BA/FS mixture and stabilized RAS have lower  $\gamma_{dmax}$  than typical compacted soils and varies between 11.3 kN/m<sup>3</sup> and 15.2 kN/m<sup>3</sup>. The maximum dry unit weight of the RAS:BA/FS mixture or stabilized RAS increases with increasing BA/FS or fly ash content. Low dry unit weight makes them favorable alternatives to natural compacted soils for construction of structural fill over weak soils.

## **Drainage Capacity**

The hydraulic conductivity of the RAS:BA/FS mixture or stabilized RAS provides adequate drainage capacity as structural fills. The hydraulic conductivity slightly decreases with increasing confining pressure due to high compressibility of RAS particles. The hydraulic conductivity of the mixture increases with increase in bottom ash/foundry slag content and becomes almost insensitive to confining pressure when the bottom ash/foundry slag content of the mixture increases to more than 50 %. The hydraulic conductivity of stabilized RAS is comparable to that of silty sands. The hydraulic conductivity is also reduced with increasing fly ash content. Due to reduction in drainage capacity, maximum fly ash content in stabilized RAS is recommended to be limited to 20%. The drainage capacity of the material increases with temperature due to reduction in water viscosity. There is no concern regarding drainage capacity of RAS:BA or fly ash stabilized RAS at elevated temperatures.

## **Shear Strength**

RAS alone exhibits sufficient shear strength as a structural fill material. Shear strength of compacted RAS:BA/FS mixtures or stabilized RAS are similar to those of compacted sandy soils and is sufficient for construction of structural fills. The shear strength of both compacted RAS:BA mixture and stabilized RAS consistently decreases with increasing temperature. As the RAS content in the RAS:BA mixture increases the temperature change has more pronounced effect on the shear strength of the mixture. However, shear strength of the embankment fills constructed with the compacted RAS:BA mixtures (with RAS content no more than 50%) or stabilized RAS with 20% self-cementing fly ash remains within the range sufficient to provide

stability of the typical road embankment fill in the climate ranges of North America (i.e., up to 35 °C fill temperatures).

### **Compressibility**

The short-term and long-term compressibility of pure RAS are significantly higher than those of compacted sandy soils. The high compressibility is due to asphalt cement and cellulose felt contents in RAS. Systematic addition of bottom ash or foundry slag to RAS or stabilization of RAS reduces compressibility of the mixture. At small to moderate stress levels typical in highway embankments, addition of more than 50% by weight bottom ash/foundry slag to RAS or stabilization with more than 10% self cementing fly ash, greatly reduces the short-term and the long-term compression and categorizes the RAS:BA/FS mixtures or stabilized RAS as slightly to very slightly compressible material. Aging by preloading for a specific time such as 150 days is an alternative method to reduce long-term compressibility of RAS. Previous research results showed that compressibility of the BA or FS is greater than natural sand. The acceptable BA or FS content of the compacted RAS:BA/FS mixture can be safely replaced by natural granular material content and the results and design graphs obtained herein can be used conservatively for the compacted RAS mixtures with sands or gravels. The results obtain in this research is also specific to the type and maximum particle size of the recycled asphalt shingles used. The developed design graphs help determine RAS content in the mixture based on overburden pressure and allowable long term settlement.

Temperature change, on the other hand, affects compressibility of the compacted RAS:BA mixture and stabilized RAS with self-cementing fly ash. The secondary compression index increases exponentially with temperature. During the cold seasons (temperatures lower

than 10 °C), the compression of the RAS:BA mixture or stabilized RAS is comparable to that of natural granular material and is practically negligible. However, the compressibility exponentially increases during warm seasons (when the temperature rises to 20 to 35 °C). This indicates that an embankment fill containing RAS or stabilized RAS constructed during the cold to mild seasons of the year may exhibit significant settlement during the warm season. In any region in North America, if the embankment is constructed during the warm season, the majority of the compression will occur during construction and negligible settlement can be expected in the seasons following the warm season. The design graphs were developed to predict subsequent settlement of an embankment constructed at a temperature around 20 °C as a function of RAS content, temperature and stress levels for RAS:BA mixtures. In using the design graph, one may meet the design specifications for the maximum allowable settlement of a road embankment.

### **Coefficient of Lateral Earth Pressure**

Coefficient of lateral earth pressure of RAS:BA/FS mixtures or stabilized RAS are comparable to those of compacted sand. Adequate drainage capacity and lower dry unit weight of RAS:BA/FS mixtures or stabilized RAS make them favorable alternatives to sand and gravel in terms of lower lateral earth pressures behind retaining structures with potential to greatly reduce the dimensions of the walls. Stabilization of RAS significantly reduces the  $K_o$  of RAS.

Based on the results of this research, stabilized RAS is considered to be a viable material for use as structural fill in highway embankments and backfill behind retaining walls. Structural fill is an alternative application to use in hot mix asphalt, which is likely to allow use of large volume of

waste asphalt shingles and help to save landfill space, reduce disposal costs, energy consumption, and green house gas emissions due to mining and production of virgin aggregates. Additionally, RAS in mixture or stabilized offers certain superior fill material characteristics compared to conventional materials such as light weight and reduced lateral pressures. However, RAS samples obtained from different sources and with different particle sizes may have different mechanical behavior and need to be tested for specific applications.

## **Appendix I**

### **Evaluation of shredded reclaimed asphalt shingles mixed with foundry slag as highway embankment fill**

#### **ABSTRACT**

Reuse of asphalt shingle waste has been identified by Environmental Protection Agency (EPA) as top 5 priority solid waste. Over 11 million Mg asphalt shingle waste is produced in the U.S. each year for which land-filling is the main end place. In this study, possible use of shredded reclaimed asphalt shingles (RAS) in highway embankment fills was investigated. The engineering properties of RAS including compaction characteristics, hydraulic conductivity, compressibility and shear strength were evaluated. Foundry slag (FS) as a granular solid waste was systematically added to RAS to improve its mechanical properties. Results showed that RAS:FS mixtures have maximum dry unit weight of  $11 \text{ kN/m}^3$ , hydraulic conductivity of over  $1 \times 10^{-4} \text{ cm/s}$ , and effective friction angle over  $33^\circ$ . Compressibility of RAS is reduced well below the maximum limit by either preloading or mixing with FS. Use of RAS:FS mixture as a lightweight material in highway embankment fills will reuse large volume of the two types of solid wastes which are produced in large quantities per year. This will help saving appreciable

amount of landfill space as well as reducing greenhouse gases by avoiding aggregate production and mining.

## **INTRODUCTION**

Sustainable construction incorporates reduction of global warming potential by reducing greenhouse gas emissions. Major part of the greenhouse gases are produced during mining and production of high volume construction materials (Wen and Edil, 2009; Lee et al. 2010;). As the world population grows the amount and type of generated solid waste increases. Use of solid waste materials in high volume construction applications is not only a promising solution to the disposal problems, also contributes to reducing greenhouse gas emissions and energy consumption by avoiding mining and aggregate production.

Approximately 11 million Mg of waste asphalt roofing shingles are generated per year in the U.S. of which 10 million Mg are tear-off roofing shingles and 1 million Mg is factory scraps (Townsend et al. 2007; NERC 2011). The most common disposal method of asphalt shingle waste is landfilling. Reuse of recycled asphalt shingles (RAS) has been identified by the U.S. Environmental Protection Agency (EPA) and Federal Highway Administration (FHWA) as a top priority.

Constituents of a typical asphalt shingle include 20-35% asphalt cement, 2-15% cellulose felt, 20-38% mineral granules/aggregates, and 8-40% mineral filler/stabilizer (Townsend et al. 2007). The primary reuse application of RAS is in production of hot mix asphalt (HMA) to benefit from the asphalt cement and granular content of RAS in HMA. Research results have indicated however, that more than 5% by weight of RAS in HMA will adversely decrease the creep stiffness and tensile strength of HMA (Grodinsky 2002; Johnson et al. 2010).

Consequently, this application uses only between 10 to 20% of the total asphalt shingle waste (Turley 2011). Another possible application of asphalt shingle waste in large quantities is to use it in structural fills including highway embankment fills or backfill behind retaining walls. In particular, in the areas where the underlying soils are compressible or weak, use of a light-weight material like RAS will potentially reduce the settlement and increase the global stability of the earth structure. Preliminary compression test results indicated that pure RAS is too compressible for use as structural fill (Benson et al. 2010; Soleimanbeigi et al. 2011). To reduce compressibility of RAS, addition of granular materials with verified suitability as structural fill was considered.

Foundry slag (FS) is a combination of limestone and metal impurities in metal casting industry, which is collected from top of the molten metal in the furnace. The molten slag is cooled, crushed and screened to create granular slag. According to the U.S. Geological Survey, about 17 to 24 million Mg foundry slag was produced in 2008 of which about 90% were reused in a variety of engineering applications such as aggregate in portland cement concrete, asphalt concrete, aggregate base, fill material and railroad ballast. Of the total reused FS, 40% was used as road base-course and 10% was used as fill material. The engineering properties of foundry slag are suitable for use as structural fill and working platforms (Emery 1982; Ahmed 1993; Edil et al. 2002; Tanyu et al. 2005).

Mixing foundry sand with RAS is expected to reduce the compressibility problem associated with RAS on one hand while allowing beneficial reuse application for two by-products on the other hand. Therefore, the objective of this research is to investigate suitability of RAS:FS mixtures as a construction material in highway embankment fills. For this purpose, relevant engineering properties of RAS:FS mixtures including compaction characteristics, hydraulic

conductivity, compressibility, and shear strength were evaluated in a systematic manner and presented herein.

## **TEST MATERIALS**

RAS samples used in this study were obtained from Stratford Building Supply Company in Stratford, Wisconsin. Visual inspection indicated that RAS samples were free of impurities such as wood chips, plastics, and nails. The Stratford Building Supply grinds the waste shingles once over and screens them through 50-mm, 25-mm, and 19-mm sieve sizes. Warner (2007) concluded that RAS particles with maximum size ( $d_{max}$ ) of 10-mm, result in higher dry unit weight ( $\gamma_d$ ), higher California bearing ratio (CBR), and higher resilient modulus ( $M_r$ ). Therefore, in this study, the RAS supply was screened to limit the  $d_{max}$  to 10-mm. FS samples were obtained from the Grede Foundries in Wisconsin. To compare the engineering properties of RAS:FS mixtures to those of natural soils, a sample of glacial outwash sand (GOS) in Wisconsin was also used in this study.

## **TEST METHODS**

The test methods include physical property tests and mechanical property tests.

### **Physical Property Tests**

The physical property tests including grain size analysis, specific gravity, and microscopic examination were conducted on RAS, FS and GOS particles.

### **Grain Size Analysis**

The grain size distribution of RAS and FS samples were determined according to ASTM D 422. The samples were first wet sieved through No. 200 sieve to separate coarse and fine particles.

The coarse portions of FS samples were oven dried for 24 hours prior to mechanical sieving. Whereas the coarse portions of RAS samples were air-dried to prevent binding of the particles at elevated temperatures.

### **Specific Gravity**

The specific gravities of RAS and FS samples were measured according to ASTM D854 (Method B). To prevent clumping of RAS particles during the test and to remove any entrapped air in the slurry, the pycnometer was continuously agitated for about one hour under a constant vacuum. De-airing was accomplished by vacuuming distilled water.

### **Microscopic Examination**

Shape, angularity and surface texture of RAS, FS, and outwash sand particles were examined using a light microscope (LM) to understand interaction mechanisms between the particles during different mechanical tests. Due to crushability of FS particles, microphotographs of the generated fines particles of FS were obtained using scanning electron microscope (SEM) to investigate the angularity and surface texture of the fines.

### **Mechanical Property Tests**

The mechanical property tests including compaction, hydraulic conductivity, one-dimensional compression, and consolidated drained (CD) triaxial compression tests were performed on RAS:FS mixtures with FS contents of 0, 25, 50, 75, and 100%.

### **Compaction**

Systematic standard Proctor compaction tests following ASTM D 698 (method B) were performed to obtain relationship between dry unit weight and water content of RAS:FS mixtures.

Minimum 5 compaction tests were conducted to obtain the variation of  $\gamma_d$  with water content ( $w$ ) of each RAS:FS mixture.

### **Hydraulic Conductivity**

Flexible wall hydraulic conductivity tests were conducted on RAS:FS mixtures according to ASTM D 5084-03 to evaluate the effect of confining stress ( $\sigma'_3$ ) on hydraulic conductivity of the mixtures. Each RAS:FS mixture was compacted to 95% of the maximum dry unit weight ( $\gamma_{dmax}$ ) at optimum water content ( $w_{opt}$ ) and consolidated to the desired effective stress ( $\sigma'_3 = 35$  kPa, 70 kPa, and 140 kPa) for 24 hours. The confining stresses were selected to represent the range of typical effective stresses in highway embankments. After the consolidation phase, the hydraulic conductivity was measured according to the falling-head rising-tail method.

### **One-Dimensional Compression**

Settlement of an embankment with large lateral extension can be considered one-dimensional and estimated from the results of one-dimensional consolidation tests. To evaluate compressibility of RAS:FS mixtures, one-dimensional compression tests were performed following ASTM D 2435-96 using a standard consolidometer ring with 64-mm diameter and 25-mm height. Each specimen was compacted at the  $w_{opt}$  and relative compaction level of 95%. The compaction in the consolidometer ring was conducted in three lifts of equal thickness by a manual hammer. RAS:FS specimens were then soaked in the consolidometers for 24 hours before applying vertical loads. Pore pressure piezometers were connected to consolidometer cells to measure any generated excess pore water pressures under each stress level. The specimens

were loaded incrementally from 12.5 kPa with load increment ratio (LIR) of 1.0 and load increment duration (LID) of 24 hours until the maximum vertical stress level ( $\sigma'_{vmax}$ ) of 1600 kPa. The range of the stress level was selected to clearly obtain compression curves and define compressibility parameters for RAS:FS mixtures. The one-dimensional consolidation test was also performed on the glacial outwash sand sample for comparison. The LABVIEW software (National Instruments, Austin, TX) and a data acquisition card (UPC601-U) were used for automated incremental loadings and recording of vertical deformations.

### **Triaxial Compression Tests**

To evaluate stress-strain and volumetric change behavior of RAS:FS mixtures under shearing and to determine the shear strength; consolidated drained (CD) triaxial compression tests were performed on compacted RAS:FS mixtures. For each mixture composition, three tests were performed under  $\sigma'_3$  of 35 kPa, 70 kPa, and 140 kPa. Each RAS:FS mixture was compacted in five layers in a split mold with 74-mm diameter and 148-mm height at a relative compaction level of 95%. The number of tamps per layer using a standard Proctor hammer was determined by trial. After assembling the cell chamber, the specimens were backpressure-saturated according to ASTM D4767 so that a  $B$  value greater than 95% was attained. The specimens were then isotropically consolidated under  $\sigma'_3$  of 35 kPa, 70 kPa, and 140 kPa. The specimen volume change during consolidation phase was monitored in the backpressure burette until no significant change in volume was observed. The shearing of each mixture specimen in drained condition was performed under constant strain rate. The axial deformation rate of 0.2 mm/min was selected based on the time for primary consolidation and the ultimate strain of the specimen at failure.

The pore water pressure was monitored to ensure no excess pore pressure is generated during shearing. The volume change of each specimen during shearing was recorded from the volume change of water in backpressure burette.

## **PARTICLE CHARACTERISTICS**

### **Grain Size Distribution**

Fig. 1 shows the grain size distribution for RAS, FS, and outwash sand. More than 80% of particles of each material are sand size with fine contents less than 5%. RAS and FS particles have almost similar grain size distributions; therefore, grain size distribution of different RAS:FS mixtures will fall within a narrow range. According to the Unified Soil Classification System (USCS) RAS and FS, although they are not soil, are classified as well graded sand, whereas outwash sand is classified as poorly graded sand. The grain size indices and the USCS classification are summarized in Table 1.

### **Specific Gravity**

The specific gravity of RAS is 1.74, which is lower than the specific gravity of outwash sand, i.e. 2.71 (see Table 1). The low specific gravity of RAS is attributed to organic cellulose felt and asphalt cement contents, which together constitute between 35 to 50% by mass of RAS. The specific gravity of asphalt binder is generally between 1.0 and 1.04 (Roberts et al. 1996). FS has a specific gravity of 2.36, which is also lower than the specific gravity of the outwash sand. The measured specific gravity of FS sample fall within the range reported in the literature (RMRC 2010).

## Morphological Characteristics

Fig. 2 shows typical shape of RAS particles, LM photomicrographs of FS and outwash sand particles and SEM photomicrographs of FS fines particles. RAS particles are plate-like, irregular in shape, highly angular and have rough surface texture. The angularity of RAS particles reduces to semi-round to round as the particle size decreases. During manufacturing, one side of the asphalt shingles is covered by sand to protect them against physical damage. The other side is covered by mineral filler to protect the shingles against adhesion during packing and shipment. The sand and mineral surface covers on the RAS particle surfaces are illustrated in Fig 2 (a). Particles of outwash sand are solid, semi-round to round and have smooth surface texture. Particle surfaces are clean, shiny and free of dust as displayed in Fig. 2 (b). FS particles are angular to highly angular, internally porous and have rough surface texture as shown in Fig. 2 (c). Fines particles of FS are highly angular, irregular in shape with sharp edges as shown in the SEM micrograph in Fig. 2 (d).

## Compaction Characteristics

Fig. 3 shows that pure RAS has a well-defined compaction curve with a  $\gamma_{dmax}$  of 11.3 kN/m<sup>3</sup> and  $w_{opt}$  of 9%. Systematic addition of FS to RAS only slightly reduces  $\gamma_{dmax}$  of the RAS:FS mixture. The  $\gamma_{dmax}$  of RAS:FS mixture varies between 11.3 kN/m<sup>3</sup> for RAS to 10.9 kN/m<sup>3</sup> for a mixture containing 50% RAS. As the FS content in the RAS:FS mixture increases, the curvature of the parabolic shape of the compaction curve decreases. This is attributed to increase in granular FS particles. Maximum dry unit weight of granular soils generally occurs at dry conditions and

decreases with increasing water content until saturation where the dry unit weight increases (Hilf 1991; Drnevich et al. 2007). Low specific gravity and high porosity of FS particles result in low  $\gamma_{dmax}$  of FS with respect to typical compacted sand. In general, the  $\gamma_{dmax}$  of the RAS:FS mixtures remains almost unchanged with different FS contents, making the RAS:FS mixture a possible favourable lightweight material for structural fill application.

### **Hydraulic Conductivity**

Fig. 4 shows the hydraulic conductivity of RAS:FS mixtures from the flexible wall hydraulic conductivity tests. Except for pure RAS under  $\sigma'_3$  of 140 kPa, the hydraulic conductivity of RAS:FS mixtures fall between  $2 \times 10^{-3}$  cm/s and  $1 \times 10^{-4}$  cm/s. The hydraulic conductivity of RAS:FS mixtures generally decreases as the  $\sigma'_3$  increases. High compressibility of RAS particles and densification of RAS:FS mixtures at higher  $\sigma'_3$  explain the decrease in hydraulic conductivity of RAS:FS mixtures with increasing  $\sigma'_3$ . As will be shown in the next section, FS is significantly less compressible than RAS under low to moderate stress levels. Therefore, as the foundry slag content increases the hydraulic conductivity of RAS:FS mixture becomes less sensitive to  $\sigma'_3$ . For the mixtures with foundry slag content more than 50%, the hydraulic conductivity is almost constant at different  $\sigma'_3$ . At a particular  $\sigma'_3$ , the hydraulic conductivity of RAS:FS mixture increases with increasing foundry slag content. This is attributed to increase in void ratio. The void ratio of compacted RAS is 0.59 while the void ratio of compacted FS is 1.44. As the FS content increases, the void ratio of the compacted RAS:FS mixture increases which consequently increases the hydraulic conductivity. In general, according to USBR (1987) classification, the RAS:FS mixtures under low to moderate confining pressures have “good” drainage capacity for use as structural fill (i.e.,  $K > 1 \times 10^{-4}$  cm/s).

## Compressibility

Fig. 5 shows the compression curves of RAS:FS mixtures in terms of vertical strain,  $\epsilon_v$ , versus logarithm of vertical effective stress,  $\sigma'_v$ . The compression curve of outwash sand specimen is also included for comparison. Compared to outwash sand, pure RAS is highly compressible for structural fill applications. High compressibility of RAS is attributed to three mechanisms: (1) the cellulose felt within RAS particles creates voids in the particles. For increasing  $\sigma'_v$ , the voids in cellulose felt tend to close rapidly. The voids between the plate-like RAS particles are also closed due to the flexibility of RAS particles; (2) the sand particles either on RAS particle surface or separated from RAS particles, penetrate into asphalt coating of other RAS particles for increasing  $\sigma'_v$ ; and (3) the smaller spherical RAS particles in the matrix (see Fig. 2(a)), tends to deform under  $\sigma'_v$  due to viscous asphalt cement. Asphalt cement and cellulose felt components together constitute between 35 to 50% by weight of RAS particles.

On the other hand, under stress levels less than 200 kPa, which represent typical overburden pressure in highway embankments, the compressibility of compacted FS is only slightly higher than the compressibility of outwash sand, which makes the FS an appropriate additive to reduce compressibility of RAS. Fig. 5 illustrates that systematic addition of FS to RAS, reduces compressibility of RAS:FS mixtures. Under  $\sigma'_v$  up to 200 kPa, addition of 50% foundry slag to RAS significantly reduces  $\epsilon_v$  of the RAS:FS mixtures from 17% to 7%.

Compared to compacted outwash sand, the compressibility of the compacted FS rapidly increases when  $\sigma'_v$  increases to higher than 200 kPa. This is attributed to crushability, high angularity and rough surface texture of FS particles. Some popcorn-like FS particles were observed to break under finger pressure. High angularity and rough surface texture of granular

particles in general, increase the possibility of particle breakage (Robert and de Souza 1958; Marshal 1967; Pestana and Whittle 1995; Chuhan et al. 2003), which, in turn, increase the compressibility. To verify this, particle size distribution of FS samples were obtained after compaction and after 1D compression test. Fig. 6 shows degradation of FS particles after compaction and compression (under  $\sigma'_v$  of 1600 kPa) tests in terms of changing grain size. The fines content increased from 3% to 6% after compaction and to 11% after 1D compression test. The average grain size,  $d_{50}$ , reduced from 1.8-mm to 1.1-mm after compaction and to 0.5-mm after 1D compression test.

Compressibility of soils is often classified based on compression indices. The classification criteria are summarized in Table 2 (Coduto 1998). The yield stress is the stress at which compressibility of granular soils changes markedly in a constrained compression test due to particle breakage or significant particle rearrangement. Pre-yield modified compression index,  $C_{pry}$ , and post-yield modified compression index,  $C_{psy}$ , which are respectively slopes of the compression curve before and after yield stress,  $\sigma'_y$ , obtained from the following relationships:

$$C_{pry} = \Delta \epsilon_v / \Delta \log \sigma'_v \quad , \quad \sigma'_v < \sigma'_y \quad [1]$$

$$C_{psy} = \Delta \epsilon_v / \Delta \log \sigma'_v \quad , \quad \sigma'_v > \sigma'_y \quad [2]$$

The  $\sigma'_y$  as well as  $C_{pry}$  and  $C_{psy}$  of RAS:FS mixtures were determined from the graphs of void ratio versus  $\log \sigma'_v$  according to the graphical construction of Casagrande (Casagrande 1936b).

Fig. 7 shows the variation of  $\sigma'_y$  of RAS:FS mixtures with FS content. The  $\sigma'_y$  of the mixtures increases with increasing FS content indicating that yield stress of RAS is improved with FS addition. Fig. 8 illustrates the variation of  $C_{pry}$  and  $C_{psy}$  with FS content in RAS:FS mixtures obtained from the compression curves. The  $C_{pry}$  decreases with FS as expected,

however,  $C_{psy}$  increases with increasing FS content. The increase of  $C_{psy}$  with FS is attributed to significant particle crushing during post-yield compression phase, which occurs at  $\sigma'_v$  higher than 200 kPa during 1D compression test as explained from Figs. 5 and 6. The settlement of typical highway embankments with overburden pressures less than 200 kPa constructed with RAS:FS fills is evaluated using the compressibility parameters in the pre-yield stress range. Therefore, addition of FS to RAS reduces the compressibility of the mixture from moderately compressible to slightly and very slightly compressible for  $\sigma'_v$  in the pre-yield stress range according to the classification criteria presented in Table 2.

Figs. 7 and 8 and Table 2 can be used as design tools to determine the required FS content in the RAS:FS mixtures given a  $\sigma'_v$  and a required compressibility. For example, if a very slightly compressible mixture of RAS:FS is desired for an embankment with  $\sigma'_v$  of 200 kPa, the designer selects a  $C_{pry}$  between 0 and 0.05, e.g. 0.03, from Table 2. Assuming that  $s'_v$  is in the pre-yield stress range, from Fig. 8 the corresponding FS content is 45%. From Fig. 7, the  $\sigma'_y$  corresponding to the FS content of 45% is 280 kPa which is higher than the given  $\sigma'_v$  of 200 kPa indicating that the stress state of the RAS:FS mixture with 45% FS remains in the pre-yield stress range.

Fig. 9 shows the variation of  $\epsilon_v$  with time for different RAS:FS mixtures under  $\sigma'_v$  of 100 kPa. The time at which excess pore water pressure,  $\Delta u$  as measured, is dissipated marks the end of primary consolidation,  $t_p$ . The generated  $\Delta u$  in RAS:FS mixtures dissipates in less than 2 min. The end of primary consolidation marked on the compression curves on Fig. 9 indicates that negligible settlement occurs due to primary consolidation in RAS:FS mixtures and the majority of settlement is due to secondary compression. The secondary compression is characterized by modified secondary compression index, which is defined as the slope of  $\epsilon_v$  versus  $\log t$  curve:

$$C_{\alpha} = \Delta \varepsilon_v / \Delta \log t \quad [3]$$

The secondary compression part of the compression curves shows that  $\varepsilon_v$  nonlinearly increases with time. Similar compression behaviour was observed by Fox et al. (1992) and Mesri et al. (1997) for Middleton peat. Long term consolidation test on pure RAS under  $\sigma'_v = 100$  kPa ( $\sigma'_v / \sigma'_y = 1.80$ ) shows that  $C_{\alpha}$  becomes constant after the standard LID of 24 h whereas in RAS:FS mixtures with 50% FS and under  $\sigma'_v = 100$  kPa ( $\sigma'_v / \sigma'_y = 0.34$ ), the  $C_{\alpha}$  increases with time after 24 h. For natural soils, all mechanisms of compression (including particle rearrangement through interparticle slip, rotation and particle damage; and particle deformation including bending and compression) that operate during primary compression are considered to continue into secondary compression (Robert and de Souza 1958; Lee and Farhoomand 1967; Lade et al. 1997; Mesri and Vardhanabhuti 2009). Flexible, plate-like RAS particles seem to reach a stable position after a rapid rearrangement under  $\sigma'_v / \sigma'_y = 1.80$ , thus the long term compression of the specimen might be only due to particle deformation as a result of compressibility of asphalt cement and cellulose felt constituents in RAS. Spherical particles seem to be more prone to rotation and rearrangement than plate-like particles. Addition of FS to RAS may increase particle rearrangement during secondary compression. In particular, crushability of FS particles may increase particle damage during secondary compression, resulting in increased secondary compression ratio over time.

To compare long-term compression of different RAS:FS mixtures quantitatively,  $C_{\alpha}$  was calculated over one log cycle of time before LID of 24 hr. Fig. 10 shows the variation of  $C_{\alpha}$  with FS content under different  $\sigma'_v$ . For a given  $\sigma'_v$ , the secondary compression of RAS:FS

mixtures decreases significantly as the FS content increases. As illustrated in Fig. 10, for typical highway embankments with  $\sigma'_v$  less than or equal to 200 kPa, addition of 50% foundry slag to RAS reduces  $C_{ae}$  from 0.023 to 0.006.

In the preceding discussions so far, the effect of addition of less compressible granular material, e.g. foundry slag, was investigated for reducing secondary compression of RAS. Preloading is another alternative approach to reduce the long term compression of compressible geo-materials like peat (Brawner 1959a, b; Samson and La Rochelle 1972; Mesri et al. 1997). In this study, the LID under  $\sigma'_v = 100$  kPa was maintained for 150 d during 1D consolidation test on RAS and RAS:FS mixture with 50% FS content. After the 150-day duration, the consolidation test with standard LID=24 h continued until  $\sigma'_v = 1600$  kPa. Fig. 11 shows the effect of secondary compression on  $\sigma'_y$  of RAS and RAS:FS mixture with 50% FS content. Table 3 summarizes the compressibility parameters of RAS and RAS:FS mixture before and after the LID=150 d. The long-term secondary compression increased the  $\sigma'_y$  of RAS from 65 kPa to 250 kPa and reduced the  $C_{pry}$  from 0.07 to 0.03. The  $C_{ae}$  of RAS was also reduced significantly from 0.023 to 0.002, reflecting a 10-fold reduction. The reason is attributed to decrease in void ratio of compacted RAS specimen over time. The secondary compression over the 150-day period, had less significant improvement on compressibility of the RAS:FS mixture. The  $\sigma'_y$  increased from 290 kPa to 340 kPa, while the  $C_{ae}$  had a 3-fold decrease from 0.006 to 0.002. The results indicate that preloading is an effective alternative way to reduce compressibility of RAS.

## Shear Strength

Figs. 12 shows the stress-strain and volume change behaviours of RAS, RAS:FS mixtures as well as the GOS sheared in triaxial compression under CD condition at  $\sigma'_3$  of 30 kPa and 140 kPa. The maximum deviator stress,  $\sigma'_{dmax}$ , of RAS is comparable to that of compacted GOS. However, the stress-strain and volume change behaviour of pure RAS resembles those of sandy soils in loose state. The  $\sigma'_{dmax}$  of RAS occurs at axial strain larger than 15% and the volume change behaviour is contractive. For FS content up to 50%, at a given  $\sigma'_3$ , the  $\sigma'_{dmax}$  of RAS:FS mixture remains almost unchanged at different  $\sigma'_3$ , while volume change behaviour is contractive. Increasing FS content to beyond 50%, increases the  $\sigma'_{dmax}$ , and changes the volume change behaviour from contractive to dilative. At low  $\sigma'_3$ , increasing FS content has more pronounced effect on  $\sigma'_{dmax}$ , and the volume change behaviour changes to contractive for FS content more than 25%. As the confining pressure increases, i.e. to  $\sigma'_3=140$  kPa, the behaviour of compacted RAS:FS mixtures changes to contractive and increasing FS has less significant effect on increasing the  $\sigma'_{dmax}$ .

The nonlinear stress-strain curves of both clay and sand may be approximated by a hyperbola (Kondner 1963; Duncan and Chan 1970). The hyperbolic relationship between the deviatoric stress and axial strain is:

$$\frac{\varepsilon}{\sigma'_d} = \frac{1}{E_i} + \frac{\varepsilon}{\sigma'_{d,ULT}} \quad [4]$$

where  $\sigma'_{d,ULT}$  is the asymptotic value of  $\sigma'_d$  which is related to  $\sigma'_{df}$  by means of a factor  $R_f$  as:

$$R_f = \sigma'_{df} / \sigma'_{d,ULT} \quad [5]$$

and  $E_i$  is the initial tangent modulus of soil expressed as:

$$E_i = K p_a \left( \frac{\sigma_3}{p_a} \right)^n \quad [6]$$

where K is the modulus number and n is the modulus exponent. To characterize Eq. [4],  $\varepsilon/\sigma'_d$  is plotted versus  $\varepsilon$ . The  $E_i$  and  $\sigma'_{d,ULT}$  are obtained from the intercept and slope of the best-fitted line to the data points. Parameters K and n are readily obtained by plotting the values of  $E_i$  against  $\sigma'_3$  on log-log scale and fitting a straight line to the data. Table 4 summarizes the hyperbolic model parameters of RAS:FS mixtures. For a given RAS content, the stiffness of the RAS:FS mixture increases with  $\sigma'_3$ . As the RAS content increases, the stiffness decreases as expected. Fig. 13 presents the comparison of the experimental data with the hyperbolic curves. The hyperbolic model approximates the stress-strain behaviour of RAS:FS mixture reasonably well up to the peak values of the deviatoric stress.

Deviator stress at failure,  $\sigma'_{df}$ , according to ASTM D4767-04, was selected as either the  $\sigma'_{dmax}$  or the  $\sigma'_d$  corresponding to 15% axial strain whichever is reached earlier. The friction angle of compacted RAS obtained from the Mohr-Coulomb failure envelope is  $33^\circ$ . Pure RAS also exhibited an apparent cohesion ( $c'$ ) of 28 kPa from the ordinate of the Mohr-Coulomb failure envelope possibly due to slight binding of RAS particles together during compaction. This apparent cohesion can be neglected for practical purposes. Fig. 14 shows the variation of  $\phi'$  and  $c'$  of RAS:FS mixtures with FS content. Similar to variation of  $\sigma'_{dmax}$  with FS content, the  $\phi'$  and  $c'$  remain almost unchanged with FS content up to 50% after which both  $\phi'$  and  $c'$  increase. The increase of  $\phi'$  is attributed to the increased number of FS particles with rough surfaces in the matrix of compacted RAS:FS mixture (see Figs. 2c, d). The ground furnace slag is a cementitious material in nature (RMRC 2011). When compacted, the fines content in granular

FS specimen increases and tend to hydrate. The increase in FS content in RAS:FS mixture, probably increases the bonding potential between the FS particles in the mixture and thus the cohesion increases. The range of  $\phi'$  for RAS:FS mixtures is between  $33^\circ$  and  $37^\circ$ , which is within the  $\phi'$  range ( $31^\circ$  to  $45^\circ$ ) for typical compacted sandy soils (US Navy 1986). Therefore, the shear strength of RAS:FS mixtures is sufficient for use as structural fill material for construction of highway embankments. For a given FS content,  $\phi'$  and  $c'$  are taken from Fig. 14 and the compressive strength,  $\sigma'_{df}$ , of the compacted RAS:FS mixture is then obtained from the Mohr-Coulomb failure criterion as:

$$\sigma'_{df} = \frac{2c' \cos \phi + 2\sigma'_3 \sin \phi}{1 - \sin \phi} \quad [7]$$

## **PRACTICAL IMPLICATIONS**

The total or differential settlement that can be tolerated by a pavement is rarely specified except in the case of bridge approaches for which the tolerable settlement is commonly specified as 12-mm to 25-mm. For roadway embankments the allowable settlement after paving depends on the length of the fill and rate at which settlement develops. If the variations in settlement are uniformly distributed along the length of the embankment, settlement of 150-mm to 300-mm can be tolerated in long embankments (NCHRP Synthesis of Highway Practice 8). Although the maximum settlement of highway embankments are allowed between 300-mm and 600-mm (NCHRP Synthesis of Highway Practice 29 and Stark et al. (2004), 300-mm is a more widely accepted limit and is adopted here.

To illustrate the performance of embankment fill constructed with RAS:FS mixtures or preloaded RAS, example calculations were made on embankments 2, 5, 10, and 15-m high constructed on a 15-m thick sand deposit. Since compacted RAS:FS mixtures have suitable drainage capacity and shear strength as highway embankment fill, emphasis was put on the evaluation of embankment settlements during the life-time period of the fill. As illustrated in previous sections, due to high hydraulic conductivity of the compacted RAS:FS mixtures, primary consolidation accounts for negligible settlement of the RAS:FS fill and short term settlements of the fill occur during construction of the embankment. The long-term settlements due to secondary compression of RAS:FS mixtures were evaluated using the following relationship:

$$s = \sum_{i=1}^n s_i = \sum_{i=1}^n h_i C_{ae,i} \log\left(\frac{t}{t_o}\right) \quad [8]$$

where  $s$  is the embankment settlement,  $s_i$  is the settlement of a layer with thickness  $h_i$  ( $h_i$  was selected 0.5 m in the calculations),  $n$  is the number of sublayers, i.e., the embankment height  $H$  divided by the sublayer thickness ( $H=nh_i$ ),  $t$  is time, and  $t_o$  is an arbitrary reference time that for the calculations herein was taken 1 d after the completion of construction. The values of  $C_{ae}$  used for settlement calculations were taken from the data points of Fig. 10. Depending on the location of each sublayer in the embankment, the corresponding  $C_{ae}$  to the vertical stress was used for settlement calculation.

Fig. 15 shows the variation of settlement of an embankment 15-m high, constructed with either compacted RAS:FS mixtures, preloaded RAS or compacted sand during 40-year lifetime after construction. The majority of settlements occur within 1 year after completion of embankment construction. The long term settlement of the embankment constructed with RAS is

about 1050-mm which is far above the allowable limits. Preloading of RAS for five months reduces the long-term settlement to 108-mm, which reflects 90% reduction. Addition of 50% FS to RAS also reduces the long-term embankment settlement to 294-mm reflecting a 72% reduction. Increase of FS content to 75% results in only 90-mm settlement during the 40-year lifetime. The average height of the embankments constructed in the U.S. is 4.5-m (Wright 1996). Having identical subgrade soil conditions, shallow embankments exhibit smaller settlement than those plotted in Fig. 15 for a 15-m high embankment. Fig. 16(a) presents the variation of settlement with height of the embankments constructed with compacted RAS, preloaded RAS, RAS:FS mixtures and glacial outwash sand. The long-term settlement of an embankment with average height, i.e. 4.5-m, constructed with these materials is smaller than the 300-mm allowable settlement. In general, for embankment height up to 15-m, preloaded RAS fills, and RAS:FS fills with 50% and 75% FS content, result in long term settlements below the allowable limit of 300 mm. Fig. 16 (b) shows the variation of long-term settlements of embankments of different heights with FS content in RAS:FS mixtures. RAS fills less than 5-m high exhibit long-term settlement within the allowable limit. For higher embankments, addition of more than 50% FS to RAS significantly reduces the long term settlement.

The results of this study are easily generalized to develop guideline criteria for incorporation of RAS in natural soil. As illustrated in Fig. 5, compacted FS is more compressible than the compacted glacial outwash sand. Therefore, the maximum recommended RAS for incorporation in RAS:FS mixture is also recommended for incorporation in RAS:granular material mixtures where the “granular material” (e.g., sand, other slags) is similar to or less compressible than FS. To maintain adequate drainage capacity and keep the long-term settlement of the average

embankment fill below the maximum allowable limit, the maximum recommended RAS content for incorporation into granular materials should be between 25% to 50%.

## CONCLUSIONS

In this study, recycled asphalt shingles (RAS) were evaluated for potential use as structural fill in highway embankments. Because of high compressibility of RAS, a granular byproduct, foundry slag (FS), was selected as granular additive to improve mechanical properties of RAS and render it an acceptable fill material. The following specific observations are made based on the test results:

1. RAS:FS mixtures have maximum dry unit weight of  $11 \text{ kN/m}^3$  which is almost 50% of maximum dry unit weight of typical compacted soils. Low dry unit weight of RAS:FS mixtures makes them favorable alternatives to natural compacted soils for construction of lighter structural fills over soft soils.
2. The hydraulic conductivity of RAS:FS mixtures is over  $1 \times 10^{-4} \text{ cm/s}$  indicating that the mixtures have good drainage capacity as structural fills. The hydraulic conductivity of the mixtures slightly decreases with increasing confining pressure due to high compressibility of RAS particles. The hydraulic conductivity of the mixtures increases with increase in foundry slag content and becomes almost insensitive to confining pressure when the foundry slag content of the mixture increases to more than 50%.
3. The short and long-term compressibility of pure RAS is significantly higher than those of compacted sandy soils. Preloading or mixing RAS with a granular material significantly

reduces the compressibility. For a typical stress level in highway embankments, addition of 50% by weight of foundry slag to RAS reduces the modified pre-yield compression index from 0.075 to 0.021 and the modified secondary compression index from 0.023 to 0.006. Preloading also reduces the secondary compression ratio of RAS from 0.023 to 0.002 which as a result, categorizes the RAS:FS mixture as slightly to very slightly compressible material.

4. Stress-strain and volumetric change behavior of pure RAS in triaxial compression is similar to those of loose sandy soils. Addition of foundry slag up to 50% to RAS does not have any noticeable effect on volumetric behavior and shear strength; however, the volumetric behavior tends to be dilative and shear strength starts to increase when the foundry slag content of the RAS:FS mixture increases to more than 50%. Depending on the FS content, the friction angle of RAS:FS mixture varies between  $33^{\circ}$  and  $37^{\circ}$  which is within the range for compacted sandy soils.

Based on the results of this research, RAS:FS mixture is considered a viable material for use as fill in highway embankments. Such an application will use the majority of asphalt shingle waste and contribute to reduction of greenhouse gas emissions by avoiding production of natural aggregates. The results obtained in this study are for the specific RAS and FS samples tested, which are however typical of such materials. However, RAS and FS samples obtained from different sources and with different particle sizes may have different mechanical behavior and need to be tested for specific applications. Further studies need to be made to generalize use of RAS:FS mixture in structural fills and to evaluate the potential effect of high ground temperatures in certain climatic regions.

## ACKNOWLEDGMENT

Support for this study was provided by the Recycled Materials Resource Center, which is supported by the Federal Highway Administration. The opinions, findings, conclusions, or recommendations expressed herein are those of the author(s) and do not necessarily represent the views of the sponsors.

## REFERENCES

- Ahmed, I. 1993. *Use of Waste Material in Highway Construction*, Noyes Data Corporation, Park Ridge, NJ.
- American Coal Ash Association. 2009. *Coal Combustion Product (CCP) Production & Use Survey Results*, ACAA, Aurora, CO. September 15, 2009 [online].
- Benson, C., Edil, T., and Soleimanbeigi, A. 2010. Use of recycled asphalt shingles in highway embankments, *Proceeding of 2010 Mid-Continent Transportation Research Forum*, Madison, WI.
- Brawner, C. O. 1959a. "Preconsolidation in highway construction over muskeg." *Roads and engineering construction*, Monetary Times Production, Toronto, 97(9), 99-104.
- Brawner, C. O. 1959b. "The principles of preconsolidation in highway construction over muskeg." *Proceeding of the 5th Muskeg Research Conference*, NRC, Ottawa, ACSSM Technical Memorandum.
- Casagrande, A. 1936. The determination of the pre-consolidation load and its practical significance, *Discussion D-34, Proc. First Int. Conf. Soil Mech. Found. Engr.*, Cambridge, 3: 60-64.
- Chuhan, F. A., Kjeldstad, A., Bjorlykke, K., and Hoeg, K. 2003. Experimental compression of loose sands: relevance to porosity reduction during burial in sedimentary basins, *Canadian Geotechnical Journal*, 40(5): 995-1011.

- Coduto, D. P. 1998. *Geotechnical Engineering Principles and Practices*. Prentice Hall.
- Drenvich, V. P., Evans, A. C., and Prochaska, A. B. 2007. A study of effective soil compaction control of granular soils, *Joint Transportation Research Program*. Paper 234.
- Edil, T., Benson, C., Bin-Shafique, M., Tanyu, B., Kim, W., and Senol, A. 2002. Field evaluation of construction alternatives for roadway over soft subgrade, *Transportation Research Record*, 1786, Transportation Research Board, National Research Council, Washington, DC: 36-48.
- Emery, J.J. 1985. Slag utilization in pavement construction, *Extending Aggregate Resources*, ASTM STP No. 774, ASTM: 95-118.
- Fox, P. J., Edil, T. B. and Lan, L. T. 1992.  $C_a/C_c$  concept applied to compression of peat, *Journal of Geotechnical Engineering*, ASCE, 118(8): 1256-1263.
- Grodinsky, C., Plunkett, N., and Surwilo, J. 2002. *Performance of Recycled Asphalt Shingles for Road Applications*, Final Report, State of Vermont's Agency of Natural Resources.
- Hilf, J.W. 1991. *Compacted Fill*, In H.-Y. Fang (Ed.), *Foundation Engineering Handbook*, 2nd Edition: 249-316. New York: Van Nostrand Reinhold.
- Johnson, E., Johnson, G., Dai, S., Linell, D., McGraw, J., Watson, M. 2010. *Incorporation of recycled asphalt shingles in hot mix asphalt mixture*, Report No. MN/RD-10/02, Minnesota Department of Transportation, Saint Paul, MN.
- Krivit, D. 2007. *Recycling of Tear-Off Shingles: Best Practices Guide*. Final report prepared for the Construction Materials Recycling Association (CMRA).
- Lade, P.V., Yamamuro, J.A., and Bopp, P.A. 1997. Influence of time effects on instability of granular materials, *Computers and Geotechnics*, Vol. 20: 179–193.
- Lee, K.L., and Farhoomand, I. 1967. Compressibility and crushing of granular soil in anisotropic triaxial compression, *Canadian Geotechnical Journal*, 4(1): 68-99.
- Marshal, R.J. 1967. Large scale testing of rockfill materials, *Journal of the Soil Mechanics and Foundations Division*, ASCE, 93: 27–43.
- Mesri, G., and Hayat, T.M. 1993. The coefficient of earth pressure at rest, *Canadian Geotechnical Journal*, 30(4): 647-666.
- Mesri, G., Stark, T.D., Ajlouni, M.A., and Chen, C.S. 1997. Secondary compression of peat with or without surcharging, *Journal of Geotechnical and Geoenvironmental Engineering*, ASCE, 123(5): 411-421.

- Mesri, G., and Vardhanabhuti, B. 2009. Compression of granular materials, *Canadian Geotechnical Journal*, 46: 369-392.
- Moulton, L.K., Seals, R.K., and Anderson, D.A. 1973. Utilization of ash from coal burning power plants in highway construction, *Transportation Research Record*, 430: 26-39.
- Northeast Recycling Council (2011). *Asphalt Shingles Manufacturing & Waste Management in the Northeast Fact Sheet*. NERC, November 2011.
- NCHRP Synthesis of Highway Practice 8: Construction of Embankments*. (1971). Transportation Research Board, National Research Council, Washington, D.C., 38 p.
- NCHRP Synthesis of Highway Practice 29: Treatment of Soft Foundations for Highway Embankments*. (1975). Transportation Research Board, National Research Council, Washington, D.C. 25 p.
- Pestana, J.M., and Whittle, A.J. 1995. Compression model for cohesionless soils, *Géotechnique*, 45: 611-631.
- Recycled Materials Resource Center. 2010. *User Guidelines for By-products and Secondary Use Materials in Pavement Construction*, <http://www.rmrc.unh.edu/tools/uguidelines/index.asp>, Accessed December 2010.
- Roberts, J.E., and de Souza, J.M. 1958. The compressibility of sands, *Proc., American Society for Testing and Materials*, 58: 1269-1277.
- Roberts, F.L., Kandhal, P.S., Brown, E.R., Lee, D.Y. and Kennedy, T.W. 1996. *Hot Mix Asphalt Materials, Mixture Design, and Construction*, National Asphalt Paving Association Education Foundation. Lanham, MD.
- Samson, L., and La Rochelle, P. 1972. "Design and performance of an expressway constructed over peat by preloading." *Canadian Geotechnical Journal*, 9, 447-466.
- Soleimanbeigi, A., Edil, T., and Benson, C. 2010. Recycled asphalt shingles mixed with granular byproducts as structural fill, *Journal of ASTM International*, 9(1).
- Stark, T. D., Arellano, D., Horvath, J. S., and Leshchinsky, D. (2004). NCHRP Report No. 529: Guidelines and recommended standards for geofabric applications in highway embankments. Transportation Research Board, National Research Council, Washington, DC.
- Tanyu, B.F., Benson, C.H., Edil, T.B., and Kim, W.H. 2005. Equivalency of crushed rock and three industrial by-products used as a working platform during pavement construction, *Transportation Research Record*, 1874, Transportation Research Board, National Research Council, Washington, DC: 59-69.

- Townsend, T., Powell, J., and Xu, C. 2007. Environmental issues associated with asphalt shingle recycling. *Construction Materials Recycling Association, US EPA Innovations Workgroup.*
- Turley, W. 2011. Personal Communication. *Construction Materials Recycling Association, Eola, IL.*
- U.S. *Bureau of Reclamation.* 1987. *Design of Small Dams.* U.S. Department of the Interior, Bureau of Reclamation.
- U.S. Geological Survey. 2008. *Minerals Yearbook.* USGS, [http://minerals.usgs.gov/minerals/pubs/commodity/iron\\_&\\_steel\\_slag/myb1-2008-fesla.pdf](http://minerals.usgs.gov/minerals/pubs/commodity/iron_&_steel_slag/myb1-2008-fesla.pdf), Accessed December 2010.
- U.S. Navy. 1986. *Design manual—Soil mechanics, foundations, and earth structures.* NAVFAC DM-7, Department of the Navy, Washington, D.C.
- Warner, J. D. 2007. The beneficial reuse of asphalt shingles in roadway construction, *MSc thesis, Department of Civil and Environmental Engineering, University of Wisconsin-Madison.*
- Wen, H. and Edil T. 2009. “Sustainable Reconstruction of Highways with In-Situ Reclamation of Materials Stabilized for Heavier Loads,” 8<sup>th</sup> International Conference on the Bearing Capacity of Roads, Railways, and Airfields, Champaign, IL, June 19, 2009.
- Wright, P. H. 1996. *Highway Engineering.* John Wiley & Sons, Inc.
- Lee, J., Edil, T., Tinjum, J., and Benson, C. 2010. “Quantitative Assessment of Environmental and Economic Benefits of Using Recycled Construction Materials in Highway Construction.” *J. Transportation Research Board*, 2158, 138-142.

Table 1-Grain size indices and USCS classifications of RAS, bottom ash and outwash sand

Material	$d_{10}$	$d_{50}$	$C_u$	$C_c$	finer	$G_s$	USCS symbol	USCS name
	(mm)	(mm)			(%)			
RAS	0.17	1.1	7.6	1.6	3.8	1.74	SW	Well graded sand
Foundry slag	0.18	1.6	11.4	2.7	4.8	2.36	SW	Well graded sand
Glacial outwash sand <sup>a</sup>	0.21	0.5	3.1	0.8	0.0	2.71	SP	Poorly graded sand

$d_{10}$ : effective particle size (particle size for which 10% of the sample is finer than  $d_{10}$ );  $d_{50}$ : average particle size (particle size for which 50% of the sample is finer than  $d_{50}$ );  $C_u$ : coefficient of uniformity,  $d_{60}/d_{10}$ ;  $C_c$ : coefficient of curvature,  $C_c^2 / (C_{10} \times C_{60})$ ;  $G_s$ : specific gravity; USCS: Unified Soil Classification System

<sup>a</sup> Data were taken from Bareither et al. (2008)

Table 2-Classification for material compressibility (after Coduto 1998)

Modified Compression Index	Classification for compressibility
0-0.05	Very Slightly compressible
0.05-0.10	Slightly compressible
0.10-0.20	Moderately compressible
0.20-0.35	Highly compressible
> 0.35	Very Highly compressible

Table 3-Effect of secondary compression on compressibility of RAS

Material	Parameters	Before LID=150 d	After LID=150 d	% change
RAS:FS (50:50)	$\sigma'_y$	65	250	280% increase
	$C_{\alpha}$	0.023	0.002	90% decrease
	$C_{py}$	0.070	0.030	60% decrease
RAS:FS (50:50)	$\sigma'_y$	290	340	17% increase
	$C_{\alpha}$	0.006	0.002	65% decrease
	$C_{py}$	0.022	0.020	9% decrease

Table 4-Summary of CD triaxial compression test data and hyperbolic model parameters

RAS (%)	$\sigma'_3$ (kPa)	$E_i$ (kPa)	$(\sigma_1-\sigma_3)_{ult}$ (kPa)	$(\sigma_1-\sigma_3)_f$ (kPa)	$R_f$	K	n
0	35	111100	354	341	0.964	49550	0.224
	70	125000	500	452	0.904		
	140	151500	714	653	0.914		
25	35	28570	313	258	0.826	12000	0.243
	70	33330	370	344	0.928		
	140	40000	625	543	0.869		
50	35	10870	189	184	0.975	2120	0.454
	70	14090	345	312	0.905		
	140	20410	455	444	0.977		
75	35	7630	200	180	0.902	1370	0.495
	70	12050	323	279	0.864		
	140	15150	526	526	0.818		

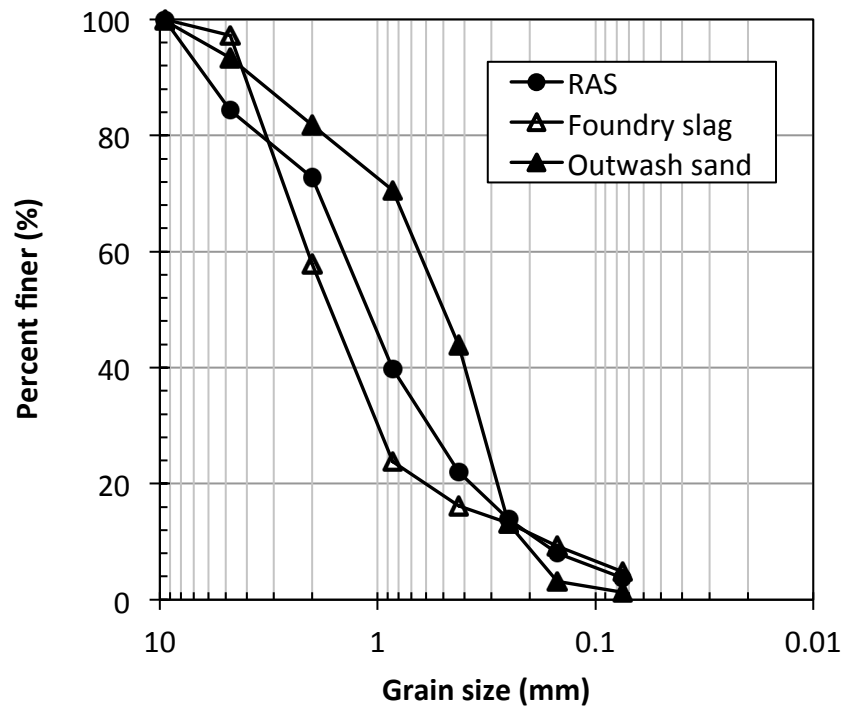
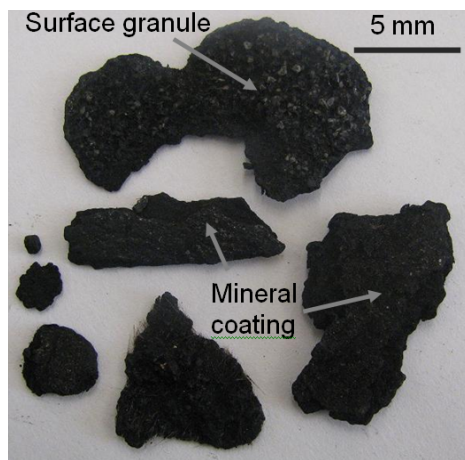
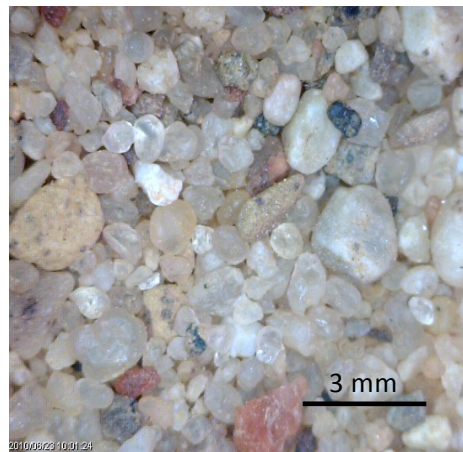


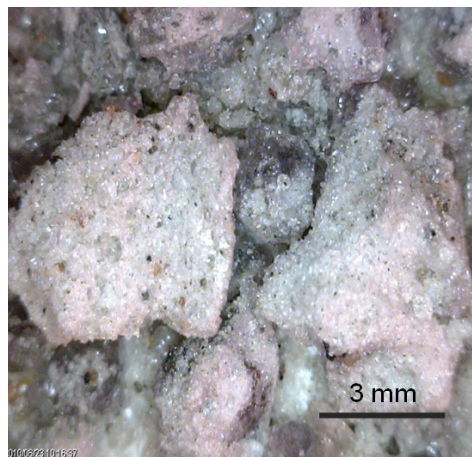
Fig. 1-Grain size distribution of RAS, foundry slag, and glacial outwash sand



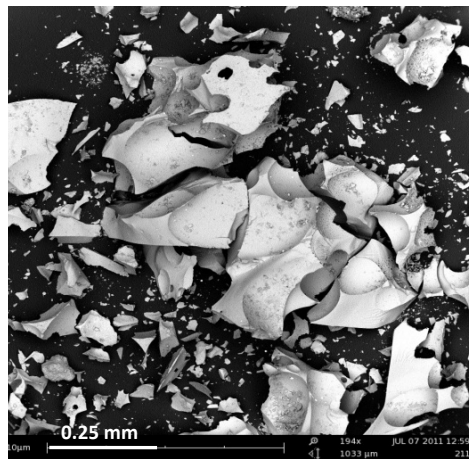
(a)



(b)



(c)



(d)

Fig. 2-Photographs of (a) RAS, (b) glacial outwash sand and (c) foundry sand and (d) SEM micrographs of foundry sand particles

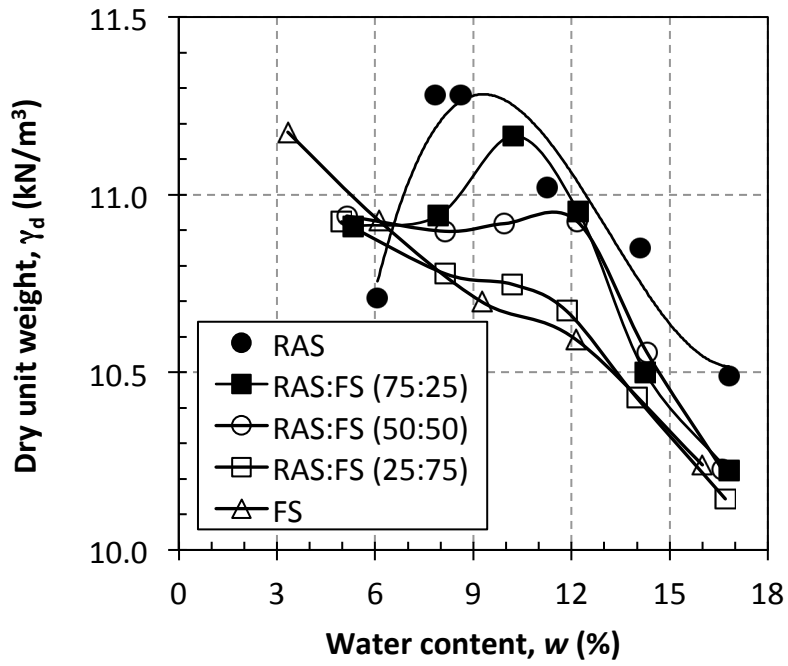


Fig. 3- Dry unit weight versus water content of RAS:FS mixtures

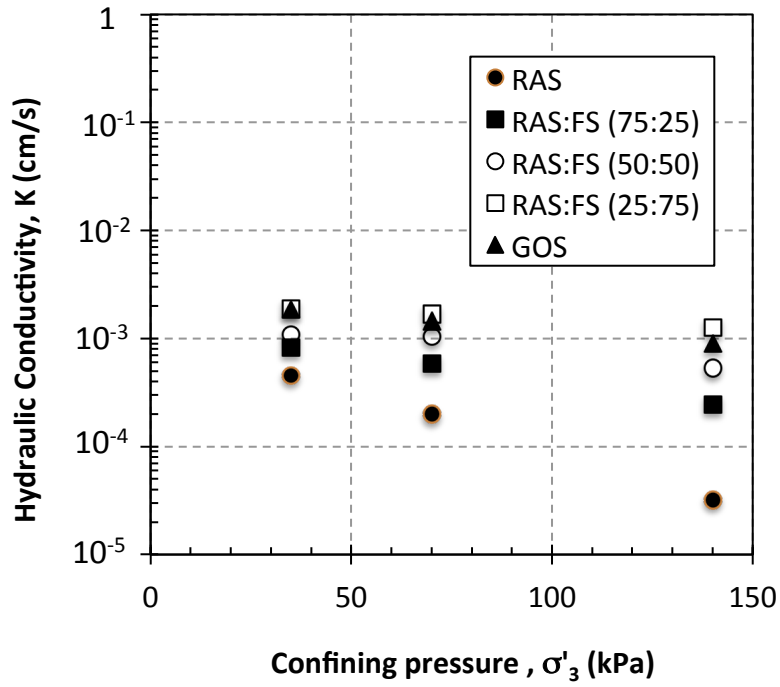


Fig. 4-Hydraulic conductivity of RAS:FS mixtures versus effective confining pressure

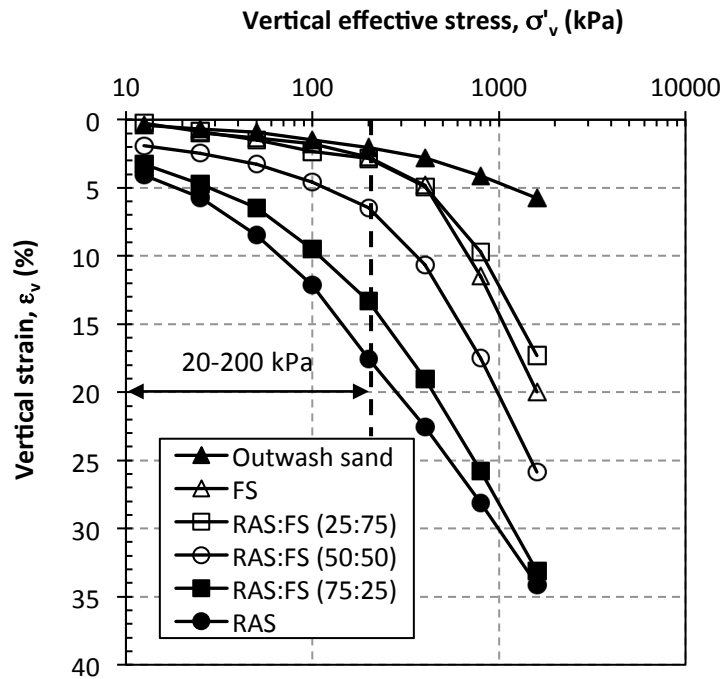


Fig. 5- One-dimensional compression curves of RAS:FS mixtures

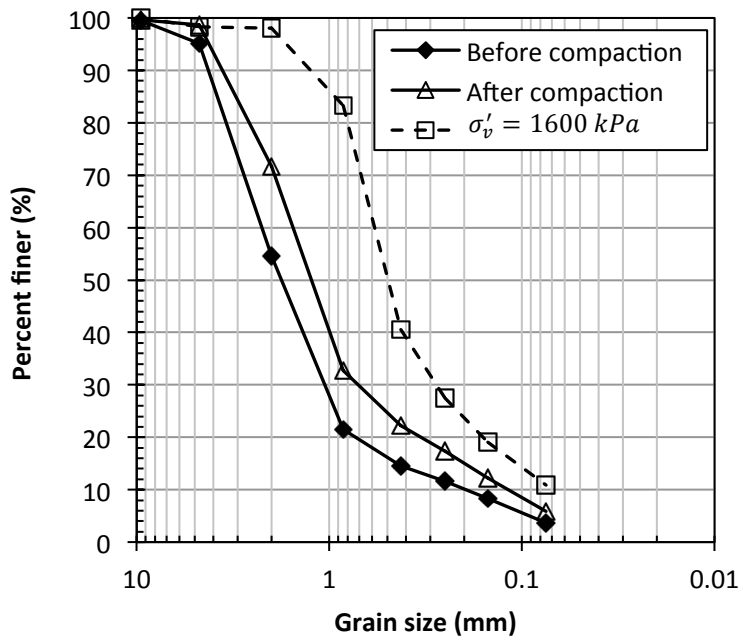


Fig. 6- Material degradation after compaction and compression tests

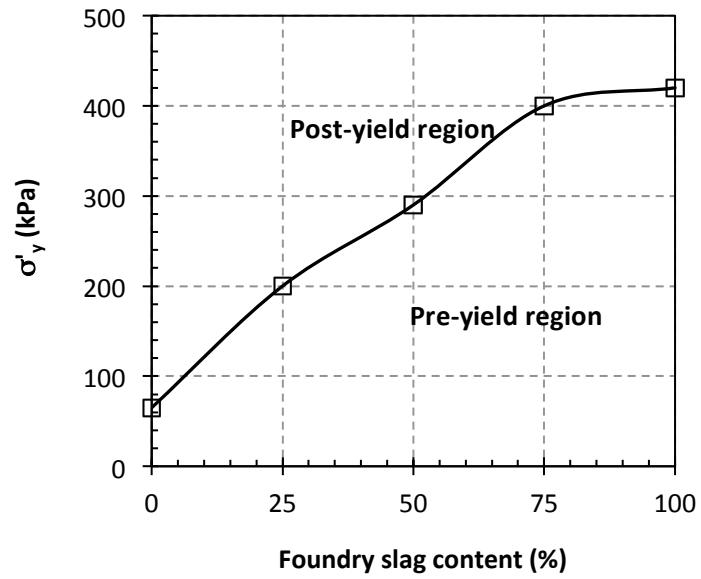


Fig. 7- Variation of yield stress of RAS:FS mixtures in compression with foundry slag content

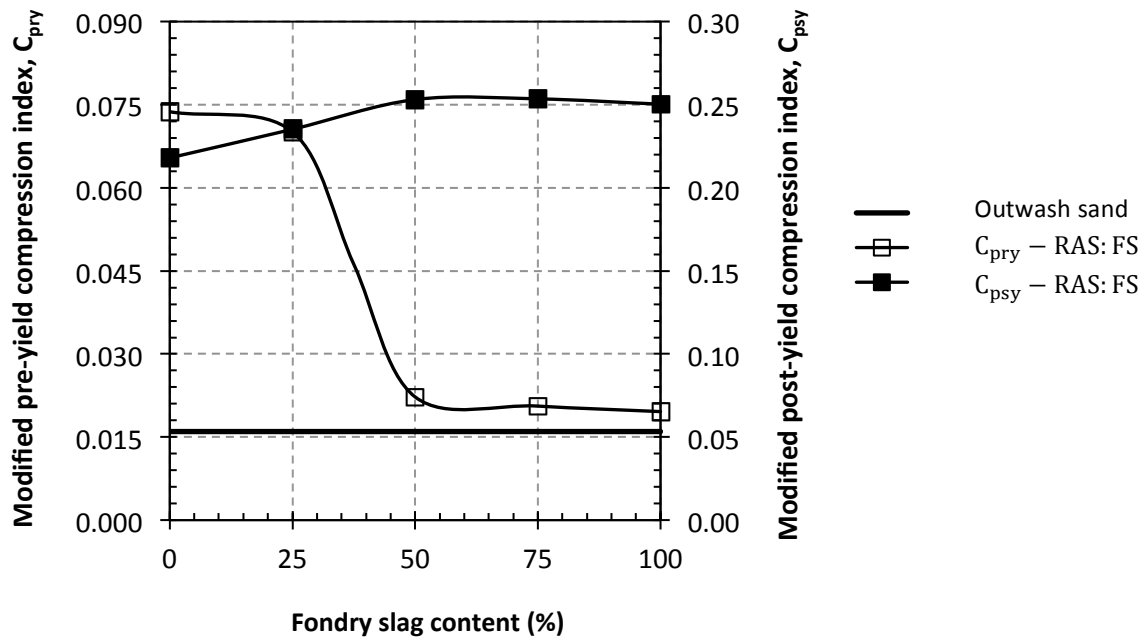


Fig. 8-Variation of pre-yield and post-yield stress, modified compression indices of RAS:FS mixtures with foundry slag content

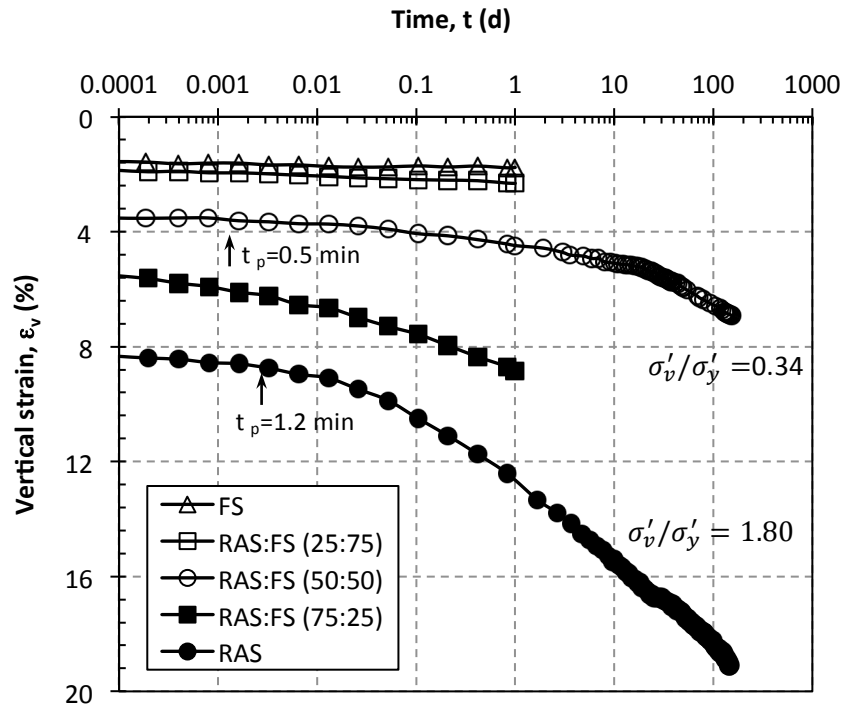


Fig. 9- Variation of  $e_v$  with time for RAS:FS mixtures

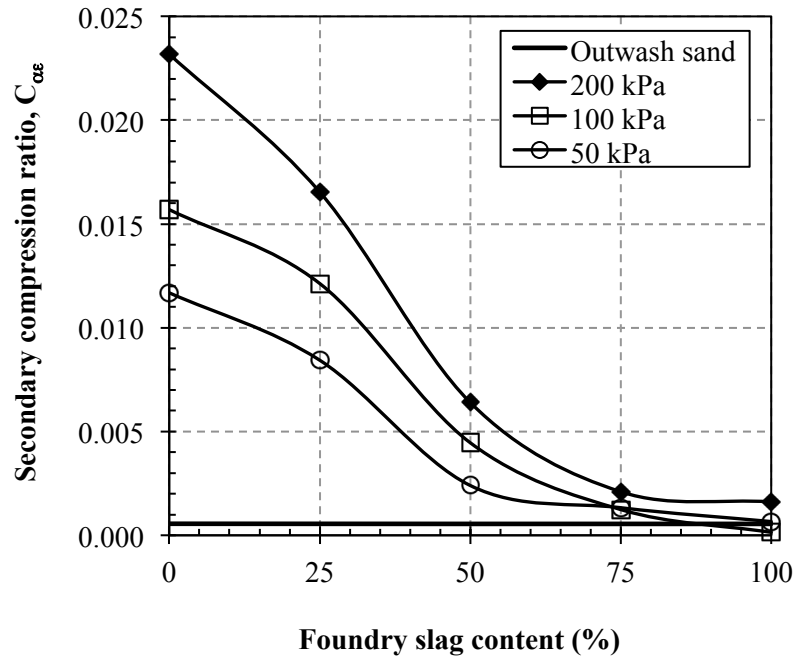


Fig. 10-Variation of modified secondary compression of RAS:FS mixtures with FS content

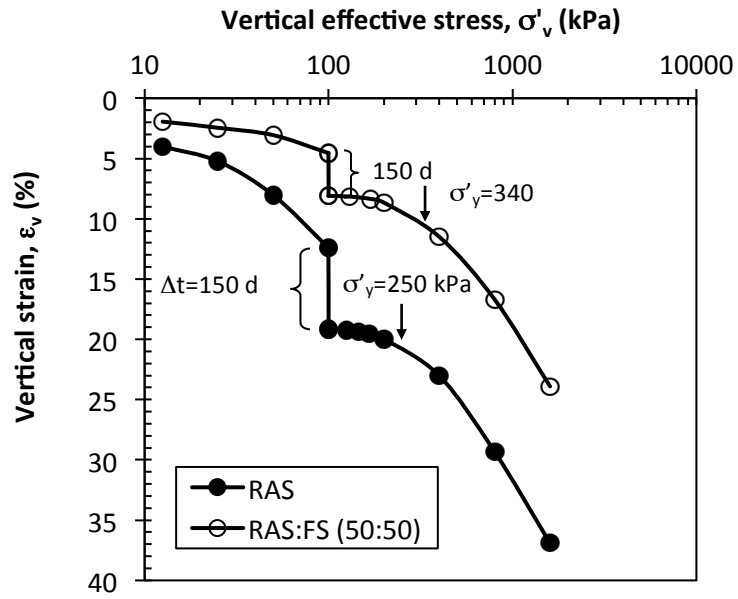


Fig. 11-Yield stress increase of RAS resulting from secondary compression

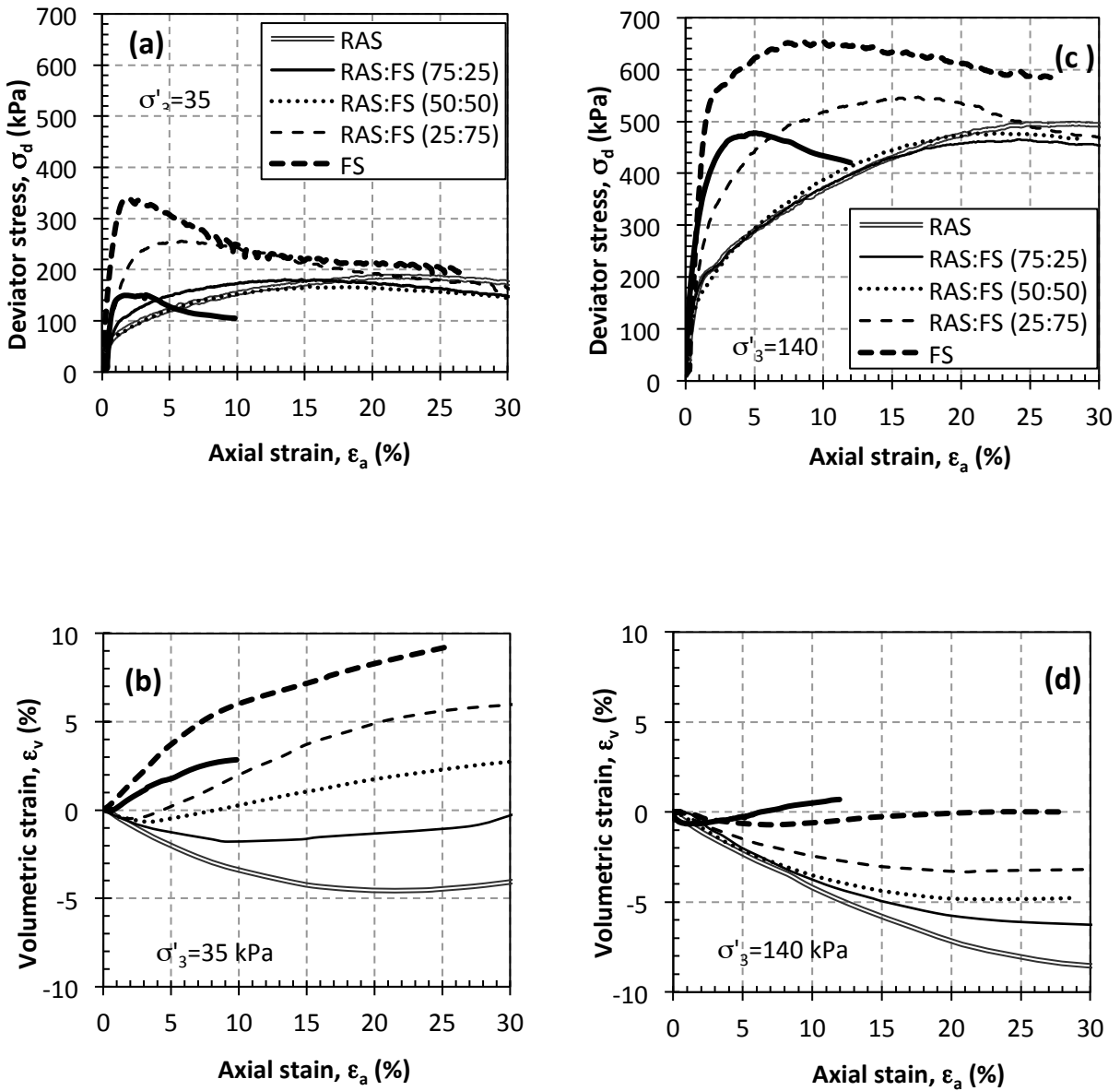


Fig. 12-Results of CD triaxial tests: (a and b) stress-strain behavior of RAS:FS mixtures; and (c and d) volume change behaviour of RAS:FS mixtures

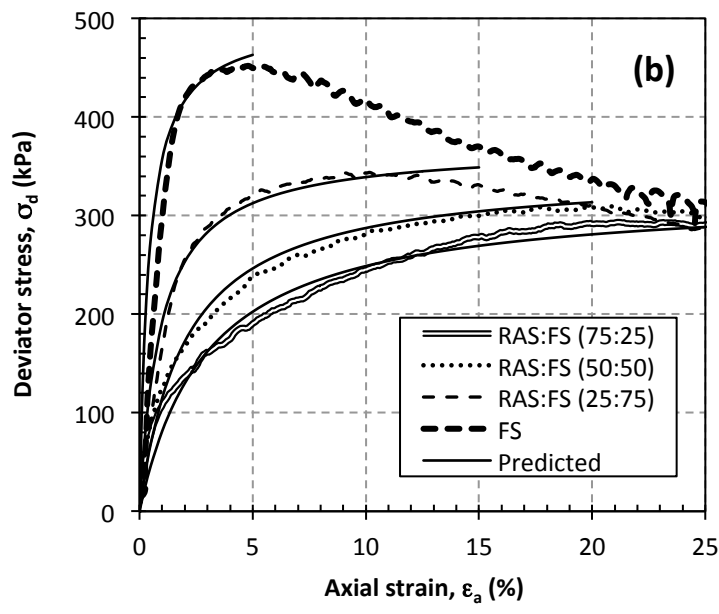
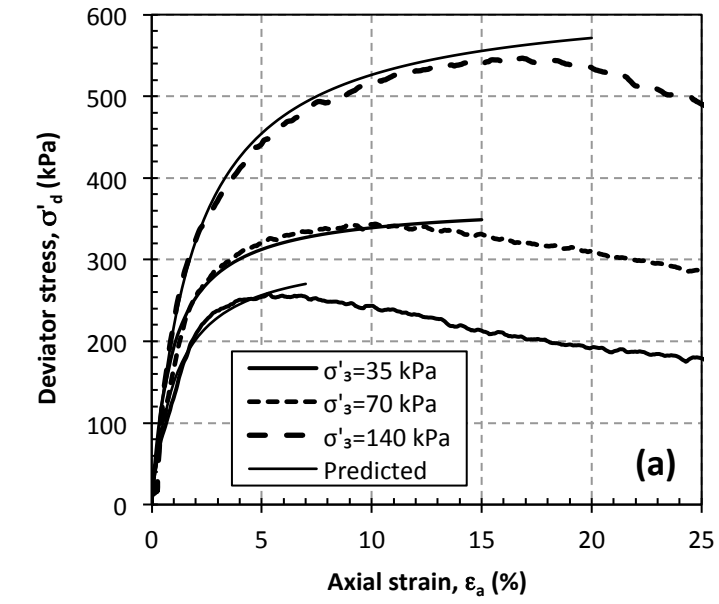


Fig. 13-Predicted versus measured stress-strain behaviour of (a) RAS:FS (25:75) at different  $\sigma'_3$  and (b) RAS:FS mixtures at  $\sigma'_3 = 70$  kPa

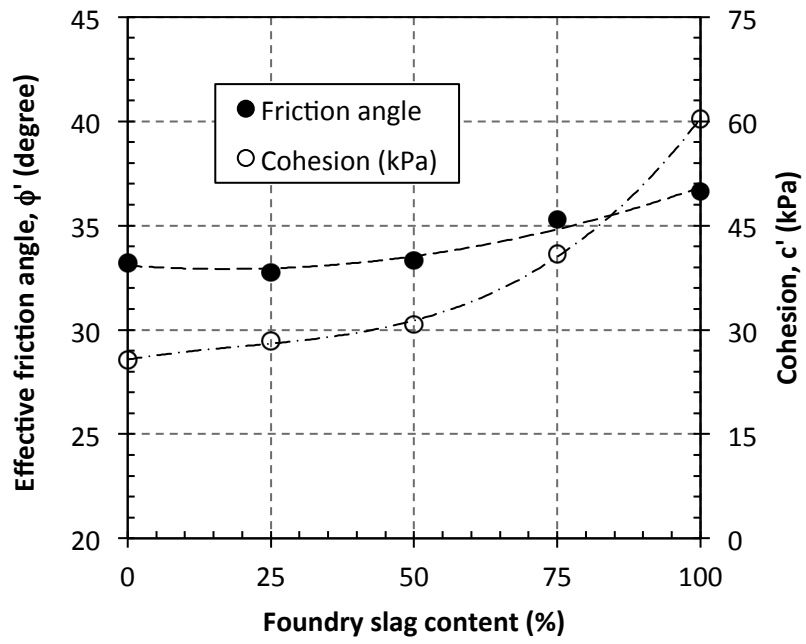


Fig. 14-Variation of friction angle and cohesion of RAS:FS mixtures with FS content

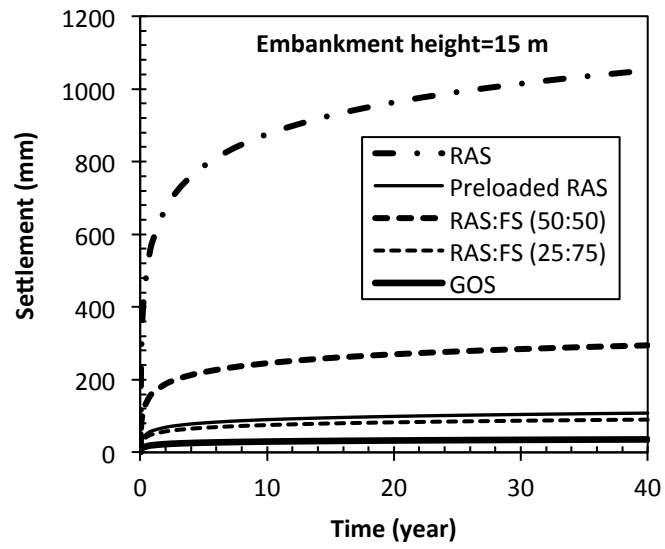


Fig. 15- Variation of embankment settlement with time

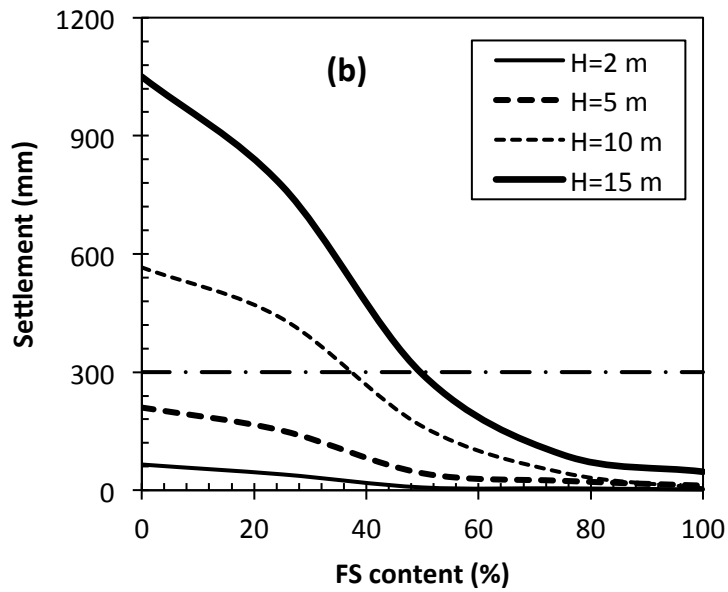
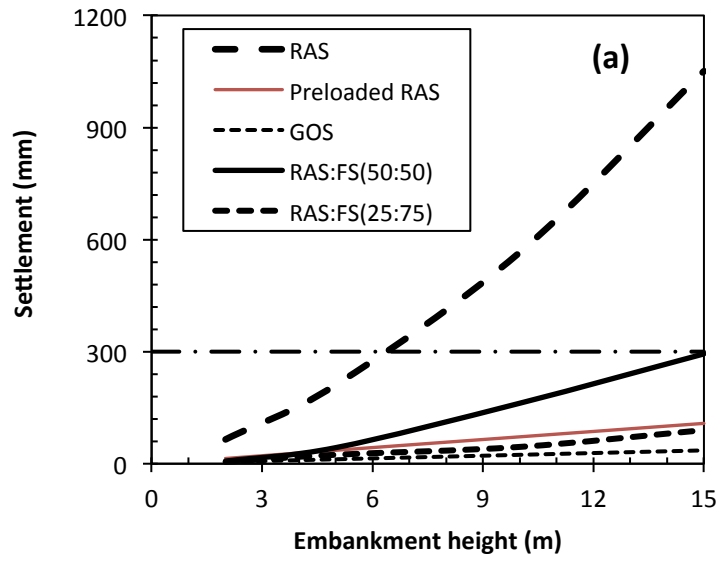


Fig. 16- Variation of embankment settlement with embankment height (a) and FS content (d)